Physica D 489 (2026) 135143

Contents lists available at ScienceDirect

Physica D

journal homepage: www.elsevier.com/locate/physd

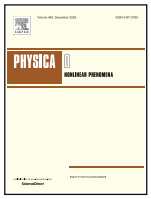

Irrational behaviour-induced suppression, enhancement and oscillations of voluntary vaccination: A stochastic model with delays

Lorenzo Cabriel [a], Chris T. Bauch [b], Fabio Anselmi [a], Piero Manfredi [c], Alberto d'Onofrio [a,1,*]

[a] Department of Mathematics, Informatics and Geosciences, University of Trieste, Via Economo 12/3, Trieste, Italy
[b] Department of Applied Mathematics, University of Waterloo, 200 University Avenue West, Waterloo, ON, N2L 3G1, Canada
[c] Department of Economics and Management, University of Pisa, Via Ridolfi 10, Pisa, 5612, Italy

ARTICLE INFO

Editor: Dr K Sznajd-Weron

Keywords:
Irrationality
Vaccine hesitancy
Evolutionary games
Stochasticity
Distributed delays
Quasi-cycles
Noise-induced transitions

ABSTRACT

We investigate how human irrationality and memory shapes voluntary vaccine uptake in the absence of disease. Building on a deterministic imitation game framework, after providing its analytical solution, we show that finite-population stochasticity alone produces either vaccine-free or full-coverage states, but with fixation times so long that the mean-field ODE model remains valid for large population sizes. To capture rapid irrational swings in public sentiment, we model them using white noise, deriving an SDE whose stationary density undergoes noise-induced transitions as noise intensity crosses critical thresholds. Larger noise can switch the population to either disease-free or full-coverage regimes, and very strong noise yields stochastic bistability reminiscent of phase transitions. Numerical simulations reveal very slow transients and rich behaviors when delays and noise interact. In particular, noise-induced quasi-cycles can onset. Generalizing to fat-tailed Cauchy noise, we find that heavy-tailed fluctuations increase the probability of fixation at zero or full coverage. Fluctuations in the imitation rate parameter produce large amplitude cycle distortions, occasionally destroying cyclic patterns. Finally, we show that a public health campaign term with 'intensity' exceeding a noise-dependent threshold eliminates the vaccine-free attractor and stabilizes full coverage.

1. Introduction

Over the past two decades, the limitations inherent in classical Mathematical Epidemiology (ME) [1,2]–a branch of Mathematical Biology exerting significant influence on current public health policies–have become increasingly apparent. Classical ME, which abstracts contagion akin to a chemical reaction, models individuals as molecules. This fundamental assumption implies that human behavior is taken as a physical constant and therefore unaffected by epidemic dynamics (and conversely). Long before the COVID-19 pandemic, it became apparent that this assumption was unable to describe various contemporary scenarios, such as non-mandatory vaccination programs [3–8].

The initial groundbreaking effort to incorporate human behavior into ME can be traced back to [9]. Later, a whole new scientific discipline emerged, termed Behavioral Epidemiology of Infectious Diseases (BEID) [3,4], which addressed the growing need to include human behavior in ME models by integrating ideas from a range of medical and social sciences.

Human behaviour is currently becoming a critical factor in the public health programs of modern industrialized countries [3,4], as well documented by the COVID-19 experience [10]. This role is amplified by two interplaying and synergizing global phenomena, namely the 'post-trust society' [11] and the 'post-truth age' [12,13].

To model agents' vaccination behaviour, most BEID models utilized either a phenomenological approach or Evolutionary Game Theory (EGT). Bauch [14] first used EGT to model the dynamic interplay between infection spread and vaccination propensity, by adding imitation dynamics for vaccination behavior to an SIR model. Since then, this model has been extended in many directions. For example, current authors have analysed the perceived risk of vaccine side effects as a function of information based on both present and past incidence of vaccine-related adverse events [15]; vaccination awareness campaigns by Public Health Systems [15]; the effects of imitation on the emergence of vaccine scares [16]; the impact of social norms [17] and bounded rationality in vaccination decisions [18]; the role of spatial information in vaccine choices [19].

* Corresponding author.
E-mail address: alberto.donofrio@units.it (A. d'Onofrio).
[1] Formerly at: International Prevention Research Institute, Lyon (France), where he developed the very first ideas of this work, see the video lecture [1]

https://doi.org/10.1016/j.physd.2026.135143
Received 18 May 2025; Received in revised form 19 November 2025; Accepted 6 February 2026
Available online 18 February 2026

Most previous works using EGT such as [14–17,20] relied on traditional game-theoretic language, based on the concept of payoff or utility (a measure of preferences). More recently, we reformulated imitation dynamics as a dual 'contagion of ideas'[4,19,21], allowing a straightforward comprehension of the opinion switching mechanism.

As the main aim of BEID models based on EGT [4,14,15,19–21] was to elucidate fundamental implications of behaviour, most such models were deterministic. Stochasticity has only been considered when studying small populations [22]. This ignores the critical fact that, in the current era dominated by social networks, opinions – including those on vaccination – tend to be highly volatile and subject to rapid, non-modellable, fluctuations in response to a succession of short-lived rumors [23–27].

Capturing such rapid opinion fluctuations is not possible with deterministic models, even when the 'rational' behaviour postulated by most models using EGT is relaxed by using other factors such as e.g., by social learning, social norms and other collective habits [17] or by the intrinsic tendency of rationality to be bounded as elucidated by the Nobel Prized Prospect Theory (whose effects on vaccination behavior were considered in [18]). When occurring through online social media, for instance, these rapid fluctuations in opinion are well described not as white noise but rather as a fat-tailed noise distribution, where extreme events (such as caused by celebrity tweets) occur with a disproportionately high frequency [28].

Another feature of real-world opinion dynamics that calls for study is the tendency of many coupled behaviour-disease systems to undergo oscillations. Examples include the behaviourally-induced infection waves of the 'Spanish flu' pandemic in the early 20th century [29], multiple waves in pertussis incidence during the whole cell pertussis vaccine scare in England & Wales in the 1970s and 1980s [14], as well as the first waves caused by successive application and relaxation of non-pharmaceutical interventions during the COVID-19 pandemic [30]. Models of such acute respiratory infectious diseases exhibit damped oscillations, due to imaginary eigenvalues [31]. It has been shown that these damped oscillations may become sustained through the addition of demographic stochasticity [31], or through strictly deterministic effects of behavioural feedback [14]. However, the possibility of generating oscillations through the interaction between stochastic effects and behaviour-disease feedbacks has generally evaded rigorous study. In this perspective, the present contribution aims to fill this gap by providing a rigorous modeling and analysis of oscillatory vaccination dynamics emerging from the joint action of stochastic opinion fluctuations and delayed behaviour-disease feedbacks.

Indeed, in this work, we investigate in depth the effects of volatile private opinions on collective vaccine uptake in the absence of infection. This problem is motivated by a critically important question in prospective terms, namely which are the determinants, and which trends might be expected, for vaccine uptake against a vaccine preventable infection that has been eliminated at an adequately large spatial scale (say, countries or entire regions) ? This question is fundamental because the subsequent policy step i.e., achieving eradication, will require maintaining elimination locally, through high vaccine uptake, for a long span of time. A major related example is that of poliomyelitis, a major infective threat prior to immunization that was targeted for eradication (i.e., global elimination) by the related Global Polio Eradication Initiative [32] in 1988. During recent decades, polio has been eliminated almost everywhere thanks to sustained immunization and is near eradication, with only two countries, Afghanistan and Pakistan, still showing endemic circulation [33]. Recently, a number of complications are recently emerging as e.g., the challenge of vaccine-derived polio virus [34], that needed a mass vaccination campaign in London in 2022 [35], the re-emergences of wild viruses in war-settings due to interruption of immunization programs [36,37] and, of course, the COVID-19 crisis [38]. However, these complications are occurring in a global landscape characterized by a steady and dramatic fall in vaccine uptake in many countries that previously reached very high immunization rates. A major example is Brazil, a country with long-standing excellence in childhood immunization. In Brazil, after many years with 99% coverage among the 1-year-old [39], polio vaccine uptake has started to decline in an oscillating region–dependent way already since 2010, long before the COVID-19 crisis, and is currently stalling at average levels well below 80%, with potential for virus re-emergence [40]. In addition to Brazil, several other Latin American countries are seeing a worrying decline in polio coverage [41]. Not to say about several Central and Sub-Saharan African countries where polio coverage started to stall or decline before having reached levels adequate for full infection control [39,42]. In UK a small but steady decline of pentavalent (Polio, Diphteria, Tetanus, Pertussis, Hib) vaccination has been observed since 2009, with a worrying percentage of 87.7% in London [43].

Abstracting from the subtle complications of polio immunization, we set up here a baseline stochastic evolutionary game-theoretic model that systematically combines behavioural feedback in vaccination decisions with stochastic fluctuations in vaccination opinions, in order to: i) reproduce in a stylised qualitative way the above mentioned trends; ii) answer the above question of which trends might be expected for vaccine uptake when the target infection has been eliminated. When infection is absent and the importation of infective cases is well controlled, the main incentive [14] for parents to vaccinate their children is removed [3,4]. In this case, the main determinants of the individual-level propensity to vaccinate, taken as a key proxy of vaccine uptake in a behavioral epidemiology approach, remain (1) the trend of vaccine adverse events (VAE) [15] and their memory over time [15], which individuals elaborate into a perceived vaccination cost, and (2) the cumulative pattern of rumors and disorientation (e.g., [24]) on vaccination opinions over online social media [11].

Consistently, we derive an imitation dynamics equation for vaccine propensity in a large-scale non-mandatory childhood immunization system where the perceived cost of vaccination depends on the (current and past) trend of vaccine adverse events (VAEs) following immunization in a background of highly volatile vaccination opinions (we term this 'irrational' behaviour) which induce large stochastic perturbations of imitation dynamics.

In particular, we pay particular attention to the interplay between opinion volatility and the form of the information set on VAEs trends used by individuals while making vaccine decisions. This is carried out using both current and delayed information indices [44], landing on a rich mathematical setting, namely stochastic integro-differential equations.

To our knowledge, apart from a video lecture of one of us [45], containing the very first steps of this work, only one very recent work published during the development of the present manuscript [46], adopted a similar mathematical approach. However, that approach considered the completely different scenario of an endemic infection without delays. Additionally, that paper made strong stochastic and biological assumptions that introduce some potential pitfalls (see appendix).

The paper is structured as follows: Section 2 summarizes the deterministic approach to evolutionary games-based modeling of vaccine hesitancy in the absence of the targeted infection; Section 3 introduces the birth-death Markov process underlying our model and infers the average time to extinction of the vaccinating population; in Section 4 the memory kernels are introduced and analysed; Section 5 models the impact of highly volatile changes in vaccine-related opinions as a stochastic differential equation driven by Gaussian white noise; in Section 6 we cover the topic of the Noise-Induced Transitions with a focus on the stationary transition density; Section 7 analyzes the long-term behavior of the system; Section 8 investigates the behavioural transitions of the system and the emergence of stochastic bistability; Section 9 deepens the investigation via numerical simulations; Section 10 study the impact of colored noises; Section 11 investigates the impact of stochastic fluctuations of a key parameter (α_1) introduced in Section 2; in Appendix H the effects of the actions of the Public Health System are considered. Concluding remarks end this work, which also includes an Appendix.

2. Imitation dynamics for voluntary vaccination

We consider vaccination against a childhood infectious disease by a perfect vaccine. Following [14,15,20], we take vaccination as a binary decision problem, encompassing two mutually exclusive strategies: a 'Vaccinator' strategy, prevalent with population frequency $x(t)$, and a 'non-Vaccinator' strategy, having frequency

$$b = 1 - x.$$

Unlike [14,15,20], where imitation dynamics was centered on the net payoff change of vaccinators, we model imitation dynamics as a 'double contagion' of ideas [4,21,47]. Indeed, general imitation games belong to the category of urn models [48]. This allows us to derive the following family of models [4,47]:

$$\begin{aligned} x' &= C(M_i)xb - \alpha(M_v)bx + \gamma(t)b, \\ a' &= -C(M_i)xb + \alpha(M_v)bx - \gamma(t)b, \end{aligned} \tag{1}$$

where: $M_i(t)$ denotes the available information index on infection spread; M_v is the corresponding information regarding trends of VAEs; $C(.)$ and $\alpha(.)$ are the transmission rates of opinions following social contacts with individuals playing the other strategy. Both information indices are assumed to be non-decreasing. Last, the term $\gamma(t)a$ represents the rate of an irreversible transition towards the vaccinator strategy possibly as a result of sustained communication activities of the Public Health System [15].

From an epidemiological viewpoint, the transmission rate $\alpha(M_v)$ and the related contagion of ideas rate $\alpha(M_v)ax$ capture the fact - mentioned in the Introduction - that VAEs become the main determinant of vaccination strategies when infections become increasingly rare [15]. Indeed, infection rarity will cause people to myopically amplify their perceptions of the risks from the vaccine. This yields

$$x' = x(1-x)\big(C(M_i) - \alpha(M_v)\big)$$

As we assume that the infection targeted by the vaccine is essentially absent ($I = 0 \Rightarrow M_i = 0$), we just take

$$C(M_i) = c_0 > 0$$

The c_0 term reflects that the fact that nonetheless individuals perceive some risk of infection e.g., resulting from outside importation. Additionally, we posit that the rate of transitioning from strategy x to strategy a is directly proportional to the dissemination of news and rumors about vaccine side effects, which is mirrored by the vaccination frequency in the initial phase

$$\alpha(M_v) = \alpha_0 + \alpha_1 M_v.$$

Previous assumptions yield

$$x' = x(1-x)(\delta - \alpha_1 M_v), \tag{2}$$

where $\delta = c_0 - \alpha_0$.

Remark *Henceforth, we assume as time unit* $1/\alpha_1$ *or we set* $\alpha_1 = 1$. Regarding the information index M_v, following [4,15,20] we assume that the extent of vaccinations per unit of time (proportional to x) is an appropriate proxy for both rumors and news on related VAEs.

Since its early developments, behavioral epidemiology studies [49, 50] have suggested that memories of the past can be a fundamental determinant of individual behavior in relation to vaccination choices and also for social distancing, see [51]. Thus, the information index M_v will depend on present and past data

$$M_v(t) = \int_0^{+\infty} W_v(\tau)x(t-\tau)d\tau \tag{3}$$

where W_v is a memory kernel

$$\int_0^{+\infty} W_v(\tau)d\tau = 1.$$

Specific types of memory kernels W_v will be discussed in later sections.

In the absence of stochastic perturbations, the system (2)-(3) straightforwardly admits, besides $x = 0, x = 1$, a unique internal equilibrium:

$$(x_e, M_e)$$

where

$$M_e = x_e = Min\left(\frac{\delta}{\alpha_1}, 1\right)$$

Henceforth, we will, unless otherwise stated, assume that

$$x_e < 1.$$

In particular, we will consider three representative memory kernels, namely (i) an unlagged kernel by which vaccination decisions do not depend on past information, (ii) an exponentially fading kernel, (ii) and acquisition-fading kernel, taken as the simplest example of a humped memory distribution.

3. Absence of memory: analytic solution and effect of intrinsic stochasticity in the imitation dynamics due to population discreteness

In this section we investigate the behavior of the model in absence of memory effects, namely

$$W_v(s) = \delta(s).$$

We first provide an analytic solution of the resulting scalar ODE model, with a comparison w.r.t the behavior of the apparently similar logistic model. Then we investigate the effect of the intrinsic stochasticity by passing form the ODE model to the corresponding Continuous Time Markov Chain. This will also allow to estimate the limits of temporal validity of the mean field approximation.

3.1. Analytic solution and comparison with logistic model

Trivially, the model is represented by the scalar ODE:

$$x' = x(1-x)(\delta - \alpha_1 x) \tag{4}$$

and x_e is globally attractive.

Setting $\alpha_1 = 1$, model (4) could apparently seem very close to the celebrated logistic growth model:

$$y' = y(\delta - y) \tag{5}$$

but in reality it is very different. To start, in the logistic model both the population size and the steady state population have only the constraint of non negativity: $y(t), \delta \geq 0$, whereas since both the $x(t)$and the steady state value δ are fractions it must be $0 \leq x(t), \delta \leq 1$. Second, the logistic model has only two equilibria 0 (unstable) and δ (stable) at variance of our IGD that has three equilibria: 0 and 1 (both unstable) and δ (stable).

Apart to these important qualitative differences, there are important quantitative differences. Suppose indeed that:

$$x(0) = y(0) = a \in [0, 1]$$

Indeed, although for $0 < a << 1$ *initially* it is $x(t) \approx y(t) \approx ae^{\delta t}$ until they remain small. If, instead, $a = 1$ the behavior of the two models is very different since for $t > 0$ it is $x(t) = a = 1$ whereas $y(t)$ decreases and tends to δ. To fully appreciate the difference between the two time behaviors it is sufficient to compare the analytical solutions of the two models. Indeed, rewriting the vaccine IGD model as follows:

$$\frac{\frac{dx}{dt}}{x(1-x)(\delta - x)} = 1$$

it easily follows that

$$t = F(x, a, \delta) = \frac{1}{\delta}\left(Log\left(\frac{x(1-x)^{\frac{\delta}{1-\delta}}}{|\delta - x|^{\frac{1}{(1-\delta)}}}\right) - Log\left(\frac{a(1-a)^{\frac{\delta}{1-\delta}}}{|\delta - a|^{\frac{1}{(1-\delta)}}}\right)\right) \tag{6}$$

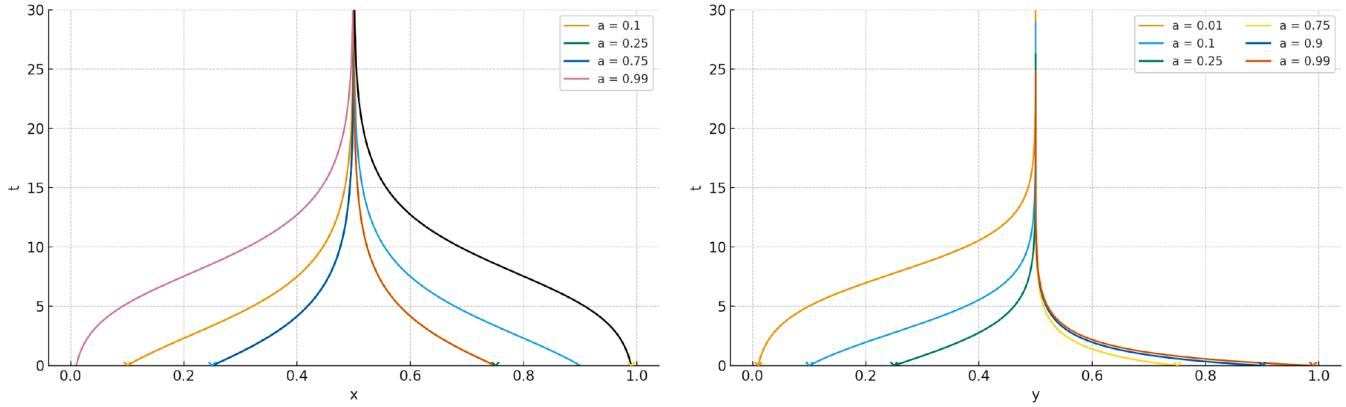

Fig. 1. Vaccine imitation game dynamics ($x(t)$) versus logistic dynamics ($y(t)$) for identical steady state $\delta = 1/2$ and various identical initial conditions $x(0) = y(0) = a$. Left panel: vaccine imitation game dynamics; Right panel: logistic dynamics.

On the contrary, the same method applied to logistic model (see [52]) yields a very different analytic solution:

$$t = L(y, a, \delta) = \frac{1}{\delta}\left[\log\left(\frac{y}{|\delta - y|}\right) - \log\left(\frac{a}{|\delta - a|}\right)\right] \tag{7}$$

The Fig. 1 clearly show the remarkable quantitative differences between the dynamics of the two models.

3.2. Impact of the intrinsic noise

To put the analysis in an appropriate stochastic perspective, we briefly consider the influence of the *intrinsic* stochasticity arising due to the discrete nature of the population.

The aim of this section is twofold. First, we want to assess the goodness of the deterministic evolutionary game model in the limit of sufficiently large populations. Second, here we explore one facet of stochasticity, the intrinsic stochasticity. In the majority of this work, instead, we will focus on the study of the impact of extrinsic stochasticity due to random fluctuations of some key behavioral parameters.

Namely, here we shall explore the continuous time population Markov process (CTPMP), which serves as the foundational framework for the deterministic evolutionary game model (4). Indeed, taking into account of the discreteness and finiteness of the population, our model becomes a CTPMP defined by the following infinitesimal probabilities:

$$Prob(n(t + dt) = n(t) + 1) = G(n)dt$$

$$Prob(n(t + dt) = n(t) - 1) = J(n)dt$$

$$G(n) := c_0 n\frac{N - n}{N} = Nx(1 - x)c_0 =: G(x)$$

$$J(n) := n\frac{N - n}{N}\left(\alpha_0 + \alpha_1\frac{n}{N}\right) = Nx(1 - x)\left(\alpha_0 + x\right) =: J(x)$$

where N is the population size and $n(t)$ is the number of people adopting the 'vaccinator' strategy at the time t.

Roughly speaking, the system, following an initial stochastic transitory phase, tends to settle near its deterministic equilibrium. However, owing to sequences of infrequent occurrences, it inevitably converges either to $n = 0$ (representing a 'non-vaccinator' equilibrium) or to $n = N$ (representing a 'pure-vaccinator' equilibrium). Briefly, once we put the analysis in a correct stochastic perspective, the seemingly stable deterministic equilibrium is, in fact, an illusion: in the long run it lacks stability, so it is metastable.

However, it is crucial to address the following practical question: *How long is the run to the loss of stability ? In other words: what is the average time, say* $\langle T_{fix}\rangle$*, necessary to reach the absorbing state* $n = 0$*, corresponding to the extinction of the vaccinator strategy?* This question holds paramount importance, as exceptionally large average times imply that the deterministic approximation is excellent. Employing the appropriate approximations (such as WKB [53–55] or other [56]) tailored to population dynamics, the average fixation time $\langle T_{fix}\rangle$ to $n = 0$ can be computed using the formula [56]:

$$\langle T_{fix}\rangle = \frac{e^{-N\phi(x_e)}}{\sqrt{N}}\frac{1}{\rho(0) - 1}\sqrt{\frac{2\pi\rho(0)}{\lambda(x_e)\mu'(x_e) - \lambda'(x_e)\mu(x_e)}} \tag{8}$$

where

$$\lambda(x) = x(1 - x)c_0$$

$$\mu(x) = x(1 - x)(\alpha_0 + x)$$

$$\rho(x) = \frac{G(x)}{J(x)}$$

$$\phi(x) = -\int_0^x \rho(z)dz = (x + \alpha_0)\Big(Log(x + \alpha_0) - 1 - Log(c)\Big)$$

This yields an average fixation time of the form

$$\langle T_{fix}\rangle = \frac{e^{c_0 N}}{\sqrt{N}}\sqrt{2\pi\alpha_0}\frac{1}{x_e^2(1 - x_e)} \tag{9}$$

Since $x_e = \delta = c_0 - \alpha_0$, it yields that $c_0 = x_e + \alpha_0$ so that it is easy to rewrite (9) as follows

$$\langle T_{fix}\rangle(\alpha_0, \delta, N) = K(N, \delta)\Psi(\alpha_0 N) \tag{10}$$

where:

$$\Psi(z) = \sqrt{z}e^z$$

$$K(N, \delta) = \frac{e^{\delta N}}{N}\frac{1}{\delta^2(1 - \delta)}.$$

It is apparent that even if δ is not unrealistically close to zero, $K(N, \delta)$ would assume unrealistically large values, even for moderately sized populations. Therefore, unless $z = \sqrt{\alpha_0 P}$ is negligible and δ unrealistically small, the average extinction time exceeds by far the range of validity of numerous implicit hypotheses we have made.

For example, if we consider $x_e = \delta = 0.5$, a small population $N = 100$ and a tiny $\alpha_0 = 0.001$, we find: $\langle T_{fix}\rangle(0.001, 100) \approx 1.445\ 10^{20}$ time units, whereas if $\alpha_0 = 1$ we have $\langle T_{fix}\rangle(1, 100) \approx 1.114\ 10^{65}$ time units. An example of relatively small average 'vaccination extinction' time would be $\delta = 0.1$, $\alpha = 0.001$ and $P = 100$, which yields $\langle T_{fix}\rangle(\alpha_0, \delta, N) \approx 8553$. However, if we increase α_0 to 0.1 we get $\langle T_{fix}\rangle(\alpha_0, \delta, N) \approx 1.704\ 10^9$.

Consequently, spontaneous stochastic fixation toward the 'no-vaccines' equilibrium becomes exceedingly improbable, especially if the initial conditions significantly deviate from 0 and 1.

Similar considerations also hold for the average time needed to reach the opposite scenario of universal vaccination ($x = 1$) reached thanks to spontaneous stochastic fluctuations.

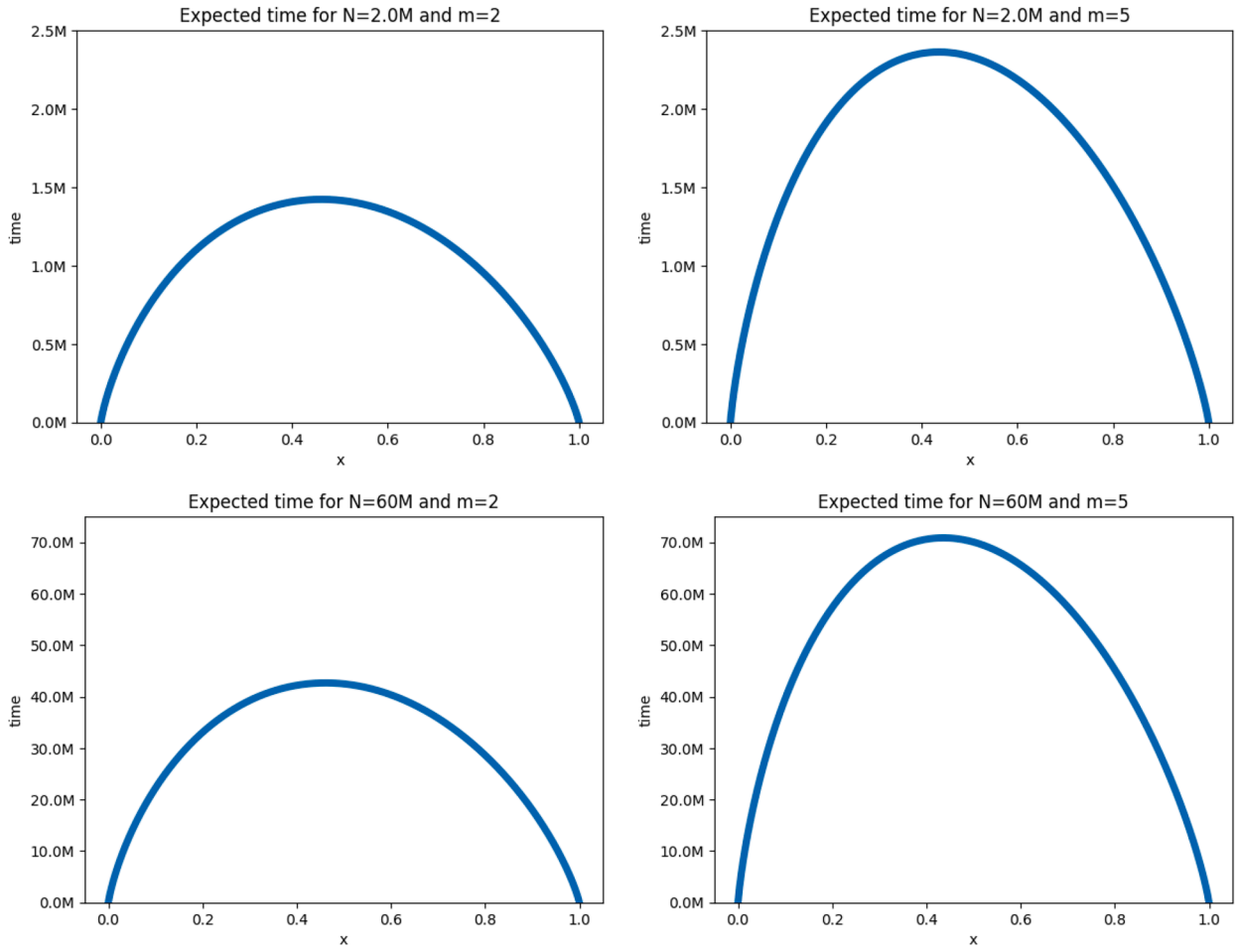

Fig. 2. Average first exit expected time to reach the boundary 0.0001 and 0.9999. Left panels: $N = 2 \cdot 10^6$; right panels: $N = 6 \cdot 10^7$; Upper panels: $m = 2$; Lower panels: $m = 5$.

It is of interest to explore scenarios where the vaccination propensities becomes not fixed but quite close to fixation. We can obtain a good estimate of these cases by means of a well known approximation of CTMC models: the Chemical Langevin Equation (CLE) [57,58]. Namely, it is straightforward to show that the CLE associated to the above CTMP reads as follows:

$$\frac{dx}{dt} = x(1-x)(\delta - \alpha x) + \sqrt{\frac{x(1-x)(\theta_0 + \alpha_0 + \alpha x)}{N}}\xi(t), \tag{11}$$

where $x(t) = n(t)/N$. Throughout all the simulations in this work, we will consider $\alpha = 1$ thus δ represents the intermediate equilibrium point of the deterministic dynamics. To have the estimation in the worst case scenario for this test, we choose $\delta = 0.5$ therefore the deterministic dynamics attracts the trajectories towards the center. We will consider $\theta_0 = m\alpha_0$ so that $\delta = (m-1)\alpha_0$ one easily gets $\alpha_0 = \delta/(m-1)$ and $\alpha_0 = \delta m/(m-1)$. We employed the values $m = 2$ and $m = 5$. As per the population size N, in our simulations we choose $N = 2 \cdot 10^6$ (corresponding to a population size between Latvia and Gabon) and $N = 6 \cdot 10^7$ (a average populations size between Italy and Tanzania). As per the parameter m, we employed the values $m = 2$ and $m = 5$, expecting a larger exit time for a larger m. Indicating with $T_a(x)$ the average time needed – starting at $t = 0$ from the point x– to reach one of the two extremes of the interval $a = (a_L, a_R)$ is given for the scalar CLE (11) by the following differential equation

$$x(1-x)(\delta - \alpha x)\partial_x T_a + 2\frac{x(1-x)(\theta_0 + \alpha_0 + \alpha x)}{N}\partial_x^2 T_a = -1 \tag{12}$$

with boundary conditions

$$T_a(a_L) = T_a(a_R) = 0$$

(clearly if at $t = 0$ the initial point is already one of the two boundaries the average hitting time is null). We choose as interval a the following: $a = (0.0001, 0.9999)$. Since the analytical solution of the scalar linear ODE (12) involves analytically unsolvable integrals (see Appendix C), we numerically solved it via the Finite Differences method. The numerical solutions are shown in Fig. 2. Note that the maximum is not coincident with the equilibrium point of the deterministic dynamics but it is shifted towards left. Interestingly, in all cases the maximum average hitting time is huge. However, for $m = 2$ it is smaller than N, whereas for $m = 5$ it is larger than N.

4. The presence of memory

Since only very recently the awareness of the importance of behavioral epidemiology became widespread, the 'empirics' of behavioral epidemiology is still rather underdeveloped. Therefore, to the best of our knowledge, no field study has attempted to investigate the relevance of memory effects regarding vaccinations of childhood. However, departing from the suggestions of theoretical works by Bauch, d'Onofrio and Manfredi, Poletti and coauthors showed empirically the relevance of exponentially fading delays in risk perceptions of the 2009 H1N1 pandemic [59,60].

However, in a number of situations a model that assume an exponentially fading memory could not be the best model. To start that model assume that the largest weight is given to the current information that in many cases are not immediately available. More, current vaccine-related decisions could be influenced by memories of the individual ex-

perience of severe infection (including also siblings or friends) when one was young, or memories of severe vaccine adverse events, are likely to be important determinants of the decision to vaccinate her/his children when the individual has grown adult. Or the experience of a vaccine adverse event while vaccinating the first child, might severely amplify the risk from vaccination that is perceived by a parent, therefore decreasing the probability of the vaccination of the second child.

This sort of memory, going back to the past, is not well represented by an exponentially fading memory, but rather calls for a humped memory distribution with a peak in the past, such as the Acquisition-Fading Kernel [51,61], which is an extension of the strong Erlang Kernel [51,62].

As a consequence, in this section, we briefly investigate the deterministic impact of the above-mentioned two memory models.

This section is complemented by two sections in the appendix where we report in detail some extensive numerical simulations.

4.1. Exponentially fading kernel

The second type of kernel we consider in this work is the exponentially fading kernel

$$W_v(s) = ae^{-as}$$

This kernel, well known in mathematical physics nd biomathematics [62,63] was introduced in Behavioral Epidemiology in the work [44]. In the epidemiological context it models scenarios where agents give the maximum weight to current information and an exponentially decaying weight to past information [4,44].

Adopting standard methods of finite-dimension reduction of the theory of delay-differential systems in case of exponentially decreasing delay kernels [63–65], in the absence of stochastic perturbations, our integro-differential system (2)-(3) reduces to the following system of ordinary differential equations:

$$x' = x(1-x)(\delta - M_v) \tag{13}$$

$$M_v' = a(x - M_v) \tag{14}$$

It is easy to show that: i) the orbits are bounded: $(x, M_v) \in [0,1]^2$; ii) a unique equilibrium point exists: $EQ = (x_e, x_e)$; ii) EQ is locally asymptotically stable: a fous if $0 < a < 4K$, and a node if $a \geq 4\ K$; iv) By applying Dulac-Bendixon theorem with $1/x(1-x)$ as integrating factor, it follows that EQ is also globally stable.

For subsequent analyses, it is useful to deep the dynamic behaviour around the stable equilibrium x_e depending on (i) the position of x_e itself, (ii) the memory length $\tau = 1/a$ and (iii) the initial conditions of the system. In the Appendix, the transitory behavior of the model (13)-(14) is illustrated.

4.2. Acquisition fading kernel (AFK)

Finally, we consider the so-called Acquisition Fading Kernel (AFK) [61], which corresponds to the sum of two exponentially distributed delays with different parameters $a_1 > 0, a_2 > 0$

$$W_v = \frac{a_1 a_2}{a_2 - a_1}(e^{-a_1\tau} - e^{-a_2\tau}),$$

whose average delay τ_m is

$$\tau_m = \frac{1}{a_1} + \frac{1}{a_2}$$

This kernel was well known in applied mathematics but without a precise name [63]. The name AFK has been introduced in [61] and it models an initial phase of acquisition of information followed by exponential decay of weight given to past information [66], which is more flexible than the exponential fading kernel where the maximum weight is given to current information, which in some cases is unavailable. Overall, the EFK and the AFK kernels are able to cope with a large amount of behavioral scenarios [4,61,66].

Again following classical methods of theory of delay differential equations [63], under this kernel the system (2)-(3) reduces to the following system of three ODEs:

$$x' = x(1-x)(\delta - M_v) \tag{15}$$

$$M_1' = a_1(x - M_1) \tag{16}$$

$$M_v' = a_2(M_1 - M_v) \tag{17}$$

It is easy to show that: i) there is a unique equilibrium point:

$$EQ = (x_e, x_e, x_e),$$

ii) the orbits are bounded; iii) if $0 < \tau_m < 1/K$ then EQ is LAS; iv) at $a_1 + a_2 = K$ a Hopf bifurcation occurs; v) if $\tau_m > 1/K$ then EQ is unstable and the system undergoes general Yabucovitch oscillations [67–69] (we recall that the Hopf is a purely local theorem). In the appendix we report a detailed numerical analysis of the model behaviour.

5. Modeling volatile opinions by means of stochastic fluctuations in presence and in the absence of 'memory'

We initially make the hypothesis that the coefficient α_1 (normalized to one) is constant, which we will relax later on. Instead, coefficients α_0 and c_0 are subject to rapid noisy perturbations

$$c_0 + \nu_c(t)$$

$$\alpha_0 + \nu_\alpha(t)$$

Letting $D\xi(t)$ denote the stochastic process $c_0 - \alpha_0$, yields the following stochastic integrodifferential model:

$$x' = x(1-x)(x_e - M_v + D\xi(t)) \tag{18}$$

$$M_v(t) = \int_0^{+\infty} W_v(\tau)x(t-\tau)d\tau \tag{19}$$

Under the assumption that both c_0 and α_0 can have large peaks and that the typical autocorrelation time [88] of $\xi(t)$ is considerably shorter than the system's typical time τ_p:

$$\tau << 1$$

Consequently, we will assume that $\xi(t)$ is a white noise, thereby resulting in the following model composed by a Stochastic Differential Equation (SDE) and by an integral equation:

$$dx = x(1-x)(x_e - M_v)dt + Dx(1-x)dB \tag{20}$$

$$M_v(t) = \int_0^{+\infty} W_v(\tau)x(t-\tau)d\tau \tag{21}$$

In the SDE (20), where B is a standard Brownian process, is a Ito SDE, which is preferable in the context of population dynamics, as evidenced by Braumann [70,71].

In the case of absence of memory, implying $W_v(\tau) = \delta(\tau)$ and $M_v(t) = x(t)$, the model (20)-(21) reduces to the following single Ito SDE:

$$dx = x(1-x)(x_e - x)dt + Dx(1-x)dB \tag{22}$$

where the drift $f(x)$ is $f(x) = x(1-x)(x_e - x)$, and the diffusion function $\sigma(x) = Dx(1-x)$. Eq. (22) is characterized by two stochastic equilibria [72,73], i.e., solutions $x(t) = x^*$ such that:

$$f(x^*) = \sigma(x^*) = 0.$$

Of course, these equilibria are $x_e^{(0)} = 0$ and $x_e^{(1)} = 1$, defining, respectively, a stochastic pure 'non-vaccinator' equilibrium (SPNVE) and a stochastic pure 'vaccinator' equilibrium (SPVE).

Also, the behaviour of SDE (22) critically depends on x_e, the internal steady-state of the underlying deterministic system (i.e., in the absence of noise), represented by the expected trajectory

$$E(dx) = x(1-x)(x_e - x)dt.$$

As such, x_e represents a key system parameter which, jointly with the volatility SDS fully determines the behaviour of (22).

In the three incoming Sections 6–8, we discuss the key properties of the SDE model (22) by showing: (i) the shape of the stationary probability density function (PDF) of x, (ii) the parametric condition on key parameters (x_e, D) ensuring that the stochastic equilibria $x_e^{(0)} = 0$ and $x_e^{(1)} = 1$ are almost surely globally attractive, (iii) the local behaviour of the SPNVE and SPVE when conditions for global attractiveness fail.

6. Noise-induced transitions: shape of the stationary transition density

The Fokker-Planck equation ruling the time evolution of the transition PDF $\rho(x,t)$ of $x(t)$ reads as follows

$$\partial_t \rho = -\partial_x\Big(x(1-x)(x_e - x)\rho\Big) + \frac{D^2}{2}\partial_{xx}\Big(x^2(1-x)^2\rho\Big) \tag{23}$$

complemented by the classical constraints $\rho(x,t) \geq 0$ and

$$\int_{0,1} \rho(x,t)dx = 1, \tag{24}$$

i.e. we are only interested in solutions of (23) that are PDFs.

Thus, provided that the constraint (24) is fulfilled, the steady-state behaviour of the vaccine uptake can be investigated by studying the properties of the steady-state density,

$$\rho_{ss}(x) = CExp\Big(-2Log(\sigma(x)) + \int_0^x 2f(u)\sigma^2(u)du\Big)$$

This yields:

$$\rho_{ss}(x) = Cx^{2\left(\frac{x_e}{D^2}-1\right)}(1-x)^{2\left(\frac{1-x_e}{D^2}-1\right)} \tag{25}$$

We preliminarily note that close to the SPNVE $x_e^{(0)}$, $\rho_{ss}(x)$ reads as follows

$$\rho_{ss}(x) \approx Cx^{2\left(\frac{x_e}{D^2}-1\right)}$$

yielding: i) if $D^2 \leq x_e$ then, close to $x = 0$, $\rho_{ss}(x)$ is increasing or constant; ii) if $x_e < D^2 < 2x_e$ then, close to $x = 0$, $\rho_{ss}(x)$ is decreasing and at $x = 0$ it has an integrable singularity; ii) if $D^2 \geq 2x_e$ then the function $\rho_{ss}(x)$ has a non–integrable singularity so that the function $\rho_{ss}(x)$ is not a PDF.

Similarly, close to the SPVE $x = 1$, $\rho_{ss}(x)$ reads as follows

$$\rho_{ss}(x) \approx C(1-x)^{2\left(\frac{1-x_e}{D^2}-1\right)}$$

yielding: i) if $D^2 \leq 1 - x_e$ then, close to $x = 1$, $\rho_{ss}(x)$ is decreasing or constant; ii) if $(1 - x_e) < D^2 < 2(1 - x_e)$ then $\rho_{ss}(x)$ is increasing and at $x = 1$ it has an integrable singularity; ii) if $D^2 \geq 2(1 - x_e)$ then the function $\rho_{ss}(x)$ has a non–integrable singularity so that $\rho_{ss}(x)$ is not a PDF.

As a consequence, in this section we will restrict our study to the cases where $\rho_{ss}(x)$ is a PDF, i.e.

$$D^2 < 2\min(x_e, 1 - x_e)$$

The behaviour of the stationary solution is governed by the sign of

$$\rho'_{ss}(x) = \rho_{ss}(x)2\left(\left(\frac{x_e}{D^2} - 1\right)\frac{1}{x} - \left(\frac{1-x_e}{D^2} - 1\right)\frac{1}{1-x}\right) \tag{26}$$

We have the following four cases:

1. if

   $$D^2 < \min(x_e, (1 - x_e))$$

   then the density is unimodal, with a maximum at:

   $$x_* = \frac{x_e - D^2}{1 - 2D^2};$$

2. if

   $$\max(x_e, (1 - x_e)) < D^2 < \min\left(2x_e, 2(1 - x_e)\right)$$

   then, the density is *bimodal* and horn–shaped, with its anti-model (minimum) at $x = x_*$. The two modes are at $x = 0$ and $x = 1$ and they are infinite;

3. if

   $$x_e < D^2 < \min(2x_e, 1 - x_e)$$

   then $\rho_{ss}(x)$ is decreasing with an infinite mode at $x = 0$;

4. if

   $$(1 - x_e) < D^2 < \min(2(1 - x_e), x_e)$$

   then $\rho_{ss}(x)$ is increasing with an infinite mode at $x = 1$.

Summing up, in the parametric space (x_e, D^2) we have detected four regions identifying sharply different behaviours of the steady-state density. Therefore, passing from one region to another one, the system undergoes a Noise-Induced Transition [74].

Remark *If (x_e, D^2) is such that $D^2 < 2Min(x_e, 1 - x_e)$, then SDE (22) defines a bounded stochastic process.*

7. The global stochastic steady-state behaviour

In this section, we explore the conditions under which the stochastic equilibria $x = 0$ and $x = 1$ i.e., the SPNVE and the SPVE, exhibit a globally attractive property almost surely (a.s.). To this aim, it is convenient to define the following variable transformation: $x = 1/(1 + e^{-z})$, i.e.

$$z = F(x) = \ln\left(\frac{x}{1-x}\right), \tag{27}$$

where the case $x = 0$ corresponds to the limit $z \to -\infty$ and the case $x = 1$ corresponds to the limit $z \to +\infty$.

Applying the Ito's formula

$$dz = \left(F'(x)f(x) + \frac{\sigma^2(x)}{2}F''(x)\right)dt + \sigma(x)F'(x)dB$$

yields the following SDE:

$$dz = \left(\left(x_e - \frac{D^2}{2}\right) + \left(D^2 - 1\right)\frac{1}{1+e^{-z}}\right)dt + DdB \tag{28}$$

whose general solution reads as follows

$$z(t) = z(0) + \left(x_e - \frac{D^2}{2}\right)t + \left(D^2 - 1\right)\int_0^t \frac{1}{1+e^{-z(s)}}ds + DB(t). \tag{29}$$

Importantly, it holds the following estimate for the integrals appearing in (29) :

$$0 < \int_0^t \frac{1}{1+e^{-z(s)}}ds < t.$$

We have:
i) for $D^2 > 1$ it is

$$z(0) + \left(x_e - \frac{D^2}{2}\right)t + DB(t) < z < \left(\frac{D^2}{2} - (1 - x_e)\right)t + DB(t)$$

ii) for $D^2 < 1$ it is

$$\left(\frac{D^2}{2} - (1 - x_e)\right)t + DB(t) < z < z(0) + \left(x_e - \frac{D^2}{2}\right)t + DB(t)$$

iii) for $D^2 = 1$ it is

$$z(t) = z(0) + \left(x_e - \frac{1}{2}\right)t + DB(t). \tag{30}$$

Hence, by considering the steady-state vaccine uptake x_e (with the constraint $x_e \neq 1/2$) and the square of the volatility, D^2, as key parameters, simple algebraic inequalities and the properties of the Wiener process, allow to identify two distinct regions. Within the first region, which is defined by

$$x_e < \frac{1}{2} \text{ AND } 2x_e < D^2 < 2(1 - x_e)$$

it is $z(t) \to -\infty$ a.s. implying

$$x(t) \to 0^+ \text{ a.s.}$$

That is to say, when the steady-state vaccine uptake rate (in the absence of noise) falls below 50%, stochastic fluctuations due to irrational

behaviour potentially make, within the above-specified range of values for D^2, the SPNVE (as) globally attractive i.e., the vaccinator strategy goes extinct for all initial vaccine uptake rates.

Within the second region, which is defined by

$$x_e > \frac{1}{2} \text{ AND } 2(1-x_e) < D^2 < 2x_e,$$

it is $z(t) \to +\infty$ a.s. implying

$$x(t) \to 1^- \text{ a.s.}$$

In other words, if the steady-state vaccination rate (in the absence of noise) surpasses 0.5, there exists a range of values for D within which stochastic fluctuations make the SPVE globally attractive. That is, all individuals opt to vaccinate their children.

8. The local stochastic stability and the onset of stochastic bistability

The scenario where the noise is large and out of the two above-specified windows, i.e. the parametric region defined by the inequality:

$$D^2 > Max\left(2x_e, 2(1-x_e)\right),$$

is interesting.

In order to analytically study the implications of the above double inequality, one needs to investigate the local stochastic stability of the two equilibrium points of the SDE (22) by means of Khasminski theory [72,73]. This states that the equilibrium point $x = 0$ of a SDE having the form of (22) is stochastically stable provided that it exists the following Ljapunov functional:

$$V(X) = \int_0^x ds Exp\left(-\int_x \frac{2f(u)}{\sigma^2(u)}\right)$$

The functional $V(X)$ for the equilibrium $x = 0$ of (22) reads as follows

$$V(x) = C\int_0^x ds\left(\frac{1}{s^{2x_e/D^2}}\frac{1}{(1-s)^{2(1-x_e)/D^2}}\right).$$

This means that if $D^2 > 2x_e$ then the equilibrium $x = 0$ is locally stochastically stable. To study the stochastic stability of the equilibrium $x = 1$ of (22) we set $x = 1 - y$, so that the problem in study is equivalent to study the stochastic stability of the equilibrium $y = 0$ of the following SDE:

$$dy = y(1-y)(1-x_e-y) - Dy(1-y)dB,$$

which it is associated the functional

$$V(y) = Q\int_0^y du\left(\frac{1}{u^{2(1-x_e)/D^2}}\frac{1}{(1-u)^{2x_e/D^2}}\right).$$

As a consequence, the local stability condition for $y = 0$ (i.e. for $x = 1$) is $D^2 > 2(1-x_e)$. It follows the interesting fact that there is an overlap between the two stochastic stability regions and the overlap is the above-mentioned region:

$$D^2 > Max\left(2x_e, 2(1-x_e)\right)$$

In such a region the behaviour of the system can be defined as stochastically bistable, thus depending on the initial condition $x(0)$ the system is attracted by one or the other stochastic attractors.

In other words, although our system is non–spatial, it experiences transitions that are very remindful of phase transitions [75]. Indeed, as pointed out by Shiino [76] non-uniqueness of the asymptotic attractors in a dynamical system is a key landmark of phase transitions.

9. Extensive numerical simulations

In this section, we numerically study mainly the effects of the noise 'strength' D.

We used an Additive Splitting approach [77]. We used for the deterministic part the 4th-order Runge Kutta method [89], and for the stochastic part the Euler-Maruyama algorithm.[90] In this way, we were able to minimize the error on the deterministic part leaving as only source of error the stochastic component. Following [78], our method is characterized by a self-regulating step along the boundary to keep the solution in the domain.

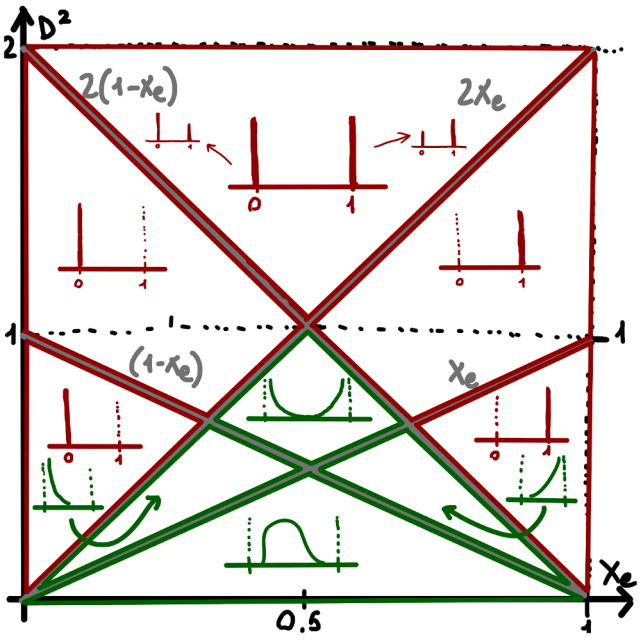

Fig. 3. Absence of delay.: stochastic NIT bifurcation in parametric space (x_e, D).

The step size was 0.01 time units and the simulation length for the steady-state analysis was of 2250 time units. All stationary distributions ρ_{SS} were obtained considering the final values of 10,000 simulated trajectories (unless a particular time label is specified). For the 3D plots and the colormeshes, we simply used the same number of simulations on a grid of 50x50 bins. For simplicity, we have not normalized the simulated probability distributions.

9.1. No delay case

Although we have analytically studied the unlagged case of eq. (22)), we numerically investigated it (22) for three reasons: i) to validate the analytical predictions; ii) to assess the transitory dynamics; iii) to develop a numerical benchmark to assess the effects of time delays.

In Fig. 3, we show a theoretical sketch of the NIT scenario in the parametric space (x_e, D^2), with the analytical stationary distribution. The corresponding numerical NIT plot matrix, shown in Fig. 4, fully validates the theoretical results.

9.2. Exponentially fading kernel

Moving to the scenario with both the exponentially fading kernel (EFK) and the opinion stochastic fluctuations, we expect a relevant role of the average delay τ. For small delays (say, $\tau < 1$) we can speculate that the impact could be limited producing situations similar to the undelayed case (Fig. 4). For larger τs, the amount of information will be more resilient to evolve. Therefore, we can imagine that a larger τ amplifies the influence of the noise on the system behaviour. Thus, we can predict that the bimodal behaviours and the two lateral ones will 'propagate' to the lower part of the theoretical figure. The above guess is confirmed: for $\tau \leq 1$, we did not notice changes w.r.t. the no-delay case, while for $\tau > 1$ some differences start to appear, as shown by the plot matrix for $\tau = 10$ (Fig. 5). It is noticeable the different types of behaviour appearing almost a row before the no delay case. Thus, for large delays

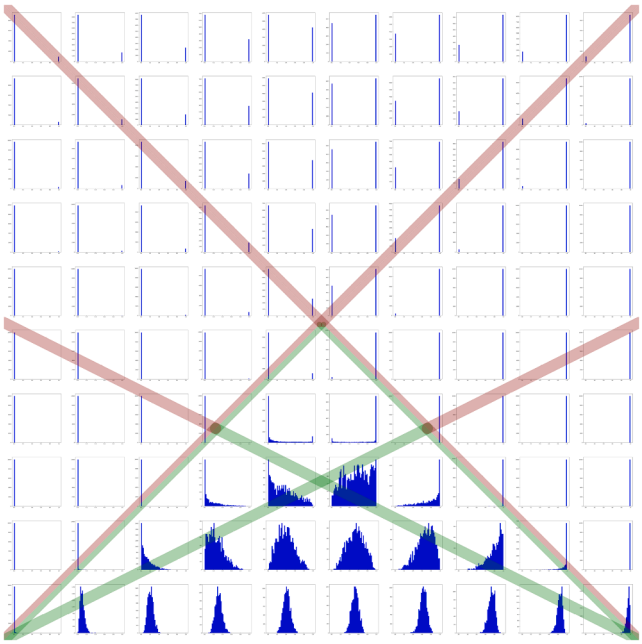

Fig. 4. Absence of delay: Plot matrix of the probability distributions obtained via simulations. Horizontal axis: $x_e \in [0, 1]$; vertical axis $D^2 \in (0, 2)$. In gray are reported the 4 reference lines: x_e, $(1 - x_e)$, $2x_e$ and $2(1 - x_e)$.

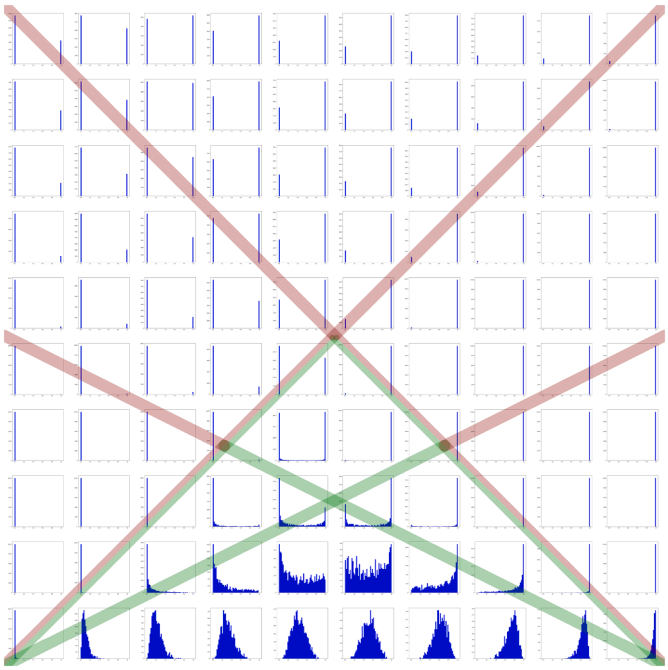

Fig. 5. EF Kernel: plot matrix of the simulated PDF for the EFK model with $\tau = 10$. Horizontal axis: $x_e \in (0, 1)$; Vertical axis: $D^2 \in (0, 2)$. In gray there are reported the 4 reference lines: x_e, $(1 - x_e)$, $2x_e$ and $2(1 - x_e)$.

the noise can characterize more sharply the mode of the system, leading to a strong probabilistic convergence towards around one of the two extreme of the domain or both of them.

9.2.1. *Projections of the parameters space*

We now deepen our focus on the capacity of D to influence the behaviour for different values of x_e and τ. Fig. 6 shows the steady-state PDF matrix plot over the parametric space (D, x_e) for the two different levels $\tau = 2$ (left panel) and $\tau = 10$ (right panel). In the left panel ($\tau = 2$),

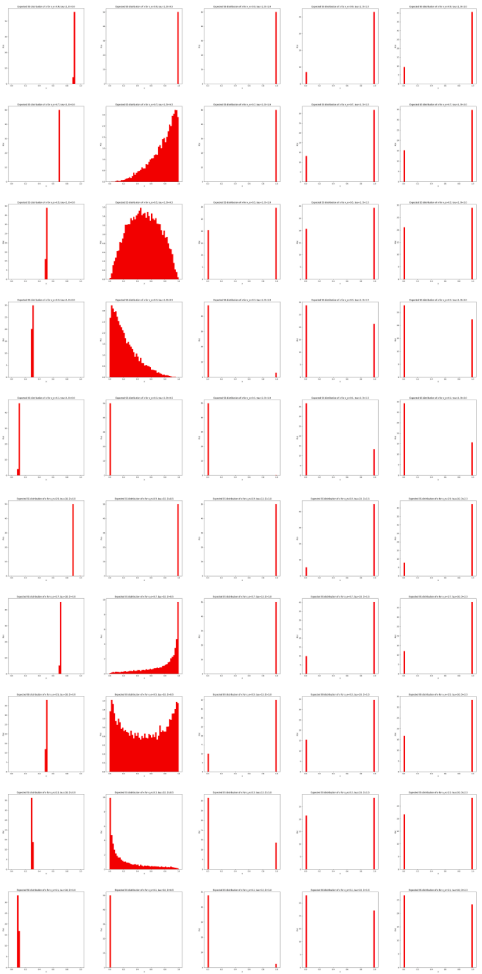

Fig. 6. EF Kernel: plot matrices of simulated stationary PDFs in the parametric space (D, x_e). Left panel: $\tau = 2$; Right panel: $\tau = 10$. Vertical axis: $D \in [0, 2]$; Vertical axis: $x_e \in (0, 1)$.

distributions reveal notable patterns. In the first column, a nearly Dirac delta centered at x_e appears, expected for $D = 0$. In other columns, small noise diffuses trajectories; eventually, a transition occurs from an extreme peak to a bimodal and then unimodal distribution at the opposite border. Overall, the system exhibits low resilience to noise.

In the right panel (where $\tau = 10$). Focusing on the differences (see Fig. 5), we note that a higher τ advances the behaviour for the same D. The unimodal distribution becomes steeper and focused near the attractors, while in the central row it shifts to a bimodal form at the domain extremes, yet with significant central values. For higher D, the two panels are similar. Note that, in both cases, at $x_e = 0.5$ we do not have a symmetric situation but is more shifted towards the upper extreme. This is probably due to our simulation approach -assuming $M_v(0) = 0$ and choosing x_0 uniformly in $(0, 1)$- which introduces asymmetry, though other simulation effects might also contribute.

Comparing the two panels, we note that in one case, the increase of τ induces a noise-induced transitions: an unimodal PDF for $\tau = 2$ becomes a bimodal one for $\tau = 10$. Fig. 7 shows the stationary PDFs matrix plot for the parametric space (D, τ). Its left panel is such that $x_e = 0.3$, whereas its right panel is such that $x_e = 0.5$

Let us look at the left part of Fig. 7 where $x_e = 0.3$. With increasing τ, the distribution for $D > 0$ becomes more focused on its attractor (second column), and since τ also suppresses behaviour along D^2, we see the same pattern for lower D as τ grows. In the third column, the distribution initially shifts toward 0, but as τ increases, the central bimodal

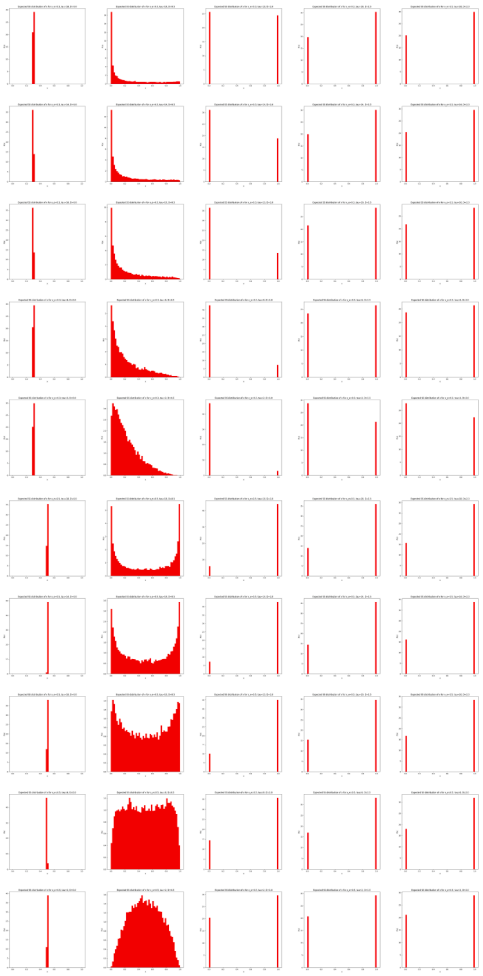

Fig. 7. EF Kernel: plot matrices of simulated stationary PDFs in the parametric space (D, τ). Left panel: $x_e = 0.3$; Right panel: $x_e = 0.5$. Horizontal axis $D \in [0, 2]$; vertical axis $\tau \in [2, 18]$.

region diminishes and the distribution becomes increasingly bimodal. In the final columns, the symmetric case appears at a certain τ, after which the symmetry between the two peaks is reversed and broken.

In the right panel of Fig. 7, where $x_e = 0.5$. In the two left columns of the plot matrix, the central distribution is evident. As τ increases, the unimodal distribution becomes bimodal, passing through an intermediate phase with nearly uniform probability. In the other columns, row differences are minimal. For $x_e > 0.5$, the situation is similar but mirrored.

Comparing the two panels, we note immediately that in the first column all the PDFs are deeply transformed when $x_e = 1/2$: four of the five become bimodal and the last one, which was decreasing, becomes unimodal. Also, the other distributions are deeply affected by the change of values of x_e.

9.3. Noise-induced quasi-regular oscillations

We now explore some specific realization of the stochastic process, by analyzing some trajectories x vs. t and the phase trajectories (x, M_v). Looking to the plot matrices, we have selected two interesting configurations:

- $\tau = 2$, $D = 0.5$ (low τ, medium D)
- $\tau = 18$, $D = 0.5$ (large τ, medium D)

In all simulations we adopt $x_e = 0.5$, since in this way system is more 'free to oscillate', and the initial condition is $(x, M_v) = (0.7, 0.0)$.

Let us start from the first one ($\tau = 2$, Fig. 8). The left panel of Fig. 8 shows that $x(t)$ stochastically oscillates around x_e, consistently with the Fig. 7. More interesting, the right panel of 8 shows that the phase plot (x, M_v) has an 'almond-like' shape. This is due to the presence of an important correlation between x and M_v: large (small) values of $x(t)$ tends to correspond to large (small) values of $M_v(t)$.

The second configuration ($\tau = 18$) shows the trajectories reported in Fig. 9. Now, the increase of the characteristic memory time up to $\tau = 18$ has a major effect: the induction of noise-induced oscillations characterized by prolonged staying close to low values. In other words, often, the system, due to the interplay between the deterministic damped oscillations and the flat spectral content of the white noise perturbation, sets in a behavior of *quasi-regular* stochastic oscillations. If, instead of considering white noise perturbation, we consider periodic perturbations of period close to the quasi-period of the damped oscillations of the linearized system (w.r.t its equilibrium point) we obtain subharmonic resonances: the systems sets in a periodic or, more interestingly (see Fig. 10), quasiperiodic oscillations with amplitude quite larger than the one of the perturbation. As for the overall 'shape' of these oscillations, we note that the x spends more time at the two extremes of the domain. Thus, for bigger τs, the delay is able to produce more important oscillations, diminishing but not eliminating the influence of the noise on the system, as shown in the right part of the Figure. The fact that during these noise-induced oscillations the vaccine propensity $x(t)$ remains for relatively long intervals at very low values has an interesting implication, since in this way there is a substantive risk of onset of large epidemics due to disease importation when $x(t)$ is very low. There is still some correlation between the two values, although the huge τ contains the values of M_v.

Nonetheless, the oscillatory behaviour requires also particular values of D. In fact, it seems to appear around 0.4-0.5. When it overlaps values such 0.8-0.9, the system will have too wide oscillations and it will be captured by one of the two bounds. Otherwise, the phenomena seems to not appear. Moreover, especially for slightly smaller τs (such as $\tau \in [10, 15]$), the oscillatory behaviour is not present in every repetition. Probably a sort of resonance due to specific transient situations is necessary in this cases.

It is of interest to briefly investigate the Fourier frequency spectrum of the above scenarios. To start, we have computed the Fourier transform of the time series of scenarios shown in Figs. 9 and 8. The Fourier power spectrum of the average value of the time series $x(t)$ in Fig. 9 is shown in the left panel of Fig. 11. There is clearly a large peak near $0.01\,Hz$, which fully justify our claim of noise-induced oscillations (aka quasi-cycles). For comparison, we also performed the Fourier transform of the average value of the non oscillating time series $x(t)$ of Fig. 8: the Fourier transform presents no special peaks.

However, as said before, sometimes the noise-induced oscillations does not clearly emerge. This is usually more frequent for lower τ but it can also happen occasionally for larger values of these parameters, for example at the considered $\tau = 18$. In this case, the power spectrum loses the above stressed large peaks (see right panel of Fig. 12), although it has number of 'not so small peaks' around some multiples of 0.01, which harmonically explains the mixed behavior observed in the time series shown in the left panel of Fig. 12. In other words, the noise induce a sort of 'noisy quasi-periodic behavior'. Here the considered same time window and simulative parameters, but the quasi-periodic regime do not appear. Certainly, there is also a plethora of intermediate cases which presents 'dirty' oscillations resulting in 'in-between cases'.

9.4. Acquisition-fading kernel

Here we will investigate the impact of the Acquisition-Fading Kernel (AFK) on the vaccination imitation dynamics affected by stochastic opinion fluctuations.

We will consider different scenarios due to the increased number of variables and parameters. In absence of stochastic perturbations, at

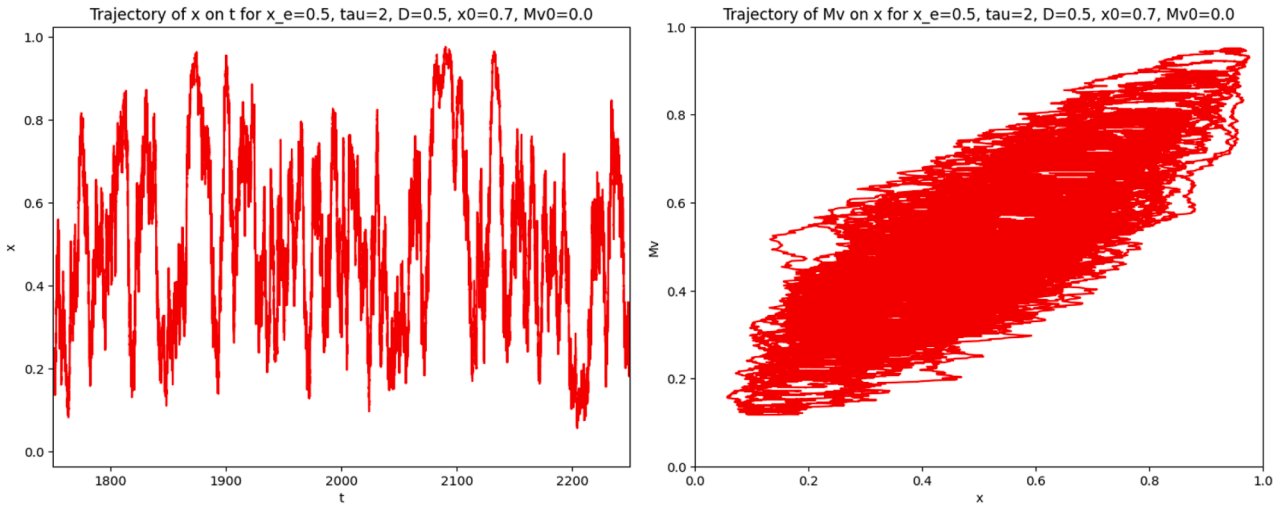

Fig. 8. EF Kernel: realizations of the stochastic process for low $\tau = 2$, medium $D = 0.5$. Left panel x v t; Right panel: phase plot (x, M_v) Parameters: $x_e = 0.5$, $x(0) = 0.7$, $M_v(0) = 0.0$.

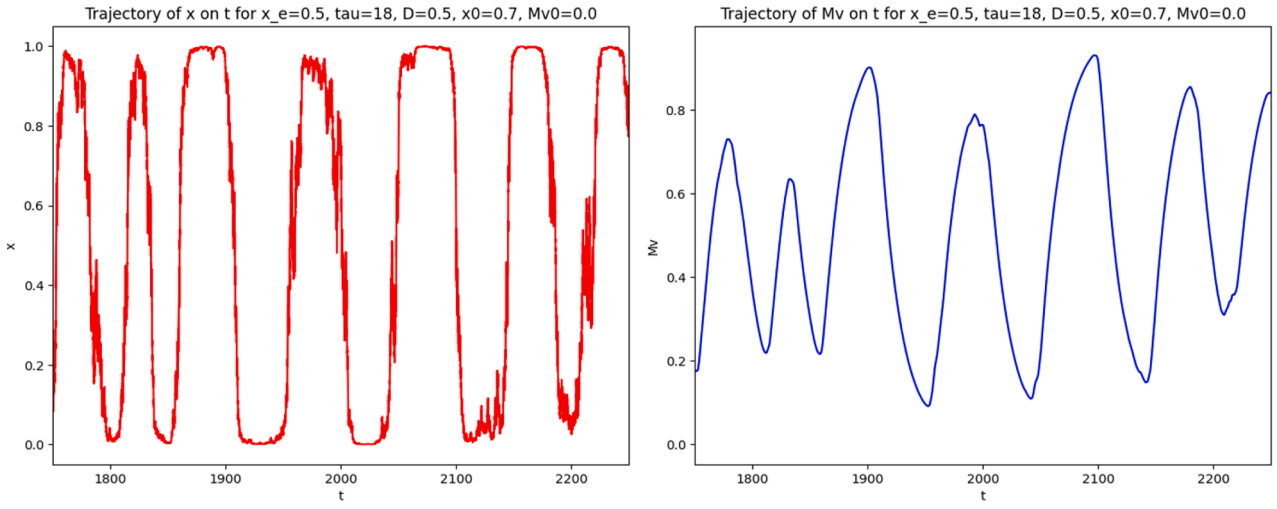

Fig. 9. Noise-induced quasi-regular oscillations. Plots of the trajectory on projections (t, x) (left) at SS and (x, M_v) (right) for the EFK model in case of large delay. These results are obtained for $x_e = 0.5$, $\tau = 18$, $D = 0.5$, $x_0 = 0.7$, $M_v(0) = 0.0$. The left plot focuses on the interval $t \in [2000, 2250]$ for an improved readability.

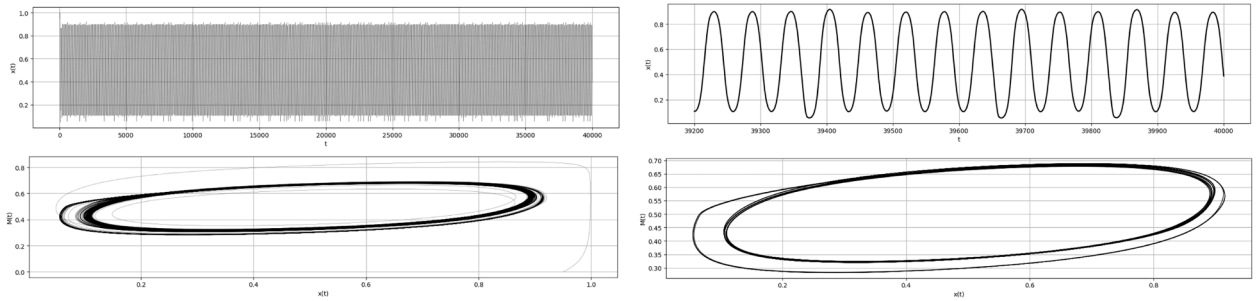

Fig. 10. Quasi-periodic resonant oscillations generated by periodic perturbations. Upper-left panel: time series of $x(t)$ for the whole simulation interval; Upper-right panel: zoom of the time series of $x(t)$. Lower-left panel: phase plot (x, M); lower-right panel: zoom of the phase plot. Parameters: $A = 1$, $T = 58$ (very close to the pseudo-period of the damped oscillations at the equilibrium).

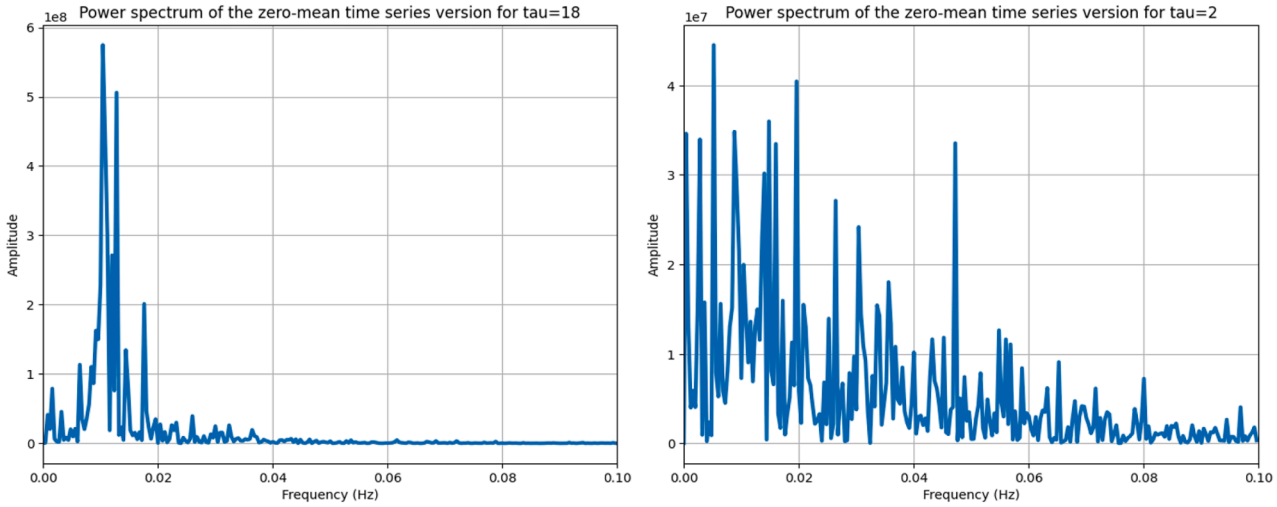

Fig. 11. Fourier transforms of the averaged values of time series of Fig. 9 (left) and the time series of Fig. 8. We have considered the showed time window to compute these transforms.

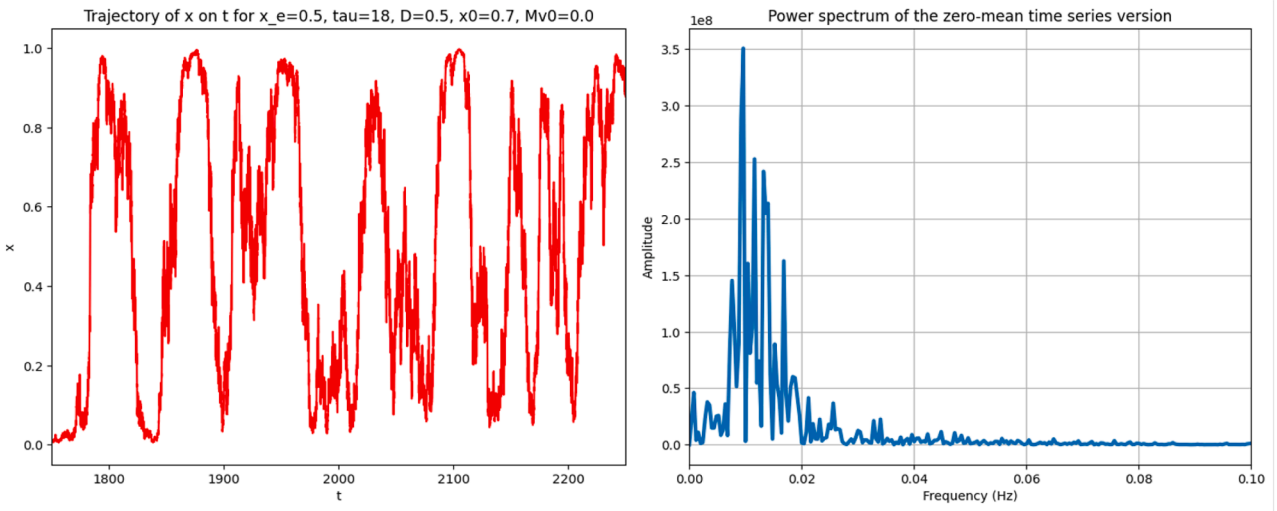

Fig. 12. Plots of the power spectrum and its time series for $x_e = 0.5$, $\tau = 18$ and $D = 0.5$. In this repetition, besides the same configuration of Fig. 9, the oscillations do not fully appear.

variance with the EFK model, we know that for $\tau_m > K$ the underlying deterministic system presents a limit cycle or other oscillating solutions via a Hopf bifurcation (which, with abuse of terminology, we will term 'Hopf cycles') from the steady-state x_e. As seen previously for the EFK, the noise can reinforce and induce a bistable regime around the two limits of the domain. Therefore, we expect that these Hopf cyclic regimes will enhance this bimodal tendency.

As per the plot matrix of the distributions in dependence of (x_e, D^2), we note that cases where $\tau_m \leq 1$ did not show differences with the no delay and the EFK scenarios. In Fig. 13, we report the matrix plot for $\tau_1 = \tau_2 = 10.0$, implying $\tau_m = 20.0$, so that for some central configurations the Hopf cycle exist. In its first row from the bottom, we observe that: i) in its rightest and leftest parts the PDFs are similar to the EFK matrix plot; ii) in its central part the PDFs are bimodal, due to the occurrence of Hopf cycle in the unperturbed model; iii) the small noise reinforces the bimodality moving the extremes of the cycle towards 0 and 1.

9.4.1. *Analysis of the evolution of the distributions: (x, M_v)*

We now analyze how D affects the PDFs, in particular when Hopf cycles occur in absence of noise.

First, we look at (x, M_v) projections of PDF in a 'reference case' where $x_e = 0.6$, $\tau_1 = 14.0$ and $\tau_2 = 8.0$. In the absence of noise and assuming uniformly distributed initial x and $M_1 = M_v = 0$, the marginalized stationary PDF is a product of Dirac deltas $\delta(x - \hat{x}(t))\delta(M_v - \widehat{M}_v(t))$ (Fig. 14), where $(\hat{x}(t), \widehat{M}_v(t))$ is the projection of the Hopf cycle onto (x, M_v). We can notice that the symbolic representation of the PDF (which is the product of two Dirac deltas) moves, roughly speaking, like a 'comet'.

By increasing the noise D up to the small value 0.1 one would expect that the small noise should produce a small perturbation of the trajectories, and, consequently, a small Gauss-like diffusion effect on the "comet". Instead, we observed that the fluctuations are distributed around the whole orbit $(\hat{x}(t), \widehat{M}_v(t))$, see Fig. 15 where a 'volcano effect' is visible. In particular: i) the PDF tends to stay most of the time close to $x = 0$ and, mainly, to $x = 1$; ii) the spread of the PDF is variable, with a

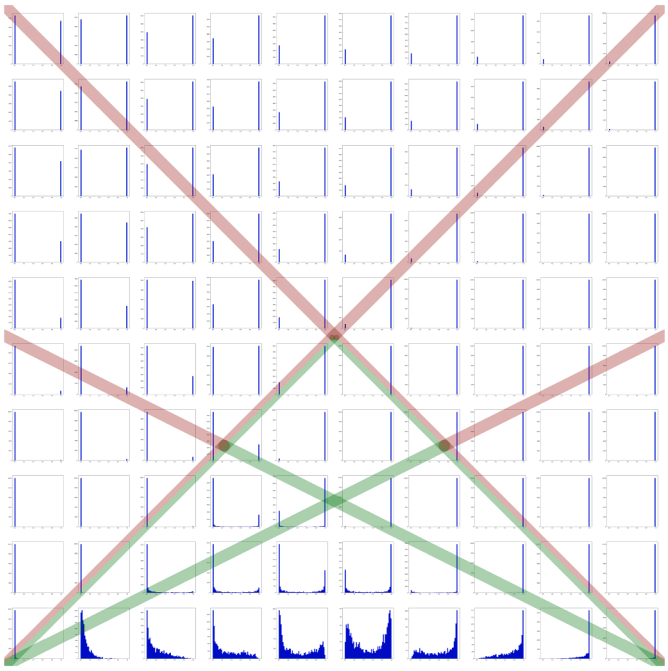

Fig. 13. AF Kernel in the presence of noise: plot matrix of the numerical steady-state PDF with $\tau_1 = \tau_2 = 10$. Horizontal axis: $x_e \in (0,1)$; Vertical axis: $D^2 \in (0,2)$. In gray there are reported the 4 reference lines: x_e, $(1-x_e)$, $2x_e$ and $2(1-x_e)$.

larger spread when x is close to 0 and a smaller spread when x is close to 1.

Increasing D up to $D = 0.3$ (Fig. 16), the 'volcano shape' disappears and the distribution is pushed towards the domain limits of x. We repeated the simulation for $(\tau_1, \tau_2) = (24, 10)$ and keeping $D = 0.1$ (Fig. 17). We note an anulus-like region where the values of the PDF are close to zero and an oscillating flux of probability between the two extremes of the cycle.

Finally, for $D = 0.3$ the synergy of the Hopf cycle is such that the PDF is a Dirac centered $(1, 1)$ (figure omitted).

Now we test a scenario where in the deterministic system no Hopf cycle occur: $(\tau_1, \tau_2) = (3.5, 2.0)$. In the left panel of Fig. 18 we show the stationary time-constant PDF in absence of noise. The situation here is straightforward since in the deterministic system the point (0.6,0.6,0.6) is globally attractive.

Increasing the noise to $D = 0.1$, we can guess that with a such small noise the system will be not able, according to our theoretically results in Fig. 3, to have a NIT. Numerical simulations confirm the intuition, see the central panel of Fig. 18. Increasing D up to 0.3 the diffusion region around the equilibrium is remarkably enlarged, see right panel of Fig. 18, and almost reach the upper limit of the (0,1) domain. The 3D plot is not smooth, due the relatively low number of employed simulations ($N_{sim} = 10000$).

9.4.2. Analysis of the evolution of the distributions: (x, t)

Here we study the dynamics of the distribution along x only. We start from the reference configuration of the previous section: $(\tau_1, \tau_2) = (14.0, 8.0)$. To start, we compare the cases $D = 0.0$ (left panel Fig. 19) and $D = 0.05$. In the left panel, corresponding to $D = 0$, we observe that the PDF is of Dirac delta type $\delta\left(x - \hat{x}(t)\right)$ where $\hat{x}(t)$ is the x component of the Hopf limit cycle, thus "comet"-like. Moreover, due to asyncronization caused by the uniform distribution of the initial condition $x(0)$, the PDF seems more diffuse in the intermediate position while at the extremes is denser.

In the right panel, corresponding to $D = 0.05$, we observe that the PDF alternates in time with its bulk of probability from values close to 0 to values close to 1, with higher and 'slim' peaks close to $x = 1$, whereas close to $x = 0$ the peaks are smaller and more diffuse. Increasing the noise amplitude to $D = 0.1$ induce the almost stationarity of the PDF, see the left panel of Fig. 20, The PDF is bimodal in $\{0, 1\}$, and the antimode is only moderately low, and it is not located at x_e. The peak at 1 is higher than the other since $x_e = 0.6 > 0.5$.

For higher D (such as $D = 0.5$, shown in the right panel of Fig. 20) the bulk of the PDF is close to 0 and the peaks are close to two Dirac deltas with different amplitudes.

As per the impact of the delays, by taking strong delays ($\tau_1 = 24.0$ and $\tau_2 = 10.0$) and $D = 0.0$, there are no real behavioural differences w.r.t. the previous couple of delays. The only changes are the wider amplitude of the Hopf cycle and the increased period of the oscillations. Moving to $D = 0.05$ (left panel of Fig. 21), the situation is a little more interesting, as we can notice in the . Indeed, the valley of the PDF is very flat and close to 0 and the PDF is more focused towards the limit, due to the synergy between the small noise and the Hopf cycle.

Increasing D up to 0.1, as shown in right panel of Fig. 21, we obtained a time-varying steady stated PDF Again, the upper extreme is the dominant peak. Moreover, the PDF cyclically diffuses and 'contracts'. These numerical findings suggest that: i) for low τ also for $D = 0.1$ the steady state PDF is constant while here it is cyclical and has an extreme profile; ii) the role of large τs to "anticipate", noise speaking, the transition to a bimodal behaviour but, this time, these delays cause also the onset of cyclic steady state PDF.

Moving back to $(\tau_1, \tau_2) = (3.5, 2.0)$, since for these values of delays in the deterministic model there is an attracting equilibrium it follows that $D = 0.0$ the steady state marginalized PDF of x is $\delta(x - x_e)$. Increasing the noise strenght to $D = 0.05$ we observe a stationary PDF peaked at x_e with a relatively small variance, as shown in the left panel of Fig. 22.

Increasing D we observe a transition phenomenon. It exists a threshold D^* such that: i) for $D < D^*$ the variance is increasing but the mode remains at x_e;: ii) for $D > D^*$ the PDF remains unimodal but its mode, as we can notice in the plot for $D = 0.5$ in the right panel of Fig. 22. Thus, it appears clear an effect of the interplay noise strength-delays: the larger are the delays, the lesser is noise strength needed to onset a NIT to a bimodal behaviour.

To end this analysis of the impact of the AFK on the proposed vaccine stochastic IGD, we may say that the role of the delays is central. Unfortunately, the results are not very reassuring under the pH viewpoint: in most cases the interplay delays-noise strenght induces a bimodal behaviour, often time-varying. The desirable target of a constant stationary PDF unimodal with mode at (or close to) $x = 1$ is difficult to reach.

10. Impact of bounded and fat tailed coloured noises

If the stochastic perturbations affecting the IGD are not fast but slow, with autocorrelation times comparable to characteristic evolution time of the IGDE, then the SDE has to be replaced by a random differential equation:

$$x' = x(1-x)\Big(x_e - x + y(t)\Big) \tag{31}$$

where $y(t)$ is a coloured stochastic process.

Here we consider noises generated by the so called Stariolo-Tsallis-Borland family of SDEs [79]:

$$dy = -\frac{1}{\tau} f(y)dt + \sqrt{\frac{2}{\tau}}\, dB \tag{32}$$

where $f(y)$ is a suitable smooth function defined for $y \in (-\infty, \infty)$ and such that i) $yf(y) > 0$ and ii) $f(-y) = -f(y)$.

In particular, we consider scenarios where exogenous events that influence vaccine sentiment are often fat-tailed and can be described by a power law. Tweets, for instance, follow power laws [80] because

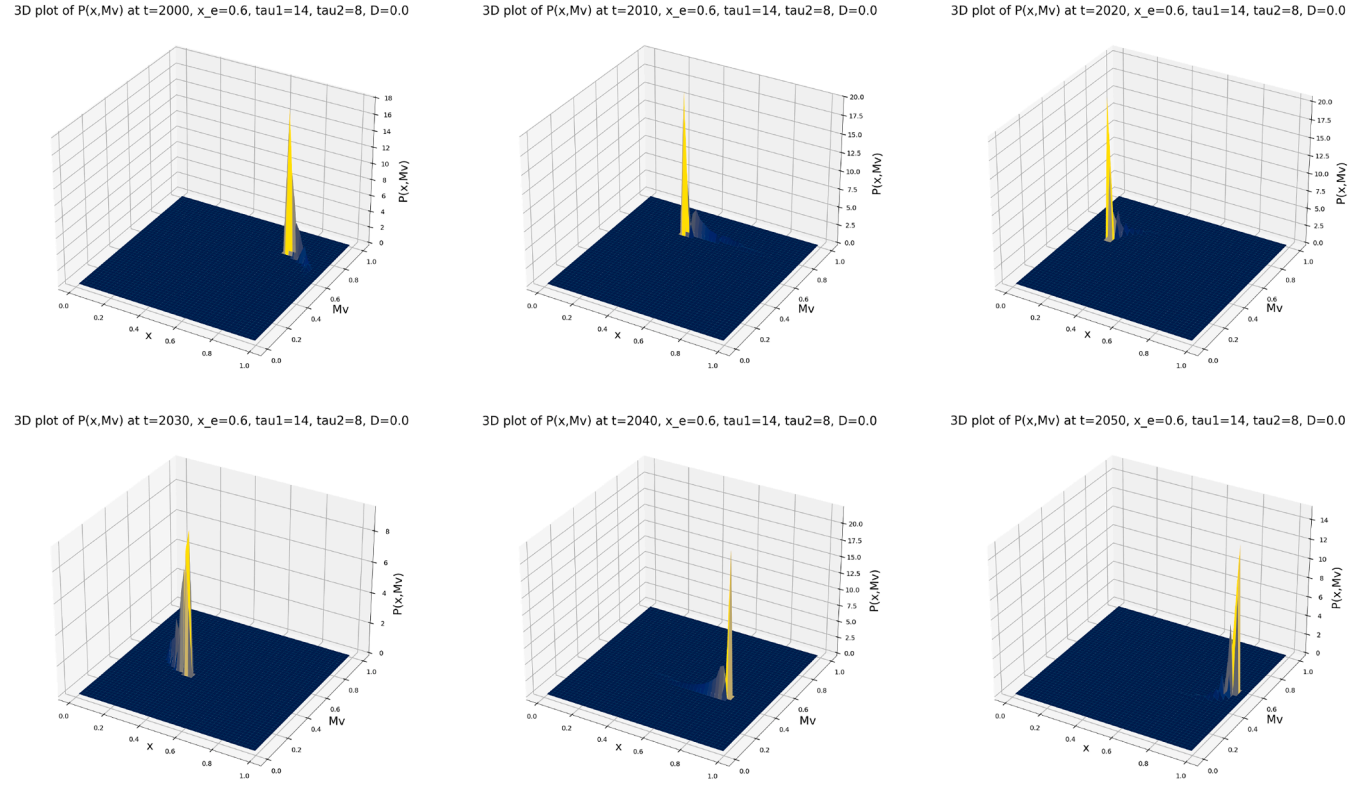

Fig. 14. Hopf cycles in the absence of noise: screenshots of a symbolic representation of the 3D plots of the PDF $\delta(x-\widehat{x}(t))\delta(M_v-\widehat{M}_v(t))$ for the case $x_e=0.6$, $\tau_1=14.0$, $\tau_2=8.0$. Upper left panel: $t=2000$; Upper Central panel: $t=2010$; Upper right panel: $t=2020$; Lower left panel: $t=2030$; Lower central panel: $t=2040$; Lower right panel: $t=2050$.

individuals are interested/concerned about dramatic events, or what celebrities say on the topic. For instance, in climate change during the past decade, the biggest spike in tweets occurred during the Pope's encyclical address, and Leonardo DiCaprio's Oscar acceptance speech. Thus, we investigate the simulations scenarios where the noise has a power law. As shown in the appendix, to simulate a stochastic process whose steady-state distribution is known and equal, say, to a function $\rho_s(y)$, the function $f(y)$ in the SDEs family (32) must be as follows

$$f(y)=\frac{\frac{d}{y}\rho_s(y)}{\rho_s(y)} \tag{33}$$

Thus, if we are assuming that the noise has a Cauchy distribution:

$$\rho_s(y)=\frac{1}{\pi B}\frac{1}{1+\left(\frac{y}{B}\right)^2} \tag{34}$$

then the generating SDE is such that:

$$f(y)=\frac{2y}{B^2+y^2} \tag{35}$$

Note that for $|y| << B$, this process is close to an OU process. This Cauchy distributed stochastic process, at the best of our knowledge, has never been previously discussed, thus in the appendix its properties are discussed in depth.

10.1. Impact of cauchy noise on the AFK system

Since for the AFK case there are numerous parameters and many scenarios are possible, we will substitute the white noise with the Cauchy noise only for the scenario where Hopf cycles can appear. For the simulations, we are warming-up the noise for $T=100$ time units.

Under various parametric values, we always obtained the bifurcation regime observed in the white noise case for very large Ds. Indeed, the Cauchy noise is heavy-tailed with divergent variance, thus, after a sufficiently long time, a trajectory of noise will certainly attain very large values and the trajectories of process x will eventually fall into one of the two bounds.

Obviously, the parameters can slow down this divergence process. Using a very small B will produce a zero-peaked noise distribution, thus the effect of the noise will be initially small but in a very long run the bifurcate distribution will be reached. An example of this transient dynamic is reported in Fig. 23. In Fig. 23, we set $\theta=21.31$, i.e. about the time needed in the deterministic scenario to pass from $x_0=1$ to the value 0.5. The only difference between the two panels is the length of the trajectory: on the left panel 1000 time units; on the right panel 10,000 time units. The right panel histogram has at its extreme values taller peaks. This stress the presence of a "flow" of probability towards the bounds. Moreover, the divergence speed is slower than in the deterministic case. Thus the noise produces a protracted and, in terms of policymaking, relevant transient phase.

11. Effects of perturbations affecting α_1

Here, we investigate the case where also α_1 is a left bounded stochastic process with mean equal to one:

$\alpha_1(t)\geq 0,\ \langle\alpha_1(t)\rangle=1$

so that

$$\dot{x}=x(1-x)\big(x_e+D\xi(t)-\alpha_1(t)M_v\big), \tag{36}$$

For simplicity, we will only explore two cases. In the first scenario (which is studied in the appendix), $\alpha_1(t)$ is a bounded stochastic process: $alpha_1^{\min}\leq\alpha_1(t)\leq\alpha_1^{\max}$.
In the second scenario,α_1 is log-normally distributed with a given standard deviation s_{α_1}. The average being one, this yields:

$$\alpha_1(t)=e^{\mu+\sigma Y(t)} \tag{37}$$

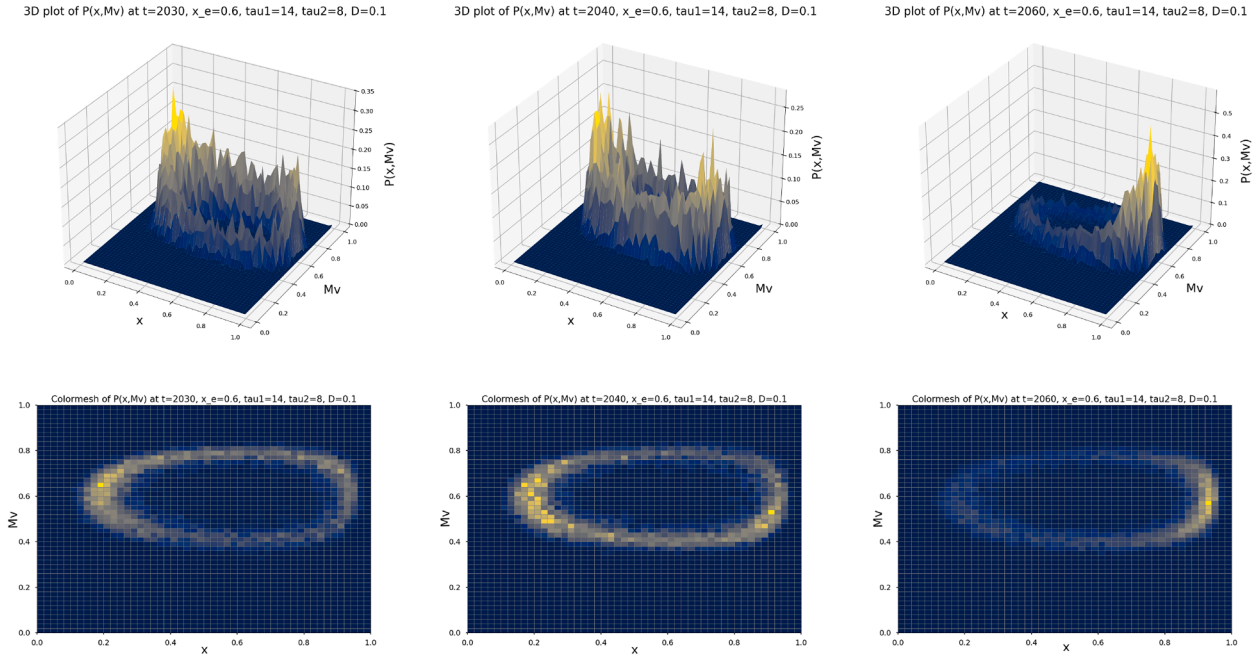

Fig. 15. AFK: impact of the noise strength on the numerical marginalized PDF in function of (x, M_v). In figure: $D = 0.1$ and (as in Fig. 14) $x_e = 0.6$, $\tau_1 = 14.0$, $\tau_2 = 8.0$. Upper panels: 3D plots, lower panels: associated colormeshes. Left panels: snapshots for $t = 2030$; Central panels: snapshots for $t = 2040$; Right panels: snapshots for $t = 2060$.

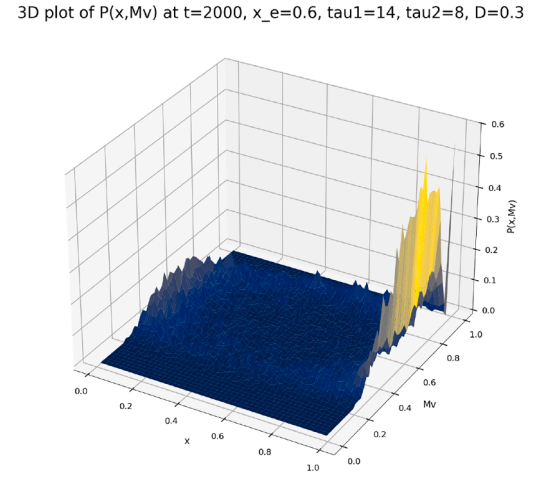

Fig. 16. 3D plot of the PDF obtained with the simulation for $x_e = 0.6$, $\tau_1 = 14.0$, $\tau_2 = 8.0$ and with noise $D = 0.3$ for $t = 2020$.

where:

$$\mu = log\left(\frac{1}{\sqrt{1+s_{\alpha_1}^2}}\right)$$

$$\sigma = log\left(1+s_{\alpha_1}^2\right)$$

and Y is an Ornstein Uhlenbeck process with unitary steady-state variance

$$\dot{Y} = -\frac{1}{\theta}Y + \sqrt{\frac{2}{\theta}}\xi_Y(t)$$

and autocorrelation time equal to θ.
Importantly, we consider that the external perturbations acting on δ and on α_1 are correlated under the assumption:

$$\xi(t) = \sqrt{1-K^2}\xi_x(t) + K\xi_y(t) \tag{38}$$

where $\xi_x(t)$ and $\xi_y(t)$ are uncorrelated; $\xi(t)$ is the white noise acting on δ and $K \in [0, 1]$ measures the degree of correlation. Thus, $K = 0$ denotes absence of correlation, whereas $K = 1$ means full correlation $\xi(t) = \xi_y(t)$.

11.1. Simulations with log-normal $\alpha_1(t)$

In this section, we will conduct some simulations to assess how log-normally distributed stochastic fluctuations of α_1 impact on our system. In particular, we will focus on the case of AFK distributed delay triggering Hopf oscillations, investigated in Section 9.4.1. Thus, also here we set $(x_e, \tau_1, \tau_2) = (0.6, 14.0, 8.0)$. As in Section 9.4.1, we will study how the SSPDF depends on D. This will be done for two different values of the new parameter s_a: $\alpha_1 = \{0.1, 0.5\}$. As per the other parameters, we set:

- $m = 1.0$;
- $\theta = 5.0$, so that the OU autocorrelation time is shorter than, but comparable to, the characteristic timescale;
- $K = 0.5$.

With parameters set, we now compare the scenarios plot by plot to identify any differences that may occur, fixing $s_a = 0.1$. In Fig. 14, we saw that the unperturbed Hopf cycle has the "comet effect" having a couple $(\tau_1, \tau_2) = (14.0, 8.0)$ able to generate Hopf oscillations. Now, if we look at Fig. 24, the situation is remarkably different. Due to this kind of noise, the time-varying comet effect of PDF in the steady-state region becomes a steady-state distribution with minimal temporal changes. Thus we will look only to a single time instant ($t = 2000$). We obtain a quite 'noisy' PDF distributed in the area of the Hopf cycle. It is immediately found once again a preference for the upper bound but the central hole, seen for noisy constant α_1 cases, has disappeared. Being this small s_a already very disturbing, we can wonder if the trajectories are still periodic (or at least quasi-periodic) to generate this kind of distribution. Producing, as example, a trajectory in this case we obtain the time series plot in Fig. 25. As we can notice, there are still quite stable oscillations, however the amplitudes stochastically vary and also the 'trend of the oscillations' fluctuates during time. On the other hand, the period seems pretty stable, as showed also by the power spectrum on the right panel of the same Figure.

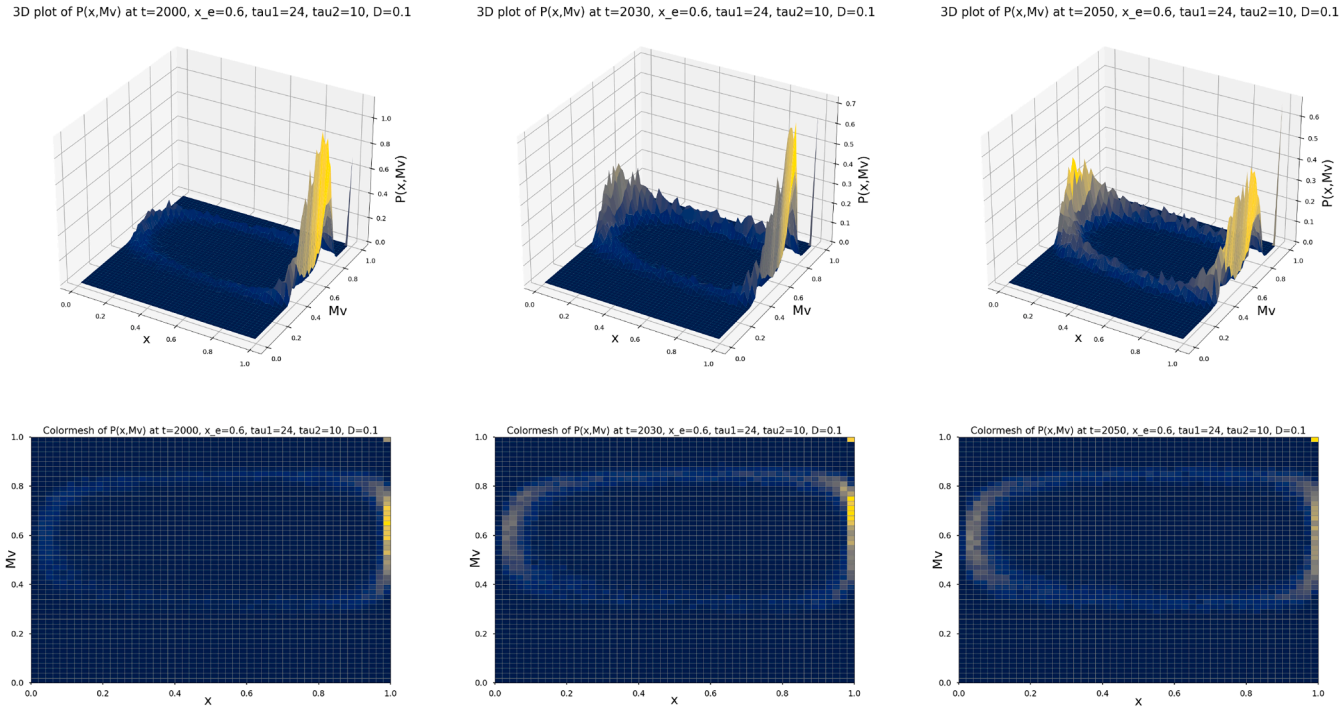

Fig. 17. AFK: impact of the noise strength on the numerical marginalized PDF in function of (x, M_v). In figure: $D = 0.1$ and $x_e = 0.6$, $\tau_1 = 24.0$, $\tau_2 = 10.0$. Left panels: snapshots for $t = 2000$; Central panels: snapshots for $t = 2030$; Right panels: snapshots for $t = 2050$.

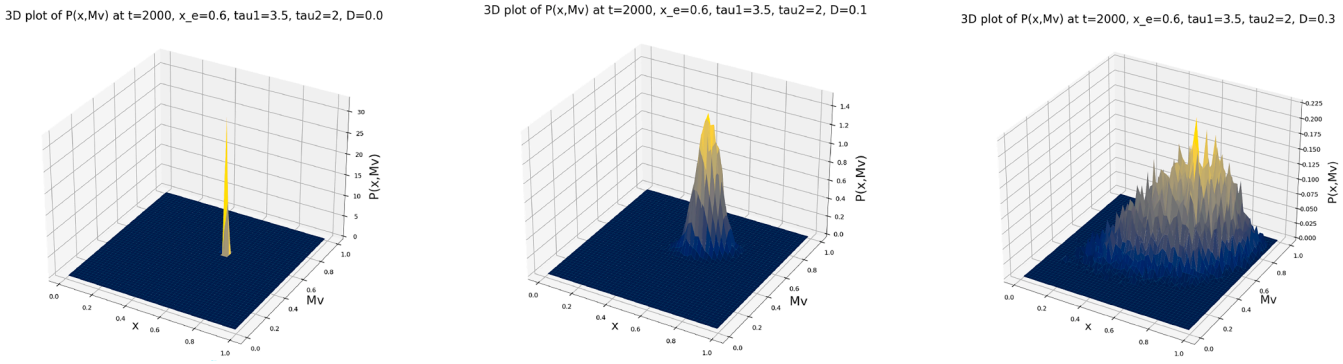

Fig. 18. AFK: 3D plots of the PDF obtained with the simulation for $x_e = 0.6$, $\tau_1 = 3.5$, $\tau_2 = 2.0$ and with noise $D = 0.0$ (left), $D = 0.1$ (central) and $D = 0.3$ (right) at SS.

Increasing D up to $D = 0.2$, we obtain some remarkably different results, see the left panel of Fig. 26. Indeed, the region around 1 has larger probability than the other regions. We can also find a large peak around $(1, 1)$. Once again, we are reporting only this time instant because the PDF have only minimal changes in time. For $D = 0.3$ the histogram almost completely collapses around $(1, 1)$, with same peaks of the type $(1, M_v)$ or, more interestingly, $(0, M_v)$ (no vaccination). Therefore, we can guess (and it is confirmed by the simulations) that the perturbations induced by s_a dominates until D grows sufficiently, and then the two noise synergizes.

Taking $s_a = 0.5$ the effects are even more extreme as shown in the right part of Fig. 26. Generally speaking, it is also interesting how this noise is capable, differently from the white noise, to almost stabilize the PDF in the steady-state region; in fact wave effects or the comet effect itself are not present anymore. In this panel, the distribution focuses on the boundary values of x with a solid preference $x = 1$ also when $D = 0.0$. As per M_v, this variable is more distributed. Incrementing D there are at first no differences ($D = 0.1$) but for $D = 0.2$ we have already the collapsed distribution almost completely peaked in $(1, 1)$. There are almost no differences considering other time instant in this steady-state region.

As per the 'force' of correlation K, surprisingly we did not notice major changes.

12. Effects of actions of public health system to favor vaccine uptake

In [15], a model was introduced to incorporate the initiatives of Public Health Systems aimed at enhancing awareness regarding the significance of vaccines, consequently elevating the rates of vaccine uptake. Representing the resulting transition rate from strategy 'No Vax' to strategy 'Vax' as $\gamma(t)$, the model (22) is adjusted in the following manner:

$$dx = x(1-x)(x_e - x)dt + Dx(1-x)dB + \gamma(t)(1-x(t))dt \tag{39}$$

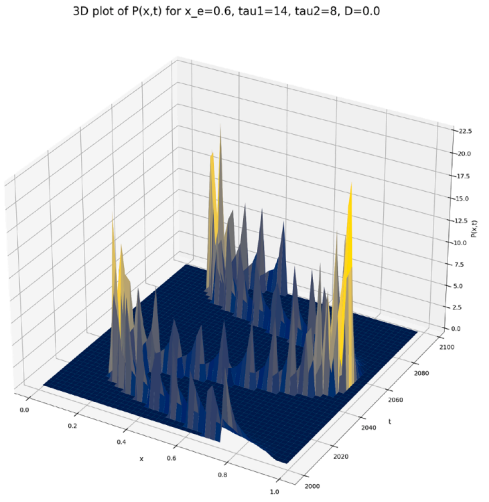

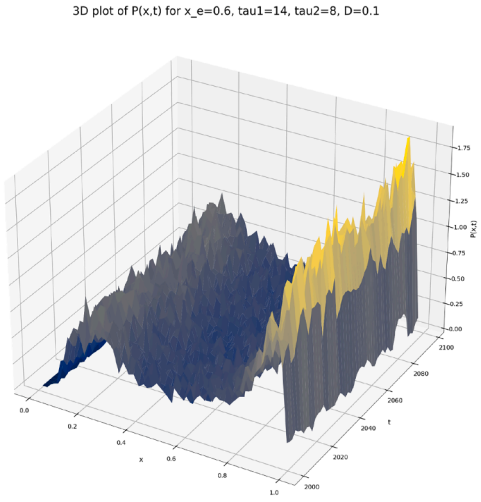

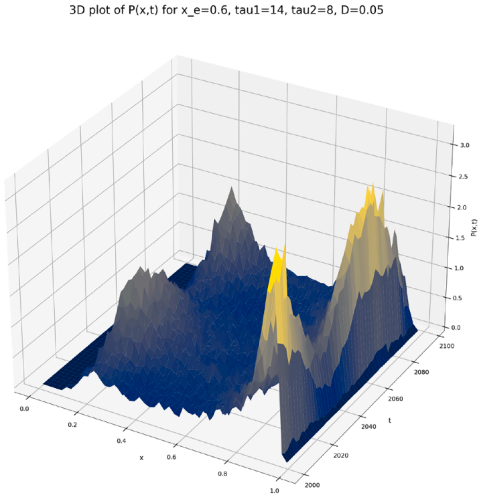

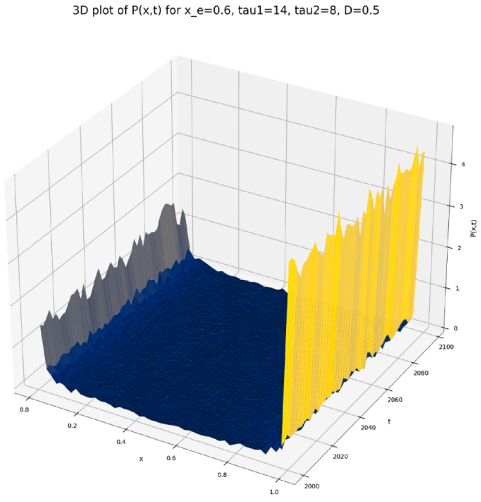

Fig. 19. AFK: 3D plots (x, t) projection of the PDF obtained with the simulation for $x_e = 0.6$, $\tau_1 = 14.0$, $\tau_2 = 8.0$ and with noise $D = 0.0$ (left) and $D = 0.05$ (right) at SS.

Fig. 20. AFK: 3D plots (x, t) projection of the PDF obtained with the simulation for $x_e = 0.6$, $\tau_1 = 14.0$, $\tau_2 = 8.0$ and with noise $D = 0.1$ (left) and $D = 0.5$ (right) at SS.

Here we will illustrate the results in the simple case where $\gamma(t) = \bar{\gamma}$ is constant. Similar results, however, are found in the general case

$$\gamma(t) = \bar{\gamma} + \eta_1 \gamma_1(t) + \eta_2 \nu(t) > 0$$

where $\gamma_1(t)$ is periodic with null mean, $\nu(t)$ is a stochastic ergodic process with null mean and $\eta_1, \eta_2 \in \{0, 1\}$ $\eta_1, \eta_2 \neq 0$. The mathematical details for all the cases are illustrated in the appendix, including the case $D = 0$, for which we provide the analytical solution.

The important beneficial effect of the enacted campaign is that the system can no more get stuck at the state 'no vaccination' since

$$dx|_{x=0} = \gamma(t)dt > 0.$$

The second effect is that the unique stochastic equilibrium point $x = 1$, when stochastically unstable in the absence of pH interventions, in presence of them can be stabilized. This occurs provided that

$$\bar{\gamma} > \gamma^* = 1 - x_e - \frac{D^2}{2} \tag{40}$$

As per the global stability of $x = 1$, if $D \in (0, 1]$ then the condition (40) also guarantees the Global Attractivity of $x = 1$. The case $D > 1$ is , instead, much more complex but in a number of cases we got that condition (40) also guarantees global stability (see the appendix).

13. Discussion

When parents vaccinate their children based on a self-interest argument i.e., by 'rationally' comparing benefits and costs of immunization, a long-standing result of behavioral epidemiology states that the collective vaccine uptake will establish at a stable equilibrium strictly below the elimination threshold. This makes infection elimination impossible. The rationale of this result, typically derived in deterministic settings [14,15], is that the rarity of infection caused by successful infection control will remove the incentive to get vaccinated.

In this work, we challenge this result, by providing extensive theoretical and simulative analyses of the consequences of stochastic fluctuations arising from highly volatile opinions about vaccination – what we termed 'irrational' behaviour. We do this in a case that will likely become more and more relevant in prospective terms, namely when the infection targeted for vaccination is not circulating anymore in the population due, e.g., to local elimination or to a strong subcritical behaviour. Arguably, under such circumstances, the main structural component of the demand for vaccines is represented by the risk of vaccine side effects that parents perceive from the current and past trends of vaccine adverse events (VAE) [14,15].

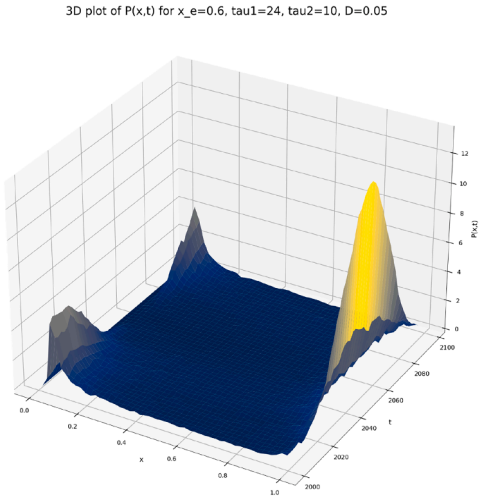

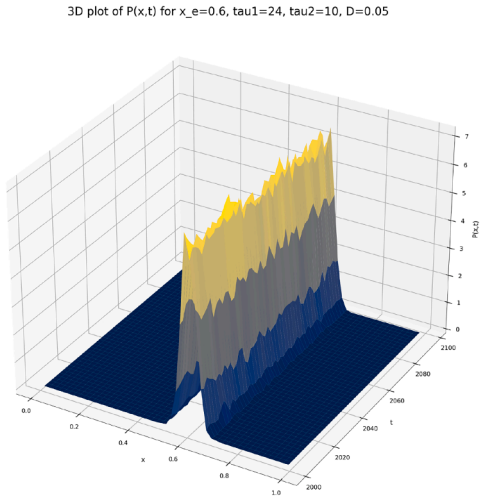

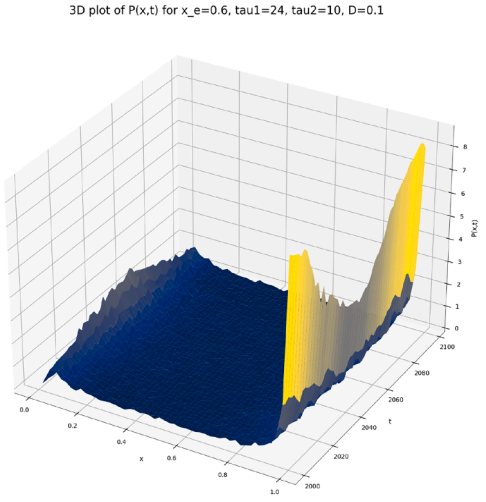

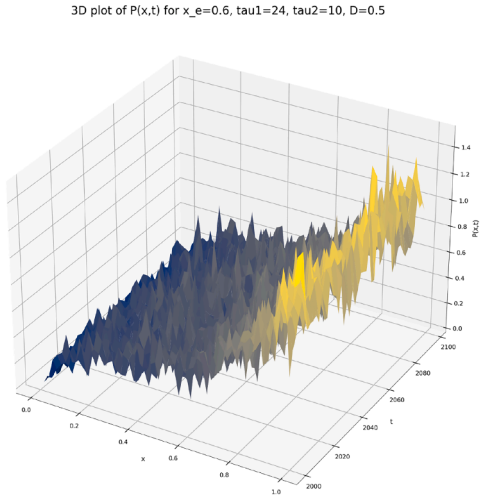

Fig. 21. AFK: 3D plots and linked colormesh (x,t) projection of the PDF obtained with the simulation for $x_e = 0.6$, $\tau_1 = 24.0$, $\tau_2 = 10.0$ and with noise $D = 0.05$ (left) and $D = 0.1$ (right) at SS.

Fig. 22. AFK: 3D plots (x,t) projection of the PDF obtained with the simulation for $x_e = 0.6$, $\tau_1 = 3.5$, $\tau_2 = 2.0$ and with noise $D = 0.05$ (left) and $D = 0.5$ (right) at SS.

The backbone of our model is represented by the evolutionary game equation for the imitation dynamics of vaccination strategies [14,15], reformulated as a process of double contagion of ideas [4].

Before plugging volatile opinions in our framework, we provided an extensive preliminary assessment of two other major causes of fluctuations in vaccine uptake that can deeply interact with stochasticity.

The first cause relates to the fact that the typical formulation of the imitation equations relies on differential equations ordinary or partial [19]. These are deterministic approximations of stochastic processes described by a continuous time Markov chains. For small to moderate population size, the Markov chain of vaccine uptake will show intrinsic stochastic oscillations that can endogenously lead to fixation in a scenario where people stop vaccinating. Nonetheless, our first result showed that the average time to fixation to such a limiting scenario is immensely large even for small/medium populations, so that the baseline mean field model remains a robust approximation as far as reasonable time horizons are considered. We also showed that the same holds for average hitting times of either very low or very high vaccination uptakes.

The second cause lies at the heart of behavioral epidemiology, namely the fact that alerts and perceptions related to VAEs, regardless of being confirmed or not, create rumours at the population level that have the potential to persist in the long-term as a collective 'memory' [81]. This implies that whilst taking their vaccination decisions, individuals will also take into account past information on the history of VAE. Model-based evidence suggests that this collective memory of VAE, typically modeled through distributed time delays, represents an important source of oscillations in vaccine uptake [15]. In this work, we considered two types of memory kernels: i) the classical exponentially fading kernel, for which we showed that no oscillations can occur; ii) the acquisition-fading kernel for which we showed that oscillations can occur via Hopf bifurcation. For both types of kernel, we provided (in the appendix) a detailed simulation analysis showing that both the transitory and oscillatory regimes can be quite heterogeneous depending on parameters and initial conditions.

Relying on these preliminary analyses, we then developed our final model for the dynamics of vaccine uptake in the presence of strongly volatile vaccination opinions. The interplay between noise and distributed delays plays a key role in the trends of vaccine uptake. We first considered the case of large and fast stochastic fluctuations in key behavioral parameters modeled as a white noise. We analysed the model both without and with the presence of a collective memory of VAE. The resulting system has two stochastic equilibria, an SPNVE where nobody gets vaccinated and an SPVE where everybody does. In the absence of

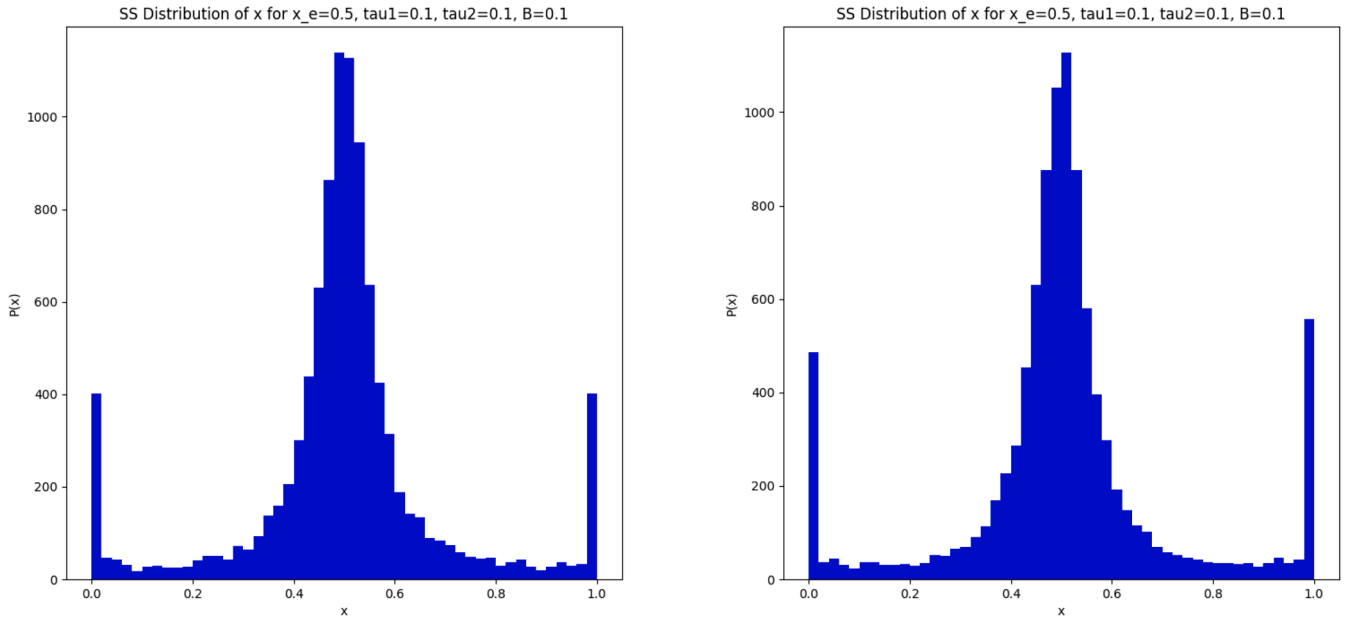

Fig. 23. Plots of PDFs for the AFK system under a perturbation of the Cauchy noise type. Noise parameter: $\theta = 21.31$ and $B = 0.1$. Other parameters: $x_e = 0.5$, $\tau_1 = \tau_2 = 0.1$. In the left case we are using simulation of 1000 time units while on the right there are used simulation of 10,000 time units.

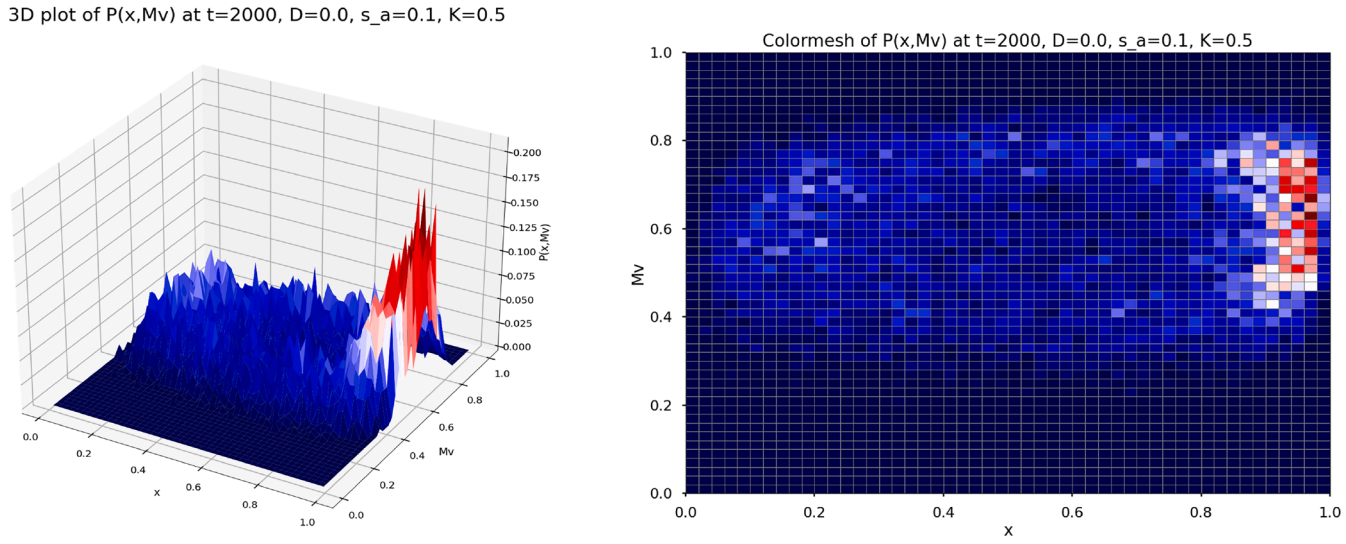

Fig. 24. Stochastic fluctuations of α_1 in the case of AFK Kernel: plot for $t = 2000$ of the PDF and corresponding colormesh, with $D = 0.0$, $s_a = 0.1$, $x_e = 0.6$, $\tau_1 = 14.0$ and $\tau_2 = 8.0$ (Hopf oscillations).

memory, we could provide a detailed analytical characterization of the model properties, showing the critical role of the noise parameter tuning the extent of opinions' volatility due to irrational behaviour.

First, a moderate volatility may cause noise-induced transitions, with the shape of the stationary distribution of vaccine uptake shifting from unimodal to bimodal, or from unimodal to monotone (decreasing or increasing).

Second, and most important from a behavioral perspective, we showed that medium-large volatility levels cause the landing of the system either on the SPNVE, where nobody vaccinates, or on the SPVE, with 100% permanent uptake. In such situations, the 'self-interest' steady-state of the deterministic system is not resilient to the volatility of opinions.

Finally, for very large volatility, stochastic bistability occurs.

In particular, the transition from stochastic stability to stochastic bistability is strongly reminiscent of phase transitions observed in systems with infinite state variables [75].

Given that the duration of the transient behavior leading to the steady-state distribution can be very long, we performed extensive numerical simulations that showed some partial differences from the theoretical analysis, which is evidence of a very slow transitory behaviour.

Once collective memories are considered in the delayed case, numerical simulations revealed further interesting phenomena.

A general result, valid under both types of memories, is that the ability of the (deterministic) equilibrium to persist under opinion volatility is further weakened. Additionally, noise-induced transitions are neatly affected by the extent of the delay. Also, in the case of exponentially fading memories (where only damped oscillations can occur in the deterministic system), pumping a sufficient opinions' volatility yields large noise-induced oscillations (of periodic or quasi-periodic types). This suggests that the noise due to irrational behavior and the dumped oscillation induced by the delay combine, triggering dramatic oscillations in vaccine uptake, even when the positive equilibrium persists.

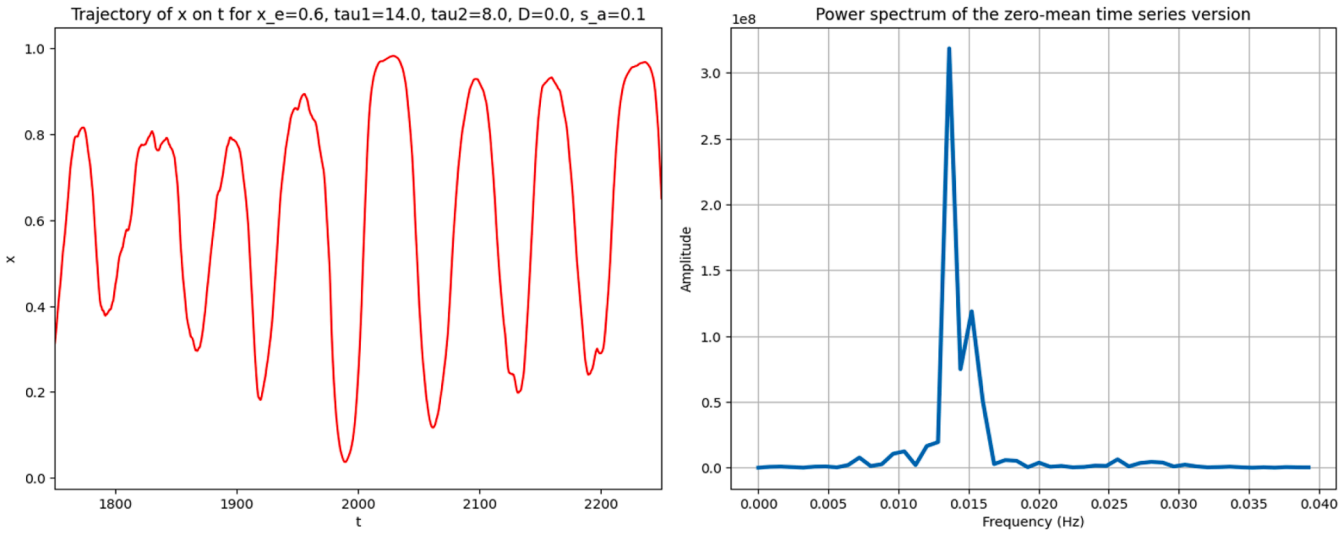

Fig. 25. Stochastic fluctuations of α_1 in the case of AFK Kernel: plot of a time series for the configuration used in Fig. 24 (left). On the right, the power spectrum of the mean-zero version of the signal in the time window $[1000, 2250]$.

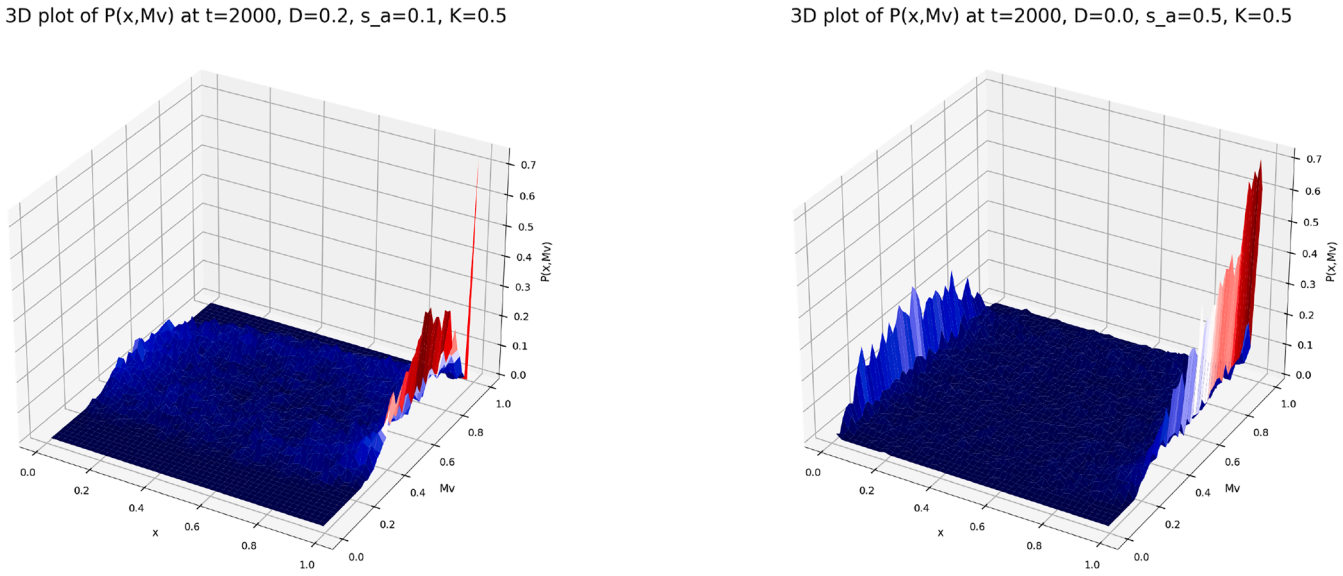

Fig. 26. Stochastic fluctuations of α_1 in the case of AFK Kernel: plots of PDF for $t = 2000$ with $x_e = 0.6$, $\tau_1 = 14.0$ and $\tau_2 = 8.0$ (Hopf oscilations). Left: $(D, s_a) = (0.2, 0.1)$. Right: $(D, s_a) = (0.0, 0.5)$.

In the case of AFK kernel, for D under same threshold the deterministic oscillations maintains its cyclical character, albeit with stochastic deviations of varying magnitude. If D increases there is a scenario of stochastic bistability, although with a substantially larger peak for the stochastic equilibrium closer to the deterministic equilibrium. Increasing the average delay, the PDF is a mixture of stochastic oscillations and of the bistable scenario.

We did not limit our investigation to the case of white noise, but we also considered an important case of a fat-tailed colored noise with Cauchy steady-state PDF, which we introduced in this work. After characterising the statistical properties of this new type of noise with respect to its characteristic parameters, we assessed its impact on our study system. Our simulations show that the effect of fat-tailed noise is to increase the probability of fixation of vaccine uptake to either the SPNVE or the SPVE.

Including fluctuations in the reactivity of vaccination decisions to (current or past) VAEs, led a strong amplification of the cycles induced in the AFK case, eventually destroying the cyclic nature of the behavior. Interestingly, in this case the impact of the correlation between the general white noise of opinions and the noise affecting the reactivity to VAEs turns out to be modest.

Finally, we analytically investigate conditions to avoid the scenario of vaccine extinction, via public health intervention incentivizing vaccination. An extended summary of key results is provided in the appendix.

Regarding future developments of this work, we will proceed along two directions that constitute two main limitations of current work. On the one hand, we aim to extend this work to include the interplay between the stochastic evolutionary dynamics of vaccine uptake and the spread of the infection to be controlled. On the other hand, we want to include the effects of human mobility as well as of spatial components of the information. This will also allow assessing the potential effects of the possible interplays between the resulting spatial non-locality with the temporal non-locality. Another limitation of our current analysis that we want to work on is a more systematic investigation with analytical and semi-analytical tools of the interplay between the stochasticity and the memory effects, and the related bifurcations, for

example by working on the associated multi-dimensional Fokker-Planck Equation.

14. Concluding remarks

This article provided a theoretical underpinning for the determinants and implications of vaccine uptake for a situation that is becoming of great importance - especially in prospective terms - namely when the target infection has been eliminated, therefore removing incentive to vaccination. Two major vaccine preventable childhood infectious diseases fall in this category, namely poliomyelitis and (to a lesser extent) measles. Although both infections have motivated empirical, public health and conceptual studies on infections that are near elimination, most such studies have focused on topics quite different from those addressed here. For example, a discussion of the challenges related to the post-elimination epoch [82], identified declining compliance with vaccination as a key treat. However, they did not propose any mechanism for compliance in the post-elimination era. Other studies have looked at the characteristic of residual transmission in elimination regimes (e.g., [83]) or at the determinants of heterogeneity in individual vaccine uptake [84]. Additionally, many theoretical studies have investigated the dynamics of subcritical infections, typically in stochastic settings (e.g., [85,86]) but also in deterministic ones, where backward bifucations can promote persistence even when reproduction is below threshold [87]. In this standpoint, we believe that our effort provides a new theoretical background for the prospective dynamics of compliance to vaccination under elimination (or near to elimination) regimes focusing, arguably, on the two key determinants of vaccine uptake, namely the memory of vaccine adverse events and the volatile vaccination opinions that pervade online social media in the current 'post-truth' phase.

Crucially, our stochastic evolutionary game framework generates a remarkably rich catalogue of dynamical scenarios for vaccine uptake, ranging from sustained high coverage to large-amplitude oscillations and dramatic collapses. These scenarios are fully qualitatively consistent with a number of facts that have recently emerged for vaccination against infections that have been eliminated in many settings. A paradigmatic example is poliomyelitis, a major infectious threat targeted for eradication since 1988 and eliminated almost everywhere thanks to sustained immunization. As reviewed in the Introduction section, contemporary polio eradication efforts are increasingly challenged by a steady, and often oscillatory, decline in vaccine uptake in several countries, including those that historically achieved very high coverage. We argue that the dynamical regimes produced by our model offer not only a coherent theoretical lens through which such empirical patterns – and their possible future trajectories in a post-truth and post-trust society – can be interpreted and explored, but also qualitatively reproduce the main trends documented for poliomyelitis in some countries and, more generally, for vaccination against other quasi-eliminated infections in the current post-truth and post-trust society.

Relatedly, our main results on key thresholds in noise strength, memory span and intervention intensity might offer quantitative guidance for designing robust vaccination campaigns in an era of absent infections but strongly volatile public opinion. We could not test our theory against data because our baseline model predicts strong oscillations in vaccination opinions on short time-scales and data on childhood immunization are instead, typically collected on much longer scales (e.g., yearly). Therefore, our predictions suggest that in the future it might be wise to collect and make available vaccine coverage data on fine temporal scales, in order to predict the potentially harmful impacts of fluctuating opinions on prevention policies.

CRediT authorship contribution statement

Lorenzo Cabriel: Writing – review & editing, Writing – original draft, Visualization, Software, Methodology, Investigation, Formal analysis; **Chris T. Bauch:** Writing – review & editing, Writing – original draft, Methodology; **Fabio Anselmi:** Writing – review & editing, Writing – original draft, Methodology; **Piero Manfredi:** Writing – review & editing, Writing – original draft, Methodology, Funding acquisition; **Alberto d'Onofrio:** Writing – review & editing, Writing – original draft, Supervision, Methodology, Funding acquisition, Formal analysis, Conceptualization.

Declaration of interests

The authors declare that they have no competing interests.

Declaration of competing interests

The authors declare that they have no competing interests.

Data availability

Code can be requested upon motivated reason

Acknowledgements

The authors warmly thank the two anonymous referees and the associated editor whose comments and suggestions helped to considerably improve this work. The work of Alberto d'Onofrio, Fabio Anselmi and Piero Manfredi was supported in part by the Italian PNRR Grant S4-02.P0001 COC-1-2023-ISS-02 INF-Act. The Work of Chris T. Bauch was funded by a NSERC Discovery Grant to Chris T. Bauch.

Supplementary material

Supplementary material associated with this article can be found in the online version at 10.1016/j.physd.2026.135143.

Appendix A. Comparison with other recent models

Balogh and Oraby published a mathematically interesting paper [46] where they use a stochastic approach to model irrational volatility in a vaccination game. However their work is very different from ours in a number of details and contains some strong biological assumptions.

First, they consider the case of spread of a SIR disease with a stochastically varying contact rate beta. They model this variation via a white noise so that the equation for the Susceptible in their model model reads (using stochastic calculus notation)

$$dS = \mu(1-x)dt - \mu S dt - SI(\beta dt + \sigma dB_1).$$

From a biological viewpoint the term

$$C = -SI(\beta dt + \sigma dB_1)$$

represents the flow of susceptibles that get infected in the infinitesimal interval $(t, t+dt)$, thus it must be negative for $dt > 0$. Unfortunately the use of a white noise, where

$$dB = G_t\sqrt{dt}, \quad G_t \sim N(0,1)$$

makes the term C very frequently negative. This is a very common pitfall in biological models, as first stressed in [91], and then specifically for epidemic models in [92].

Secondly, and from the viewpoint of the vaccine IGD, the noise is inserted in a purely mathematical way so that authors, after defining as X_1 and X_2 the number size of 'VAx' and 'NoVax' groups, write two replicator-like equations of the IGD as follows:

$$dX_1 = X_1X_2\Big(u_1(X_1,X_2)dt + v_1(X_1,X_2)dB_1\Big) \tag{A.1}$$

$$dX_1 = X_1X_2\Big(u_2(X_1,X_2)dt + v_2(X_1,X_2)dB_2\Big) \tag{A.2}$$

where $(B_1(t), B_2(t))$ is a bidimensional Wiener process that is postulated to perturb the system.

The consequence is that due to a *non-demographic* fluctuation the total population $N = X_1 + X_2$ becomes not constant, which requires the

adoption of the Ito formula. Moreover, the dynamics of N is not considered in the SIR stochastic differential equations, where the state variables (S, I, R) are fractions with respect to the stochastically varying N.

As we have shown by a semi-mechanistic derivation, the random perturbations in the IGD cannot induce a population dynamics, because they merely model instantaneous changes of the rates of transition from a strategy to its opposite strategy.

Appendix B. Table of the main symbols and parameters

Here we summarize all main symbols and parameters in table (Table B.1) for facilitating the reading of this work.

Table B.1
Summary of main symbols and parameters used in the manuscript.

Symbol	Description	Typical Domain/Units
Core State Variables and Functions		
$x(t)$	Fraction of individuals using strategy "vaccine" at time t	$[0, 1]$
$1 - x(t)$	Fraction using strategy "no vaccine"	$[0, 1]$
x_e	Deterministic equilibrium fraction (no noise)	$[0, 1]$
$b(t) = 1 - x(t)$	Alternate notation for "no vaccine" fraction	$[0, 1]$
Memory Variables / Kernels		
$M_v(t)$	Weighted memory of side-effect information	$[0, 1]$
$W_v(\tau)$	Memory kernel for vaccination side effects	$\int_0^\infty W_v(\tau)\, d\tau = 1$
$M_1(t)$	Auxiliary memory variable (AFK model)	$[0, 1]$
τ_1, τ_2	Rates for acquisition-fading kernel (AFK)	$\tau_1, \tau_2 > 0$
a	Rate parameter for exponential-fading kernel (EFK)	$a > 0$
Deterministic Rates and Parameters		
$\alpha_0,\ \alpha_1$	"No-vax" transition rates; e.g. $\alpha(M_v) = \alpha_0 + \alpha_1 M_v$	$\alpha_1 > 0$; sometimes $\alpha_1 = 1$
c_0	Baseline rate favoring vaccination	$c_0 > 0$
$\delta = c_0 - \alpha_0$	Effective difference for the drift term	Real, often $\delta > 0$
$\gamma(t)$	Public health intervention rate promoting vaccination	$\gamma(t) \geq 0$
Discrete / Markov Model Parameters		
N	Total population in discrete model	$N \in \mathbb{N}$
$n(t)$	Number vaccinating at time t	$n \in \{0, \ldots, N\}$
P	Population scaling or WKB parameter	Typically $P \sim N$
Noise / Stochastic-Process Parameters		
D	Noise intensity for fast/white fluctuations	$D \geq 0$
$\xi(t)$	White noise, $\langle \xi(t) \rangle = 0$, $\langle \xi(t)\xi(s) \rangle \propto \delta(t - s)$	Real-valued in time
θ	Correlation timescale in Ornstein-Uhlenbeck or colored noise	$\theta > 0$
B	Scale parameter for Cauchy (fat-tailed) colored noise	$B > 0$
K	Correlation parameter if multiple noises are correlated	$[0, 1]$
$y(t)$	Generic slow/colored noise process	Real or bounded interval
Auxiliary Transforms and Symbols		
$z(t) = \ln\left(\frac{x}{1-x}\right)$	Logistic transform used in some SDE analyses	$z(t) \in \mathbb{R}$
λ, ω_H	Eigenvalues or Hopf frequency in linearization	Determined by char. equations
$f(x),\ \sigma(x)$	Drift/diffusion in SDE form	E.g. $f = x(1-x)(x_e - x)$
…	Other short-lived symbols (e.g. normalizing constants)	Defined locally in text

Appendix C. Issues in solving analytically the hitting time equation

In this Appendix section we will try to solve as much as possible analytically the differential equation for the mean first time for the system to reach the extreme region a presented at the end of Section 3 in the Eq. (12).

Starting from the expression we can immediately simplify the situation moving to the variable $S(x) = \partial_x T_a(x)$ and dividing for the coefficient in front of the highest order derivative. This will produce the following differential equation.

$$\partial_x S(x) + \frac{N(\delta - \alpha x)}{2(\lambda + \alpha x)} S(x) = -\frac{N}{2x(1-x)(\lambda + \alpha x)} \tag{C.1}$$

where $\lambda := \theta_0 + \alpha_0$. Now, we are going to solve using the integrating factor method therefore we need to find $\mu(x) = \exp(\int f(x))$ where $f(x)$ is the function in front of the $S(x)$ term. The integral is can be solve easily by parts obtaining

$$\int \frac{N(\delta - \alpha x)}{2(\lambda + \alpha x)} dx = \frac{N(\delta + \lambda)}{2} \ln(\lambda + \alpha x) - \frac{Nx}{2} \quad \Rightarrow \quad \mu(x) := (\lambda + \alpha x)^{\frac{N(\delta+\lambda)}{2}} e^{-\frac{Nx}{2}} \tag{C.2}$$

However, our analytical solution stops at the next step in fact using the integrating factor method we need now to solve:

$$\mu(x) S(x) = -\int \frac{N(\lambda + \alpha x)^{\frac{N(\delta+\lambda)}{2} - 1} e^{-\frac{Nx}{2}}}{2x(1-x)} dx + C_1 \tag{C.3}$$

Aside the integration constant, the integral has no analytical solution in closed form due to the co-presence of two different polynomials at the numerator and denominator and the exponential function. Thus, this integral can be solved only numerically or posing some assumption and simplifications.

Actually these is only the first step into the issues of solving analytically this differential equation. Moving over this integral more unsolvable ones will appear when substituting back $S(x)$ and solving for $T_a(x)$ and also the boundary conditions at a produces compounds of such analytically unsolvable integrals.

Appendix D. Some properties of the transient behavior in the EF kernel case

In this Appendix section we will illustrate some interesting properties of the transitory of the EF kernel. In particular, the system exhibits critical oscillations. Indeed, for larger values of the parameter τ, the damping coefficient decreases and becomes less than one, which means that the EQ is reached by means of damped oscillations. For example, in both panels of Fig. D.1 it is $z = 0.52$ so the EQ is reached by means of oscillations that are rather damped. Note, however, that z provides only qualitative and strictly local indications on the behaviour, whereas the simulations provide also interesting information linked to the role of initial conditions. For example, and in reference again to the Fig. D.1, the amplitude and number of oscillations is different in the two panels . For example, in the figure the system starts with an apparent direct divergence to run over the EQ point and then, at last, converge to the EQ.

This phenomenon of the critical oscillation disappears moving x_e towards the centre of the domain and becomes a proper shrinking oscillatory behaviour centred in the EQ. Nonetheless, we will talk about it more deeply then.

Looking at the trajectories for varying x_0, one can notice that there are no differences in the characteristics of the oscillation. If the starting point is more distant from the EQ, the initial approaching phase will be steeper and the starting point will be accordingly different. However, the time position of the characterizing points is almost the same as well their values. This fact is particularly visible looking at the M_v plots, where a varying x_0 produces almost no differences in the evolution of the trajectory. An example of this is reported in Fig. D.2 for M_v, nevertheless this is also valid for x.

Totally different is the capacity of $M_v(0)$ to influence the system. This initial condition can modify the critical oscillation, both in the time position of the main elements and both in the depth of the parts composing the oscillation.See Fig. D.3. As we can observe, having a $M_v(0)$ more distant from the x_e enhances the amplitude of the critical oscillation as well extends the time duration of the oscillation. The partial preservation of the characteristics of the second peak is also very interesting, and it is clear that the effects of $M_v(0)$ are relevant on the first part of the trajectory. Secondly, we can trivially notice that the changes on the time extensions produce a delay of the second peak in time. We can make eventually an educated guess about the role of the domain border. In fact, it can be potentially the cause of the suppression of a full converging oscillatory regime, limiting the full expression of the oscillation. This is particularly visible in the bottom right plot where we have an almost constant region at the border, while, in the top left plot, we can fully appreciate the semi-critical oscillation.

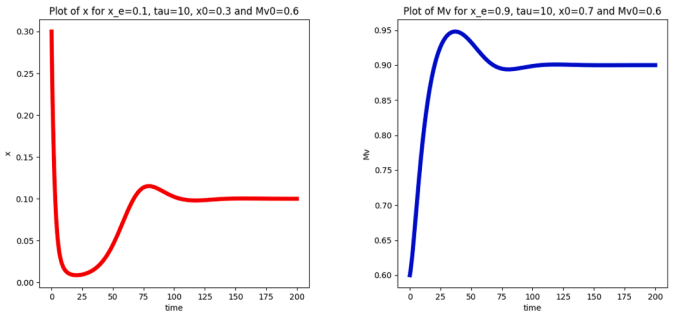

Fig. D.1. Trajectories of x (left) and M_v(right) for some particular configurations. Both are characterized by $\tau = 10$. On the left the $x_e = 0.1$, on the right is $x_e = 0.9$. In both cases, a critical oscillation appears.

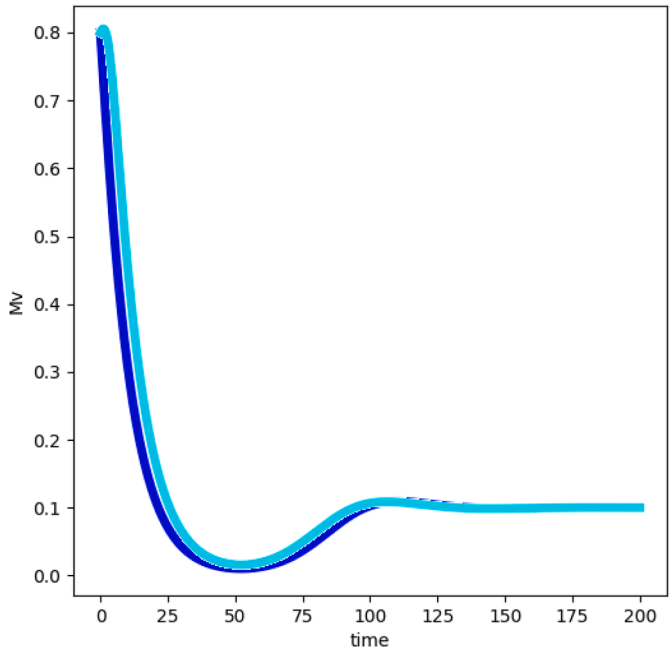

Fig. D.2. Comparison between two M_v trajectories. Both are characterized by $x_e = 0.1$, $\tau = 10$ and $M_v(0) = 0.8$. The blue trajectory has $x_0 = 0.2$, while the aqua one has $x_0 = 0.9$. Even if the two plots have a substantially different starting x_0, the M_v trajectories are remarkably similar.

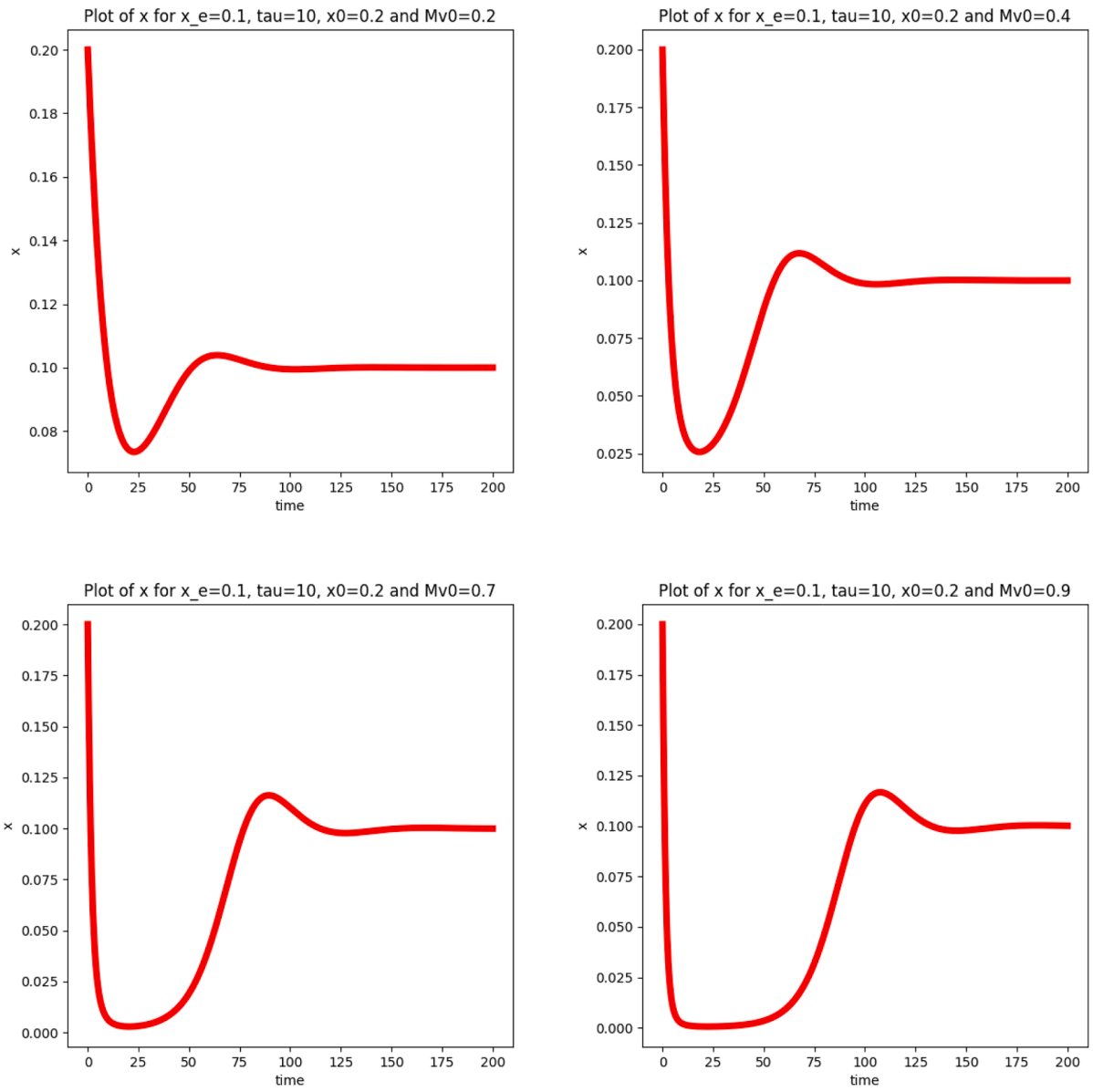

Fig. D.3. EF kernel: impact of $M_v(0)$ on damped oscillation. On top left $M_v(0) = 0.2$, on top right $M_v(0) = 0.4$, on bottom left $M_v(0) = 0.7$ and on bottom right $M_v(0) = 0.9$. All share $x_e = 0.1$, $\tau = 10$ and $x_0 = 0.2$, and exhibit critical oscillations, but the characteristics are substantially different to one another.

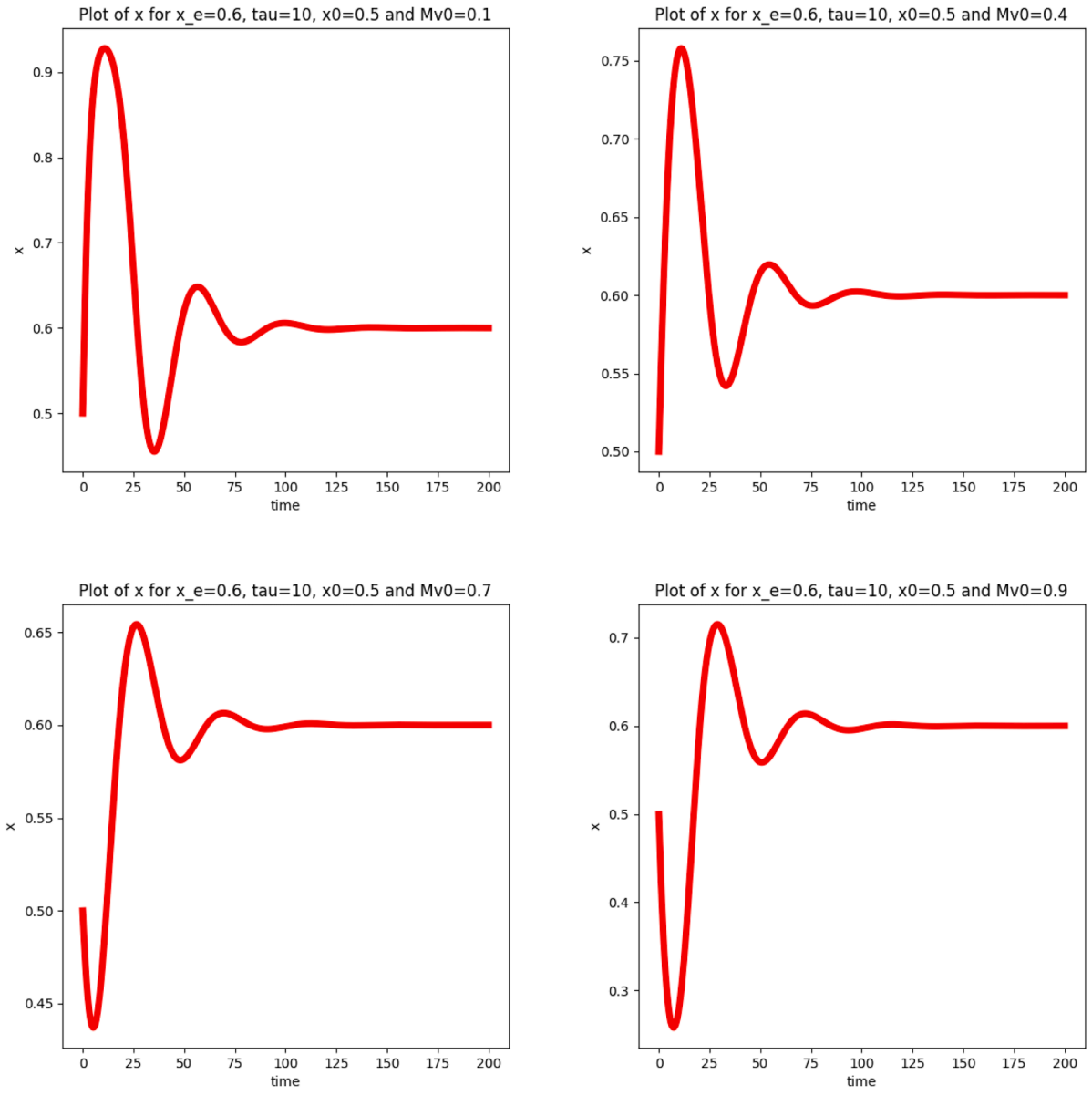

Fig. D.4. EF kernel: impact of $M_v(0)$ on the trajectories in case of mildly damped oscillations. All of the panels are such that $x_e = 0.6$, $\tau = 10$ and $x_0 = 0.5$. Upper left panel: $M_v(0) = 0.1$; Upper right panel: $M_v(0) = 0.4$,; Lower left panel: $M_v(0) = 0.7$; Lower right panel: $M_v(0) = 0.9$.

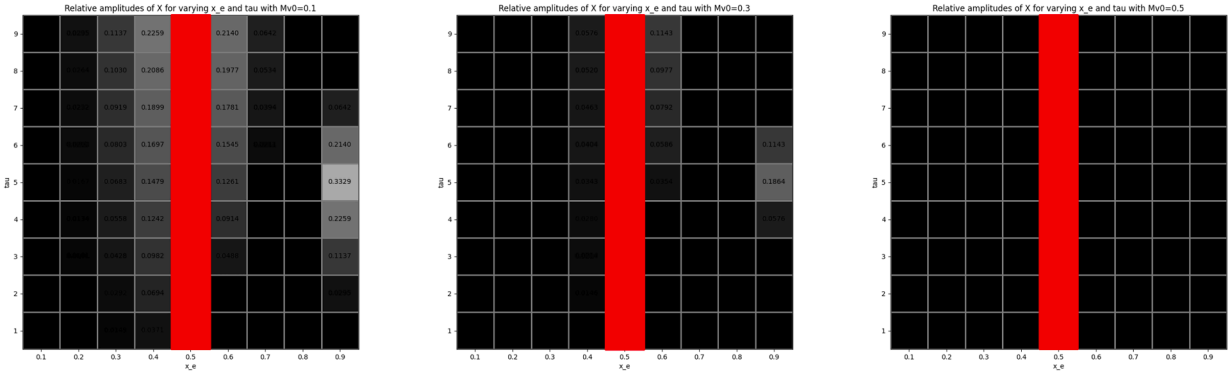

Fig. D.5. EF kernel: colormesh of the rectified maximum relative distance $(maxdist - initdist)_+$. Left panel: $M_v(0) = 0.1$; Central panel:, $M_v(0) = 0.3$; Right panel: $M_v(0) = 0.5$. In lighter shades, we have the configurations with oscillations bigger than the starting values. The central column is removed because we assumed $x_0 \equiv x_e$.

Similar observations can be made looking at the M_v plots here not reported.

Damped oscillations: moving x_e towards the centre of the domain the damping coefficient decreases (for example $z(10, 0.5) \approx 0.31 < 0.52$), thus the oscillations are less damped. Moreover, we noticed that the role of $M_v(0)$ is important, whereas the x_0 values have a scarce influence. See for example the Fig. D.4.

Summarizing the influence of initial conditions and other parameters, we can identify macroscopically two scenarios: 1) starting from the initial condition, we reach EQ but at any point the trajectory will be not farther away from the equilibrium than the distance we had at the starting point; 2) group of points where the trajectory is more distant from EQ in comparison with its starting position, ad in lower right panel of Fig. D.4. In the first case, we are sure that our system will be always limited by the initial position, in the second case the system will reach EQ but with a more traumatic evolution.

To quantify and visualize these behaviours, we may proceed as follows: given $(x_e, \tau, x(0), M_v(0))$ one computes the maximum absolute distance from the trajectory to the EQ throughout all the simulations. Then, one subtracts the initial distance from the initial conditions to the EQ. Finally, one sets to zero the cases where the distance was negative. We call this measure of behaviour of solutions Rectified Maximum Relative Distance (RMRD) $(maxdist - initdist)_+$. Since, we have seen so far that x_0 has small impact on the dynamics, we computed the RMRD in function of (τ, x_e) for some selected $M_v(0)$. We will plot the RMRD by using colormeshes in Fig. D.5.

As we can appreciate, the overshooting distances appear for the high values of τ, but also for intermediate values of it when $x_e = 0.9$, even if in a lesser extended form. The closer $M_v(0)$ is to EQ, the lesser are in number, and in entity, the configurations producing an oscillation bigger than the initial condition, even for the same values of the parameters. In the right, we can see that, if $M_v(0) \equiv x_0$, we will have the initial condition as maximum distance in all scenarios.

Appendix E. Some properties of the model under acquisition fading kernel

In this Appendix Section, we numerically illustrate some properties of the model under Acquisition Fading Kernel. For this model, we can perform the tests similaf to those done for the case of exponentially fading kernel. However, here the scenario is deeply different since the "memory" here is characterized by two characteristic times: τ_1 and τ_2. Even only considering the average delay $\tau_m = \tau_1 + \tau_2$ can be fallacious because two systems having the same average delay may have different behaviours as shown in Fig. E.1. And, of course, here the major novelty is the occurrence of Hopf bifurcation and the oscillations for $\tau_m > 1/K$. Thus, the presence of the AFK makes the system increasingly complex, so that an analysis aimed at finding predictable patterns in the evolution of the trajectory is more difficult and of uncertain utility.

Due to all these causes, we will move directly to study the impact of the parameters values on the system bifurcations, with particular focus on $x(t)$, the fraction of vaccinated newborns.

To study the effects of the parameters, we will plot the trajectories for the different parameters configuration to gather them in different 'plot matrices', where we will vary along on each one of the two axis one of the three parameters of our system. We will sample each parameter in 10 points, therefore, fixing the evaluated couple of parameters (τ_1, τ_2), we need to consider actually 10 plot matrix with a x_e having 10 possible different values. Certainly, we are going to report in this paper only the most significative results. Nonetheless, before looking at the results, we can try to solve the equation $a_1 + a_2 < K$ to understand what kind of shape the bifurcation line associated to the Hopf bifurcation should have. Trivially, we can obtain that:

$$\tau_1 + \tau_2 < K\tau_1\tau_2$$

Therefore, considering the couple of parameters, we should expect a hyperbolic bifurcation line and above this the Hopf region if K is sufficiently low for the considered domains of τ_1 and τ_2. If we want to study another interesting couple such as (x_e, τ_1), the situation is far more complicate. We can use the definition $K = x_e(1 - x_e)$ remembering that $0 < x_e < 1$. We can, in this way, obtain

$$\tau_1 = -\frac{\tau_2}{\tau_2 x_e^2 - \tau_2 x_e + 1} \tag{E.1}$$

Differently from before, the validity of this expression is not only a burden of the considered couple, but it is required that $\tau_1, \tau_2 > 0$. For this reason,

$$\tau_2 > \frac{1}{(1 - x_e)x_e} \qquad \Rightarrow \qquad \tau_2 > \min\left(\frac{1}{(1 - x_e)x_e}\right) = 4 \quad \text{having } x_e \in (0, 1)$$

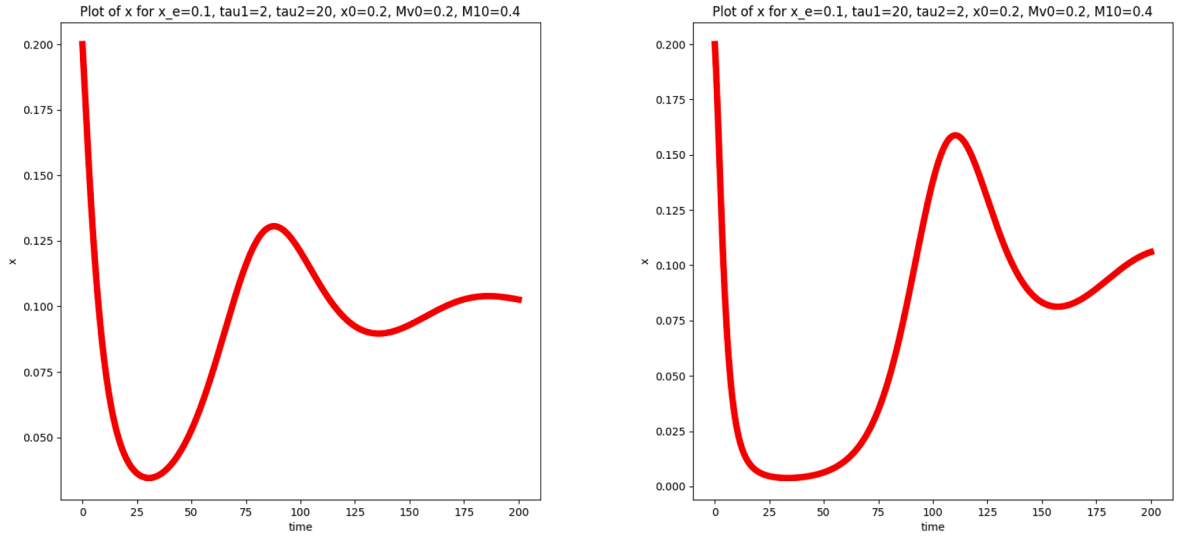

Fig. E.1. AF kernel: damped oscillations. Both are characterized by $\tau_m = 22$ and $x_e = 0.1$. Left panel: $\tau_1 = 20$ and $\tau_2 = 2$; Right panel: $\tau_1 = 2$ and $\tau_2 = 20$. In both cases, there is a damped oscillatory behaviour, but the two evolutions are quite different.

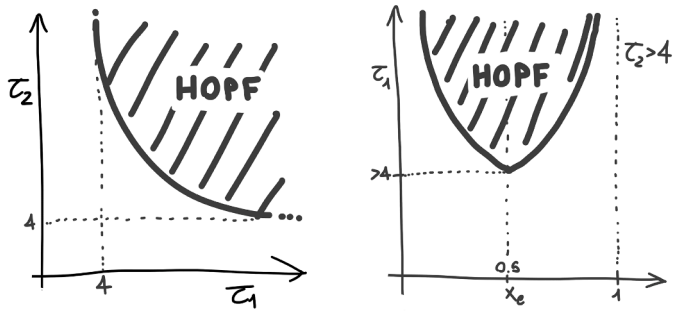

Fig. E.2. AF kernel: sketches of the bifurcation diagram in the parameters space. Left panel (τ_1, τ_2) parameter space; Right panel (x_e, τ_1) space. The plot for the (x_e, τ_2) is similar to the right panel and it omitted.

Thus, if $\tau_2 > 4$ we will be able to have a Hopf bifurcation for our system, at least for some values of x_e. If this condition holds, the region where the Hopf behaviour appears, for x_e, is

$$\frac{1}{2}\left(1 - \sqrt{\frac{\tau_2 - 4}{\tau_2}}\right) < x_e < \frac{1}{2}\left(1 + \sqrt{\frac{\tau_2 - 4}{\tau_2}}\right)$$

and we need also to have τ_1 greater than the right term in (E.1) to have the Hopf bifurcation. It is trivial to say, due to the symmetry of the expression, that a similar condition and situation happens for τ_1 when considering the couple (x_e, τ_2). The expected shapes for the two couples are reported in the two pictures of Fig. E.2.

Having understood what is the expected behaviour given the system, we can finally have a look at the plot matrices: starting from the one based on the (τ_1, τ_2) pair, shown in Fig. E.3.

Looking at the plot, we can see that it perfectly mirrors the bifurcation diagram shown in the left panel of Fig. E.2, with further details. The upper right corner is characterized by the Hopf oscillatory behaviour and, moving away from it, we move then to the damped oscillations and eventually, in the bottom left corner, to the semi-critical oscillation case. In Fig. E.4, it is shown the plot matrix concerning the pair of parameters (x_e, τ_1). Also here, the matrix mirrors the right panel of Fig. E.2, with further details.

The phase plot matrix of Fig. E.5 shows the impact of the parametric pair (τ_1, τ_2) on the phase plots (x, M_v).

We can notice that both the Hopf cycle and the damped oscillations have a bigger extension along the horizontal axis. In the top right corner, this characteristic is particularly strong: while x occupies entirely the domain, M_v values are extended in a much smaller portion of the $(0, 1)$ interval. This fact is actually quite explainable because τs influence how much the two information values "follow" the x variable. To obtain oscillations we need to increase these two terms, as seen also in the theory above, thus this leads to an augmentation in the resilience of the information variables. Due to these, it is quite direct and obvious that M_v has a far smaller extension in its domain than x.

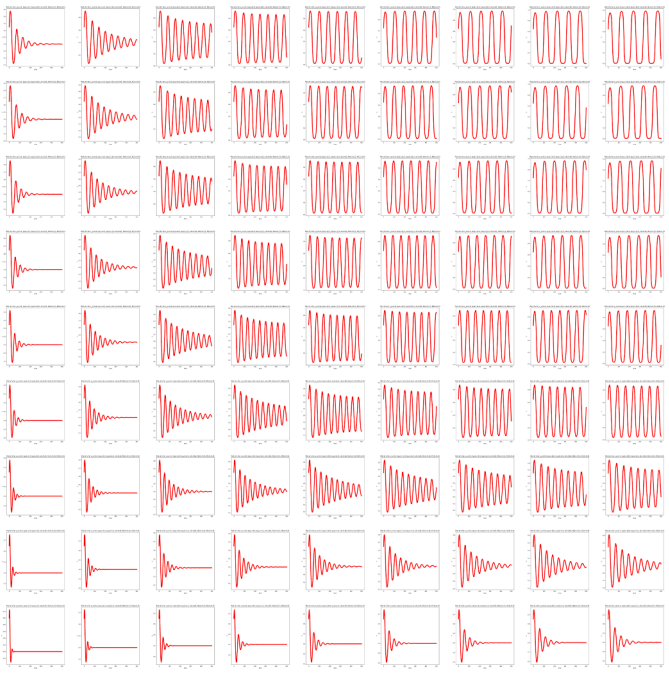

Fig. E.3. AF kernel: plot matrix of trajectories (t, x). Other parameters: $x_e = 0.4$, $x_0 = 0.65$, $M_v(0) = 0.15$ and $M_1(0) = 0.35$. Horizontal axis $\tau_1 \in [2, 18]$; Vertical axis: $\tau_2 \in [2, 18]$.

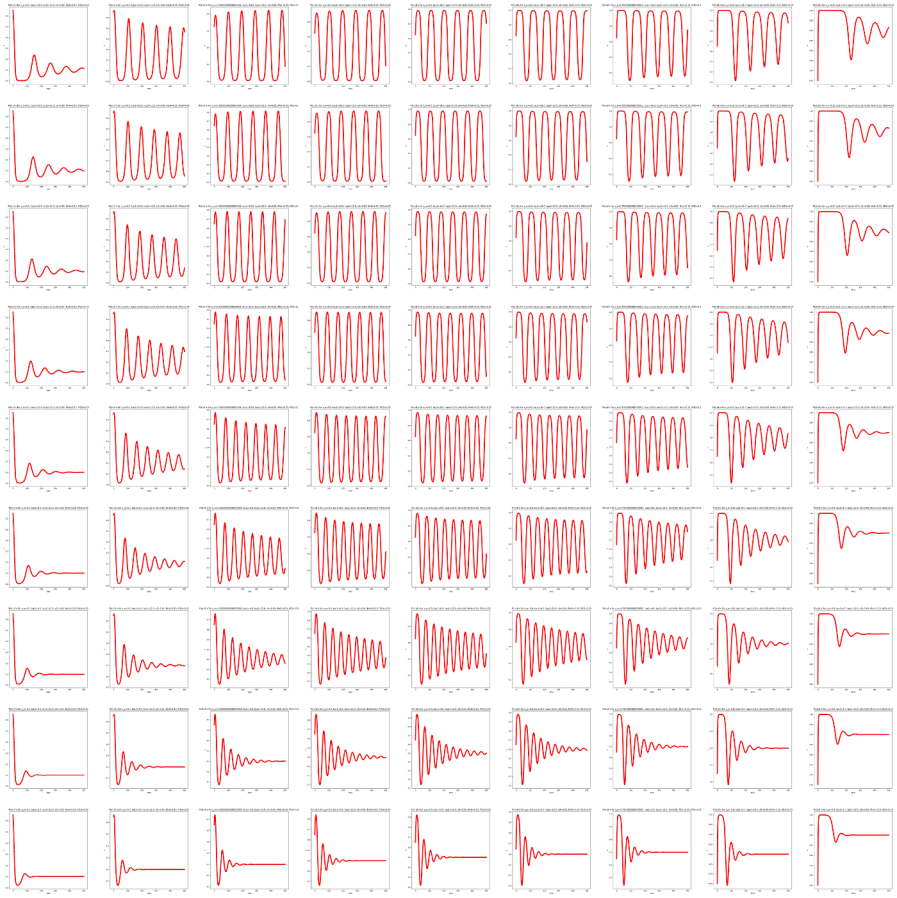

Fig. E.4. Plot matrix of trajectories (t, x), all characterized by $\tau_2 = 12$, $x_0 = 0.65$, $M_v(0) = 0.15$ and $M_1(0) = 0.35$. Along the x axis, x_e is increasing from 0.1 to 0.9. Instead, τ_2 is along the vertical one and is increasing from 2 to 18.

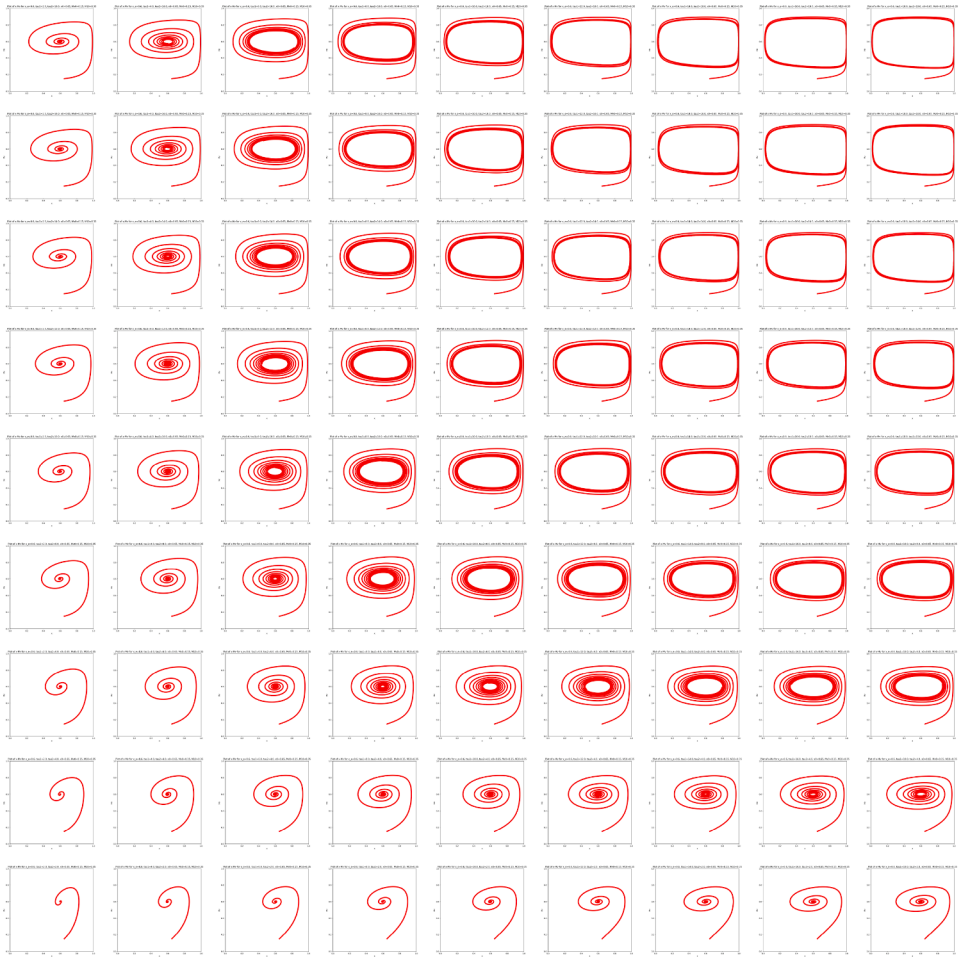

Fig. E.5. AF kernel: Phase plot matrix showing the impact of the parametric pair (τ_1, τ_2) on the phase plots (x, M_v). Other parameters: $x_e = 0.6$, $x_0 = 0.65$, $M_v(0) = 0.15$ and $M_1(0) = 0.35$. Horizontal axis $\tau_1 \in [2, 18]$; Vertical axis: $\tau_2 \in [2, 18]$.

Appendix F. Properties of the cauchy distributed stochastic processes

To start, the impact of B on the numerical steady-state PDF is shown in Fig. F.1. As per the autocorrelation, we must note that it is influence both by θ and by B.

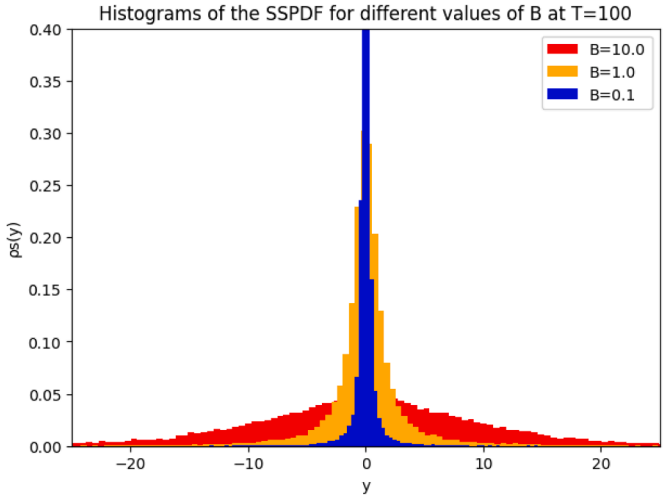

Fig. F.1. Cauchy-distributed fat tailed noise: histograms of the numerical steady-state PDF, for $T = 100$ and for $B \in \{0.01, 1, 10\}$.

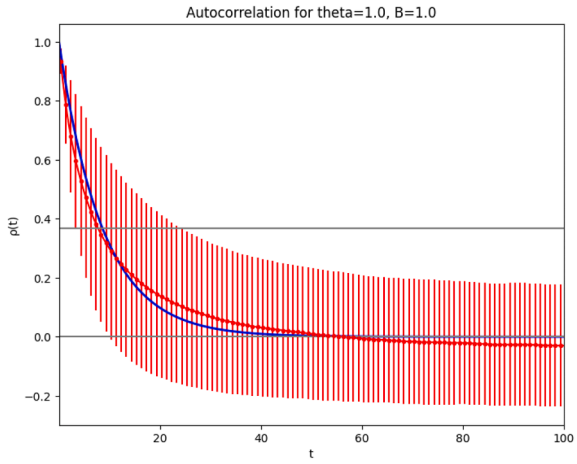

Fig. F.2. Autocorrelation of the Cauchy-distributed stochastic process for the reference parametric pair $(\theta, B) = (1, 1)$. The best fit for an exponential function is in blue; the mean autocorrelation is in red, and the error band given by the standard deviation is in pink. In gray, the $y = 0$ and $y = 1/e$ lines.

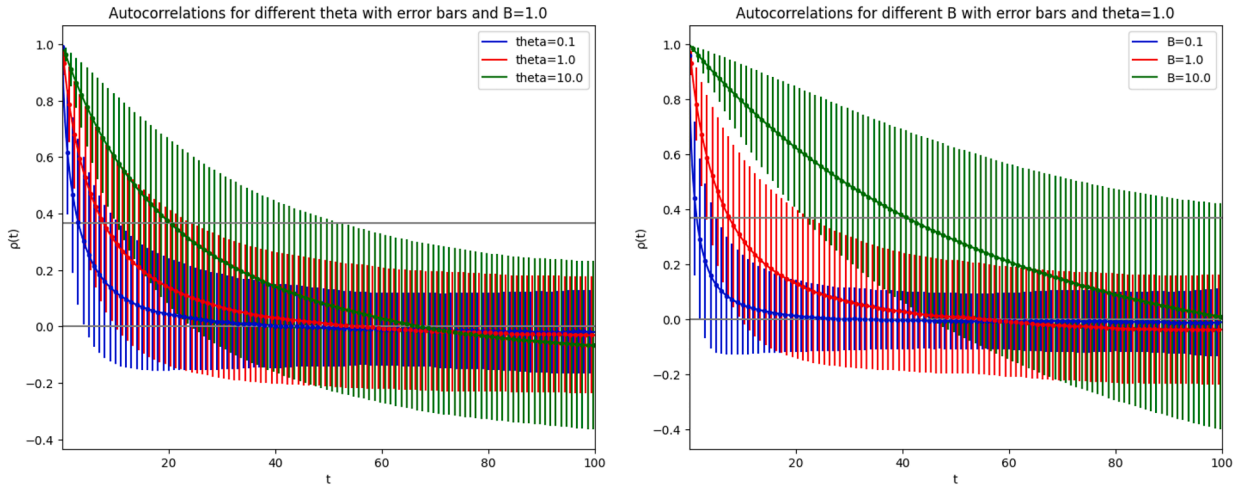

Fig. F.3. Impact of parameters θ and B on the autocorrelation of the Cauchy-distributed process. The autocorrelations are shown in the format: mean value (in solid line) plus SD error bars (vertical lines). Left panel: the AC is shown for $\theta = 0.1, 1, 10$ and $B = 1$; Right panel: the AC is shown for $B = 0.1, 1, 10$ and $\theta = 1$. The $y = 0$ and $y = 1/e$ lines are in gray.

As per the noise autocorrelation, it is shown in Fig. F.2 for the reference parametric pair $(\theta, B) = (1, 1)$. The plot shows that i) for a long time the autocorrelation follows an exponential decay; ii) the simulated autocorrelation has a large Standard Deviation iii) the characteristic time of this exponential is much larger than θ. Namely, the fitting to $g(t) = e^{-t/\tau_E}$ is as follows: $\tau_E \approx 8.61 \pm 0.02$.

Going beyond the reference parametric pair, Fig. F.3 shows the impact of parameters θ and B on the autocorrelation of the Cauchy-distributed noise. In the left panel of Fig. F.3, the AC is shown for $\theta = 0.1, 1, 10$ and $B = 1$; in the right panel, the AC is shown for $B = 0.1, 1, 10$ and $\theta = 1$. As per the relationship between the characteristic time and the two parameters, we got: i) the characteristic time is a power law function of θ (see Fig. F.4)

$$\tau_E \approx (8.498 \pm 0.002)\, \theta^{0.407 \pm O(-5)}$$

ii) The characteristic time τ_E is not a power-law function of B (see right panel of Fig. F.5). We obtained the following nonlinear fit:

$$\tau_E \simeq (48 \pm 6.22 \cdot 10^{-3}) - (47 \pm 6.06 \cdot 10^{-3}) \exp\left(-(0.15 \pm 4.48 \cdot 10^{-5})B\right) \tag{F.1}$$

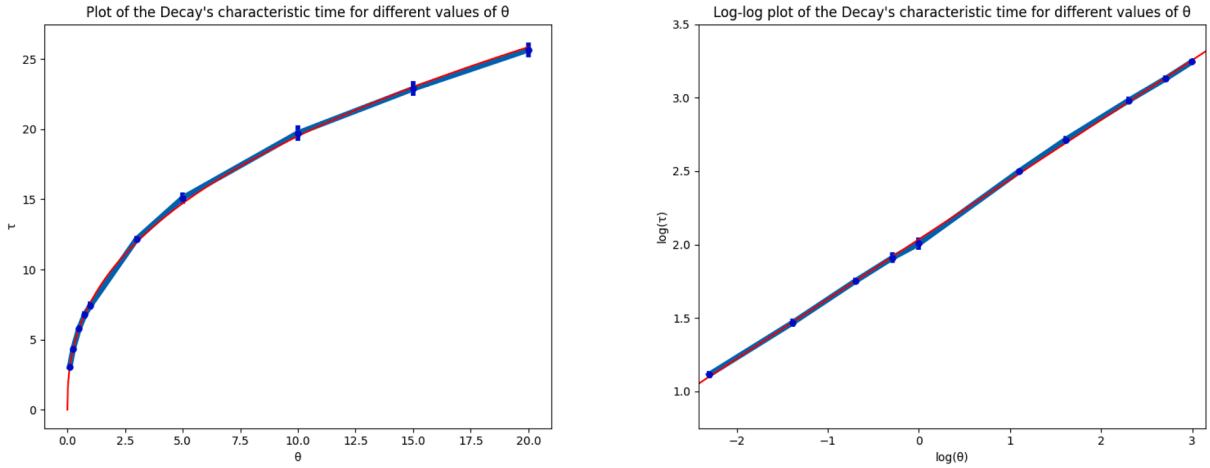

Fig. F.4. Characteristic time of autocorrelation (τ_E) vs θ. Left panel: τ_E vs θ; Right panel: log-log plot of τ_E vs θ, which is practically linear.

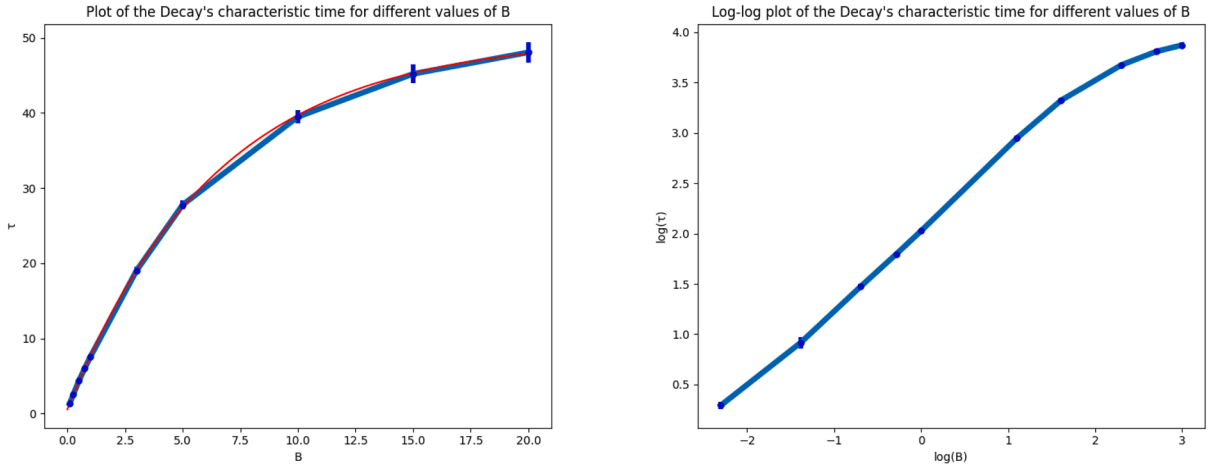

Fig. F.5. Characteristic time of autocorrelation (τ_E) vs B. Left panel: τ_E vs B; Right panel: log-log plot of τ_E vs B, which is not linear.

Appendix G. The case of bounded $\alpha_1(t)$

If $\alpha_1(t)$ is a bounded process, it is possible to provide simple analytical conditions on the asymptotic behavior of the model. Indeed, by applying the transformations seen in the previous sections one gets

$$dz = \left(\left(x_e - \frac{D^2}{2}\right) + \left(D^2 - \alpha_1(t)\right)\frac{1}{1+e^{-z}}\right)dt + D dB \tag{G.1}$$

whose general solution reads as follows

$$z(t) = z(0) + \left(x_e - \frac{D^2}{2}\right)t + \int_0^t \frac{\left(D^2 - \alpha_1(t)\right)}{1+e^{-z}}dt + DB(t). \tag{G.2}$$

For $q_1 = 0$ we have three cases:
Case A:

$D^2 > \alpha_1^{max}$

(i.e. $D^2 > \alpha_1(t)$) To start, from

$$\frac{D^2 - \alpha_1(t)}{1+e^{-z}} > \frac{D^2 - \alpha_1^{max}}{1+e^{-z}} > 0$$

yields

$$z(t) > q(t) = z(0) + \left(x_e - \frac{D^2}{2}\right)t$$

So that if

$$x_e - \frac{D^2}{2} > 0 \quad \text{AND} \quad D^2 > \alpha_1^{max}$$

ie

$$\alpha_1^{max} < D^2 < 2x_e$$

then

$$q(t) \to +\infty \Rightarrow z(t) \to +\infty \Rightarrow x(t) \to 1$$

Moreover, from

$$\frac{D^2 - \alpha_1(t)}{1+e^{-z}} < \frac{D^2 - \alpha_1^{min}}{1+e^{-z}} < D^2 - \alpha_1^{min}$$

one gets

$$z(t) < r(t) = z(0) + \left(x_e - \frac{D^2}{2}\right)t + (D^2 - \alpha_1^{min})t = z(0) + \left(x_e + \frac{D^2}{2} - \alpha_1^{min}\right)t$$

so that if

$$x_e + \frac{D^2}{2} - \alpha_1^{min} \quad \text{AND} \quad D^2 > \alpha_1^{max}$$

ie

$$\alpha_1^{max} < D^2 < 2(\alpha_1^{min} - x_e)$$

then

$$r(t) \to -\infty \Rightarrow z(t) \to -\infty \Rightarrow x(t) \to 0$$

Case B:

$D^2 < \alpha_1^{min}$

(i.e. $D^2 < \alpha_1(t)$) From

$$\frac{D^2 - \alpha_1(t)}{1+e^{-z}} < 0$$

it yields

$$z(t) < f(t) = z_0 + \left(x_e - \frac{D^2}{2}\right)t$$

thus if

$$2x_e < D^2 < \alpha_1^{min}$$

then

$$f(t) \to -\infty \Rightarrow z(t) \to -\infty \Rightarrow x(t) \to 0$$

Finally, we have the Case C:

$\alpha_1^{min} < D^2 < \alpha_1^{max}$

implying

$$\frac{D^2 - \alpha_1(t)}{1+e^{-z}} < \frac{D^2 - \alpha_1^{min}}{1+e^{-z}} < D^2 - \alpha_1^{min}$$

yielding

$$z(t) < h(t) = z_0 + \left(x_e - \frac{D^2}{2}\right)t + (D^2 - \alpha_1^{min})t = z_0 + \left(x_e + \frac{D^2}{2} - \alpha_1^{min}\right)t$$

Thus if

$$x_e + \frac{D^2}{2} - \alpha_1^{min} < 0 \quad \text{AND} \quad \alpha_1^{min} < D^2 < \alpha_1^{max}$$

ie if

$$\alpha_1^{min} < D^2 < Min\left(\alpha_1^{max}, 2(\alpha_1^{min} - x_e)\right)$$

then

$$h(t) - \infty \Rightarrow z(t) \to -\infty \Rightarrow x(t) \to 0$$

Moreover from

$$\frac{D^2 - \alpha_1(t)}{1+e^{-z}} > \frac{D^2 - \alpha_1^{max}}{1+e^{-z}} > D^2 - \alpha_1^{max}$$

it follows that

$$z(t) > c(t) = z_0 + \left(x_e - \frac{D^2}{2}\right)t + (D^2 - \alpha_1^{max})t = z_0 + \left(x_e + \frac{D^2}{2} - \alpha_1^{max}\right)t$$

Thus if

$$x_e + \frac{D^2}{2} - \alpha_1^{max} > 0 \quad \text{AND} \quad \alpha_1^{min} < D^2 < \alpha_1^{max}$$

ie

$$Max\left(\alpha_1^{min}, 2(\alpha_1^{max} - x_e)\right) < D^2 < \alpha_1^{max}$$

then

$$c(t) \to +\infty \Rightarrow z(t) \to +\infty \Rightarrow x(t) \to 1$$

Appendix H. Detailed analysis of the effects of actions of public health system to favor vaccine uptake

Here we will analyze in detail the role of public health in favoring vaccine uptake. The main results of this section for the case where the action γ is constant have been summarized in the main body of this work.

For the commodity of our readers we report also here the main model

$$dx = x(1-x)(x_e - x)dt + Dx(1-x)dB + \gamma(t)(1-x(t))dt \tag{H.1}$$

And we recall that we assume

$$\gamma(t) = \bar{\gamma} + \eta_1\gamma_1(t) + \eta_2\nu(t) > 0 \tag{H.2}$$

where $\gamma_1(t)$ is periodic with null mean:

$\langle\gamma_1(t)\rangle = 0,$

$\nu(t)$ is a stochastic ergodic process with null mean and $\eta_1, \eta_2\{0,1\}$ $\eta_1\eta_2 \neq 0$. This corresponds to some worthwile cases: i) $\eta_1 = \eta_2 = 0$ i.e. $\gamma(t) = \bar{\gamma}]$ is constant; ii) $\eta_1 = 1$ $\eta_2 = 0$: periodic $\gamma(t) > 0$ with average equal to $\bar{\gamma}]$

$$\bar{\gamma} = \frac{1}{T}\int_0^T \gamma(t)dt;$$

iii) $\eta_1 = 1$ $\eta_2 = 0$: $\gamma(t)$ is positive and stochastic with:

$\gamma(t) = \bar{\gamma} + \nu(t),$

where $\nu(t)$ is a bounded stochastic ergodic process with zero average:

$\langle\nu(t)\rangle = 0$

iv) $\gamma(t) > 0$ is the bounded stochastic perturbation of a periodic positive function.

As far as the bounded ergodic noise $\nu(t)$ note that if we define the stochastic process

$$K(t) = \bar{\gamma} + \frac{1}{t}\int_0^t \nu(s)ds$$

due to the ergodic properties of $\nu(t)$ it holds that for large times the second addendum tends to the average of $\nu(t)$

$$\lim_{t\to+\infty} K(t) = \bar{\gamma} + \langle \nu(t)\rangle = \bar{\gamma}$$

In the following, we will consider only the case (iii) since the other cases leads to practically identical calculi.

As mentioned in the text, an important effect is that when stochastically unstable, the unique stochastic equilibrium point $x_e = 1$, can be stabilized. Indeed, as far as the local stability is concerned, applying the theorem of stochastic linearization [72,73] and linearizing at $x = 1$ by setting $y = 1 - x$ one gets the following equation:

$$dy = (1 - x_e - \gamma(t))ydt + DydB$$

Whose solution is

$$y(t) = y(0)Exp\left(\left(1 - x_e - \frac{D^2}{2}\right)t + DB(t) - \int_0^t \gamma(u)du\right)$$

thus if:

$$\bar{\gamma} > \gamma^* = 1 - x_e - \frac{D^2}{2} \tag{H.3}$$

then the equilibrium point $x = 1$ is locally stochastically stable. As far as the stability in the large, applying the transformation (27) one gets the following SDE:

$$dz = \left(\left(x_e - \frac{D^2}{2} + \gamma(t)\right) + \gamma(t)e^{-z} + \left(D^2 - 1\right)\frac{1}{1+e^{-z}}\right)dt + DdB$$

whose solution is

$$z(t) = z(0) + \int_0^t \gamma(u)du + \left(x_e - \frac{D^2}{2}\right)t + \int_0^t (\gamma(u)e^{-z(u)} + \frac{\left(D^2-1\right)}{1+e^{-z(u)}}du + DB(t).$$

Four cases can occur. The first case is trivial if in the absence of control $x = 1$ is globally attractive, then even the controlled system has the same property. The proof of this claim is trivial. The other two cases depends on whether D is equal to, or smaller or greater than 1.

Namely:

i) if $D = 1$ then

$$z(t) = z(0) + \int_0^t \gamma(u)du + \left(x_e - \frac{1}{2}\right)t + \int_0^t \gamma(u)e^{-z(u)}du + DB(t) >$$

$$z(0) + \int_0^t \gamma(u)du + \left(x_e - \frac{1}{2}\right)t + DB(t)$$

yielding the following condition for the global attractiveness of $x = 1$:

$$\bar{\gamma} > \frac{1}{2} - x_e \tag{H.4}$$

which is precisely the local condition (H.3) for $D = 1$. The interest of the constraint (H.4) stands in the case $x_e \in (0, 1/2]$, because for $x_e \in (1/2, 1)$ even in the non-controlled system globally tends to $x = 1$.

If $0 < D < 1$ then

$$\int_0^t (\gamma(u)e^{-z(u)} + \frac{\left(D^2-1\right)}{1+e^{-z(u)}}du > \left(D^2-1\right)t$$

so that

$$z(t) > z(0) + \int_0^t \gamma(u)du + \left(x_e + \frac{D^2}{2} - 1\right)t + DB(t)$$

The corresponding condition for the global attractivity of $x = 1$ is thus the local stability condition (H.3).

H.1. Case $D > 1$

Defining the function

$$\psi(w,t) = \gamma(t)w + \frac{\left(D^2-1\right)}{1+w}$$

one can see that if

$$\gamma(t) \geq D^2 - 1, \tag{H.5}$$

then $\psi_{\min} = \psi(t,0) = D^2 - 1$. Thus from

$$z(t) > z(0) + \int_0^t \gamma(u)du + \left(x_e - 1 + \frac{D^2}{2}\right)t + DB(t),$$

it follows that condition (H.3) implies $z \to +\infty$. Thus if (H.5) and (H.3) holds than the equilibrium $x = 1$ is also global stochastic stable.

This the double condition *'(H.5) AND (H.3) '* is of course sharper than the local stability condition alone (H.3). However in the case of constant γ the above-mentioned double condition is summarized by

$$\gamma > Max\left(D^2 - 1, 1 - x_e - \frac{D^2}{2}\right)$$

By setting

$$D^2 - 1 < 1 - x_e - \frac{D^2}{2}$$

yields that if

$$1 < D^2 < \frac{3}{2}\left(2 - x_e\right)$$

then (H.3) guarantees the global attractiveness of $x = 1$.

Moreover, since $D^2 - 1 > 0$, it further follows that

$$z(t) > z(0) + \int_0^t \gamma(u)du + \left(x_e - \frac{1}{2}\right)t + DB(t),$$

so that if (H.5) and $x_e > 1/2$ also guarantees the global stochastic attractiveness of $x = 1$. If

$$\gamma(t) < D^2 - 1$$

Observing that

$$\psi_{min}(t) = q(t) := -\gamma(t) + 2\sqrt{(D^2-1)\gamma(t)}$$

yielding:

$$z(t) > z(0) + \left(x_e - \frac{D^2}{2}\right)t + 2\sqrt{D^2-1}\int_0^t \sqrt{\gamma(u)}du + DB(t).$$

Applying the ergodic property, it follows the following stochastic GAS condition:

$$\left\langle \sqrt{\gamma(t)} \right\rangle > \frac{D^2 - 2x_e}{4\sqrt{D^2-1}} \tag{H.6}$$

which is very complex.

Finally, if

$$\gamma_{min} < D^2 - 1 < \gamma_{Max}$$

defining

$$\psi_{min}(t) = \omega(t) = min(D^2 - 1, q(t))$$

yields

$$z(t) > z(0) + \left(x_e - \frac{D^2}{2}\right)t + \int_0^t \omega(u)du + DB(t).$$

The associated sufficient condition for the stochastic GAS of $x = 1$ is

$$\langle \omega(t)\rangle > x_e - \frac{D^2}{2}.$$

H.2. Constant γ: study of the local stochastic stability at $x = 1$

In the case where γ is constant, it is appropriate to set $y = 1 - x$, leading to

$$dy = \big(y(1-y)(1-x_e-y)+\gamma y\big)dt + Dy(1-y)dB \tag{H.7}$$

If $q_1 = 0$, then one can find a stochastic Lyapunov function $V(y)$ solving the Kashminski-Kushner equation [72,73]:

$$L(V(.)) = y(1-y)(1-x_e-y)-\gamma y)V'(y) + \frac{D^2}{2}y^2(1-y)^2V''(t) = -k(y)$$

setting

$$V'(y) = Z(y)e^{(2/D^2)(\gamma-(1-x-e))}$$

and

$$k(y) = y^{2+(2/D^2)(\gamma-(1-x_e))}k_3(y)$$

one gets the equation

$$\big((\gamma+x_e)y-(2\gamma+x_e)\big)Z + \frac{D}{2}(1-y)^2Z' = -k_3(y)$$

the most convenient choice for $k_3(y) > 0$ (in $y \in [0,1]$) is

$$k_3(y) = -(\gamma+x_e)y + (2\gamma+x_e) > 0$$

since it implies $Z(y) = Const$ and

$$V(y) = \frac{Z_0}{1+(2/D^2)(\gamma-(1-x_e))}y^{1+(2/D^2)(\gamma-(1-x_e))}.$$

Similar results can be obtained by linearization in the case $q_1 > 0$.

H.3. Impact of a small or relatively small constant γ if $x = 1$ is stochastically unstable

If γ is constant under the threshold $\gamma < \gamma^*$, then $x = 1$ is stochastically unstable and it is of interest to solve the Fokker Planck equation to assess the impact of γ on the stationary distribution of x.

The stationary distribution reads as follows

$$\rho_{ss}(x) = AExp(-\frac{2\gamma}{xD^2})x^{2(-1+(1/D^2)(x_e+\gamma))}(1-x)^{(2/D^2)(1-x_e-\gamma)-2}$$

is increasing or stationary provided that

$$f(x) \geq \sigma'(x)\sigma(x)$$

which yields the following inequality

$$\pi(x) = (2D^2-1)x^2 + (x_e - D^2)x + \gamma \geq 0$$

The function $\pi(x)$ is such that $\pi(0) = \gamma > 0$ and

$$\pi(1) = \frac{D^2}{2} - \gamma^*$$

.

Thus if $\pi(1) < 0$, i.e. $\gamma^* > D^2/2$ then it exist a $x_1(\gamma)$ such that the PDF $\rho(x)$ is unimodal with mode at $x_1(\gamma)$.

If $\pi(1) > 0$ and $2D^2 - 1 < 0$ then $\pi(x) > 0$, i.e. $\rho(x)$ is increasing.

Finally, the case $2D^2 - 1 > 0$ and $\pi(1) > 0$ is more complex. Indeed, the parabula has a minimum at

$$x_{min}(\gamma) = \frac{D^2 - x_e}{2(2D^2-1)}$$

We have two cases: i) $x_{\min}(\gamma) > 1$, implying $\pi(x) > 0$ in $x \in (0,1)$, i.e. the PDF is increasing. This case implies $1/2 < D^2 < (1/3)(2-x_e)$ in turn implying $x_e < 1/2$; ii) $x_{\min}(\gamma) \in (0,1)$. In such a case the behavior depends on the sign of

$$\pi(x_{min}) = \frac{D^2-x_e}{4(2D^2-1)} + \gamma,$$

i.e.: if $\pi(x_{\min}) \geq 0$ then the PDF is increasing, otherwise denoting as $x_1(\gamma)$ and $x_2(\gamma) > x_1$ the two solutions of $\pi(x) = 0$ the PDF has a mode at x_1, a minumum at $x = x_2$ and it is growing for $x \in (x_2, 1)$.

H.4. Absence of noise and constant γ: analytical solution

In case of absence of noise and constant control rate, an analytical solution of the type $t = \psi(x; x_0, \gamma)$ can be easily found after some simple calculus. Indeed, in such a case the model is:

$$x' = x(1-x)\Big(x_e - x\Big) + \gamma(1-x) \tag{H.8}$$

and it reads as follows:

$$x' = (1-x)\Big(x_e x - x^2 + \gamma\Big) \tag{H.9}$$

which can be rewritten as follows

$$x' = (1-x)(x_2-x)(y_2+x) \tag{H.10}$$

where

$$x_2(\gamma, x_e) = \frac{\sqrt{x_e^2+4\gamma}+x_e}{2} > 0,$$

is the positive solution of the equation

$$x^2 - x_e x - \gamma = 0 \tag{H.11}$$

and

$$y_2(\gamma, x_e) = \frac{\sqrt{x_e^2+4\gamma}-x_e}{2} > 0$$

is such that $-y_2$ is the negative solution of (H.11).

Finally, rewriting (H.10) as follows:

$$\frac{\frac{dx}{dt}}{1-x)(x_2-x)(y_2+x)} = 1 \tag{H.12}$$

and applying elementary integration we easily get:

$$Log\Big(\frac{(1-x)^P(x+y_2)^Q}{|x_2-x|^R}\Big) = Log\Big(\frac{(1-x_0)^P(x_0+y_2)^Q}{|x_2-x_0|^R}\Big) + t$$

ie

$$\frac{(1-x)^P(x+y_2)^Q}{|x_2-x|^R} = \frac{(1-x_0)^P(x_0+y_2)^Q}{|x_2-x_0|^R}e^t, \tag{H.13}$$

where:

$$P(\gamma, x_e) = \frac{1}{(1+y_2)(1-x_2)},\ Q(\gamma, x_e) = \frac{1}{(1+y_2)(x_2+y_2)},$$

$$R(\gamma, x_e) = \frac{1}{(1-x_2)(x_2+y_2)}.$$

H.5. Colored noises and the control by public health authorities

If we take into the account the control by Public Health Authorities the dynamics of x is ruled by the following random differential equation

$$x' = x(1-x)\Big((x_e-x)+y(t)\Big) + \gamma(t)(1-x). \tag{H.14}$$

Since $x \in (0,1]$

$$\frac{x'}{x(1-x)} = x_e + y(t) - x + \frac{\gamma(t)}{x} > x_e + y(t) - x + \gamma(t) \tag{H.15}$$

Again taking into account ergodicity of $\gamma(t)$ and of $y(t)$ it is easy matter to show that

$$\bar{\gamma} > 1 - x_e \Rightarrow x(t) \to 1 \tag{H.16}$$

Appendix I. Summaries of key scenarios

Short-Memory Scenario

- Fast Adaptation: When the memory kernel has a small characteristic time, individuals promptly update their vaccination choice based on recent information.

- Near-Deterministic Regime: Short memory tends to produce a behavior close to the no-delay deterministic model, except for minor transient discrepancies.
- Minimal Oscillations: Damped oscillations (if any) have small amplitude because past side-effect information quickly “expires” and does not accumulate.
- Interpretation: The system is comparatively straightforward–noise may still induce boundary fixation, but memory-driven complexity is reduced.

Large-Memory Scenario

- Long-Term Information Retention: An extended memory window means individuals weigh side-effect signals over a longer history, potentially reinforcing perceived risks.
- Delayed Responses: Transients can be more pronounced, with slower convergence or more persistent oscillations because outdated information lingers.
- Enhanced Noise Effects: Larger memory can amplify certain noise-driven phenomena, such as quasi-cycles or boundary fixation at extreme vaccination levels.
- Interpretation: The slow washout of historical data heightens the interplay between stochastic “irrational” spikes and the system’s drift toward equilibrium.

Hopf Bifurcation and Oscillatory Dynamics

- Onset of Cycles: For certain parameter thresholds (e.g., combined memory rates, vaccination propensity, and noise intensity), the system exhibits a Hopf bifurcation.
- Sustained Oscillations: Once the bifurcation is passed, vaccine uptake and perceived side-effect intensity can oscillate indefinitely in the deterministic model.
- Interpretation: The Hopf region highlights a qualitatively distinct regime wherein feedback via memory conspires with behavioral imitation to sustain periodic dynamics.

Noise Affected Systems:

- Noise-Induced Quasi-Cycles: Under stochastic forcing, in the systems presenting deterministic cycles these become noisy limit cycles or erratic swings. Moreover, also deterministic systems that do not present cycles in their dynamics can be subjected to noise-induced transitions when perturbed eventually able to induce cyclic behaviours in certain conditions.
- Bifurcate behaviour propensity: Increasing the noise amplitude via the different parameters leads sistematically to the absorption of the trajectories to one of the two boundary states. This bifurcate situation is the common final behaviour for all the noise affected systems when the noise effects on the dynamics become too relevant, at least at the steady-state.

References

[1] N.T.J. Bailey, The Mathematical Theory of Infectious Diseases and its Applications (2nd edition), Charles Griffin & Company Ltd, 1975.
[2] V. Capasso, V. Capasso, Mathematical Structures of Epidemic Systems, 88, Springer, 1993.
[3] P. Manfredi, A. d’Onofrio, Modeling the Interplay Between Human Behavior and the Spread of Infectious Diseases, Springer, New York, New York, 2013.
[4] Z. Wang, C.T. Bauch, S. Bhattacharyya, A. d’Onofrio, P. Manfredi, M. Perc, N. Perra, M. Salathé, D. Zhao, Statistical physics of vaccination, Phys. Rep. 664 (2016) 1–113.
[5] R. Casiday, T. Cresswell, D. Wilson, C. Panter-Brick, A survey of UK parental attitudes to the MMR vaccine and trust in medical authority, Vaccine 24 (2) (2006) 177–184.
[6] E. Dubé, C. Laberge, M. Guay, P. Bramadat, R. Roy, J.A. Bettinger, Vaccine hesitancy: an overview, Human Vaccin. Immunother. 9 (8) (2013) 1763–1773.
[7] V.A.A. Jansen, N. Stollenwerk, H.J. Jensen, M.E. Ramsay, W.J. Edmunds, C.J. Rhodes, Measles outbreaks in a population with declining vaccine uptake, Science 301 (5634) (2003) 804–804.
[8] S.B. Omer, D.A. Salmon, W.A. Orenstein, M.P. Dehart, N. Halsey, Vaccine refusal, mandatory immunization, and the risks of vaccine-preventable diseases, N. Engl. J. Med. 360 (19) (2009) 1981–1988.
[9] V. Capasso, G. Serio, A generalization of the Kermack-McKendrick deterministic epidemic model, Math. Biosci. 42 (1-2) (1978) 43–61.
[10] N. Perra, Non-pharmaceutical interventions during the COVID-19 pandemic: a review, Phys. Rep. 913 (2021) 1–52.
[11] R. Löfstedt, Risk Management in Post-Trust Societies, Palgrave–McMillan, 2005.
[12] M. Carlson, The information politics of journalism in a post-truth age, Journalism Stud. 19 (13) (2018) 1879–1888.
[13] C. Hagiopol, P.M. Leru, Scientific truth in a post-truth era: a review, Sci. Educ. 272 (2025) 2923–2956.
[14] C.T. Bauch, Imitation dynamics predict vaccinating behaviour, Proc. R. Soc. Lond. B Biol. Sci. 272 (1573) (2005) 1669–1675.
[15] A. d’Onofrio, P. Manfredi, P. Poletti, The impact of vaccine side effects on the natural history of immunization programmes: an imitation–game approach, J. Theor. Biol. 273 (1) (2011) 63–71.
[16] C.T. Bauch, S. Bhattacharyya, Evolutionary game theory and social learning can determine how vaccine scares unfold, PLoS Comput. Biol. 8 (4) (2012) e1002452.
[17] T. Oraby, V. Thampi, C.T. Bauch, The influence of social norms on the dynamics of vaccinating behaviour for paediatric infectious diseases, in: Proc. R. Soc. B, 281, The Royal Society, 2014, p. 20133172.
[18] T. Oraby, C.T. Bauch, Bounded rationality alters the dynamics of paediatric immunization acceptance, Sci. Rep. 5 (1) (2015) 10724.
[19] A. Lupica, P. Manfredi, V. Volpert, A. Palumbo, A. d’Onofrio, Spatio-temporal games of voluntary vaccination in the absence of the infection: the interplay of local versus non-local information about vaccine adverse events, Math. Biosci. Eng. 17 (2020) 1090.
[20] A. d’Onofrio, P. Manfredi, P. Poletti, The interplay of public intervention and private choices in determining the outcome of vaccination programmes, PLoS ONE 7 (10) (2012) e45653.
[21] B. Buonomo, G. Carbone, A. d’Onofrio, Effect of seasonality on the dynamics of an imitation–based vaccination model with public health intervention, Math. Biosci. Eng. 15 (1) (2018) 299–321.
[22] M. Ochab, P. Manfredi, K. Puszynski, A. d’Onofrio, Multiple epidemic waves as the outcome of stochastic SIR epidemics with behavioral responses: a hybrid modeling approach, Nonlinear Dyn. 111 (1) (2023) 887–926.
[23] A.L. Schmidt, F. Zollo, A. Scala, C. Betsch, W. Quattrociocchi, Polarization of the vaccination debate on Facebook, Vaccine 36 (25) (2018) 3606–3612.
[24] S. Ajovalasit, V.M. Dorgali, A. Mazza, A. d’Onofrio, P. Manfredi, Evidence of disorientation towards immunization on online social media after contrasting political communication on vaccines. Results from an analysis of Twitter data in Italy, PLoS ONE 16 (7) (2021) e0253569.
[25] D.A. Broniatowski, A.M. Jamison, S. Qi, L. AlKulaib, T. Chen, A. Benton, S.C. Quinn, M. Dredze, Weaponized health communication: Twitter bots and Russian trolls amplify the vaccine debate, Am. J. Public Health 108 (10) (2018) 1378–1384.
[26] J.T. Jost, P. Barberá, R. Bonneau, M. Langer, M. Metzger, J. Nagler, J. Sterling, J.A. Tucker, How social media facilitates political protest: information, motivation, and social networks, Polit. Psychol. 39 (2018) 85–118.
[27] J. On, H.-A. Park, T.-M. Song, Sentiment analysis of social media on childhood vaccination: development of an ontology, J. Med. Internet Res. 21 (6) (2019) e13456.
[28] G. Bonifazi, B. Breve, S. Cirillo, E. Corradini, L. Virgili, Investigating the COVID-19 vaccine discussions on Twitter through a multilayer network-based approach, Inf. Process. Manage. 59 (6) (2022) 103095.
[29] D. He, J. Dushoff, T. Day, J. Ma, D.J.D. Earn, Inferring the causes of the three waves of the 1918 influenza pandemic in England and Wales, Proc. R. Soc. B Biol. Sci. 280 (1766) (2013) 20131345.
[30] B. Tang, W. Zhou, X. Wang, H. Wu, Y. Xiao, Controlling multiple COVID-19 epidemic waves: an insight from a multi-scale model linking the behaviour change dynamics to the disease transmission dynamics, Bull. Math. Biol. 84 (10) (2022) 106.
[31] R.M. Anderson, R.M. May, Infectious Diseases of Humans: Dynamics and Control, Oxford University Press, 1991.
[32] Global polio eradication initiative, (https://polioeradication.org/). Accessed on 2025-09-30.
[33] K. Chumakov, E. Ehrenfeld, V.I. Agol, E. Wimmer, Polio eradication at the crossroads, Lancet Global Health 9 (8) (2021) e1172–e1175.
[34] M. Pons-Salort, C.C. Burns, H. Lyons, I.M. Blake, H. Jafari, M.S. Oberste, O.M. Kew, N.C. Grassly, Preventing vaccine-derived poliovirus emergence during the polio endgame, PLoS Pathog. 12 (7) (2016) e1005728.
[35] D. Klapsa, T. Wilton, A. Zealand, E. Bujaki, E. Saxentoff, C. Troman, A.G. Shaw, A. Tedcastle, M. Majumdar, R. Mate, et al., Sustained detection of type 2 poliovirus in London sewage between February and July, 2022, by enhanced environmental surveillance, Lancet 400 (10362) (2022) 1531–1538.
[36] M. Eichner, S.O. Brockmann, Polio emergence in Syria and Israel endangers Europe, Lancet 382 (9907) (2013) 1777.
[37] V. Cetorelli, The impact of the Iraq war on neonatal polio immunisation coverage: a quasi-experimental study, J Epidemiol Community Health 69 (3) (2015) 226–231.
[38] D.A. Kalkowska, A. Voorman, M.A. Pallansch, S.G.F. Wassilak, S.L. Cochi, K. Badizadegan, K.M. Thompson, The impact of disruptions caused by the COVID-19 pandemic on global polio eradication, Vaccine 41 (2023) A12–A18.
[39] World Health Organization, Immunization, 2023. Accessed: 2025-10-27, https://www.who.int/health-topics/immunization.
[40] T.M.R. da Silva, A.C. M. G. N.d. Sá, E.J.S. Prates, R.d. Freitas Saldanha, T.P.R. Da Silva, A.M.d. Silva Teixeira, M.A. Beinner, S.R. de Oliveira, A.T.N. de Sá, F.P. Matozinhos, et al., Temporal and spatial distribution trends of polio vaccine

coverage in less than one-year old children in Brazil, 2011–2021, BMC Public Health 23 (1) (2023) 1359.
[41] L.H. Falleiros-Arlant, J.R. Torres, M.L. Ávila-Agüero, J.B.-d. Castillo, A. Gentile, R. Debbag, Increasing polio coverage with safer vaccines: a pressing need in Latin America, Rev. Chil. Infectología 39 (5) (2022) 614–622.
[42] G. Antehunegn Tesema, M. Sarfo, S.R. Okeke, E.K. Ameyaw, S. Yaya, Unveiling the drivers of polio vaccine uptake: insights from a multi-country study of 37 nations in sub-Saharan Africa, PLoS ONE 20 (3) (2025) e0316884.
[43] Vaccination statistics in UK, (https://digital.nhs.uk/data-and-information/publications/statistical/nhs-immunisation-statistics/england-2023-24). Accessed on 2025-09-30.
[44] A. d'Onofrio, P. Manfredi, E. Salinelli, Vaccinating behaviour, information, and the dynamics of SIR vaccine preventable diseases, Theor. Popul. Biol. 71 (3) (2007) 301–317.
[45] A. d'Onofrio, Exposé de Alberto d'Onofrio dans le cadre du groupe de travail maths-4-COVID-19 : 8 juin 2020, 2020, (https://www.youtube.com/watch?v=BF4NCSXe-A8). Video lecture, published on the YouTube channel of the 'Laboratoire Jacques-Louis Lyons' of Sorbonne University, Paris.
[46] A. Balogh, T. Oraby, Stochastic games of parental vaccination decision making and bounded rationality, Math. Biosci. Eng. 22 (2) (2025) 355–388.
[47] B. Buonomo, P. Manfredi, A. d'Onofrio, Optimal time-profiles of public health intervention to shape voluntary vaccination for childhood diseases, J. Math. Biol. 78 (4) (2019) 1089–1113.
[48] E. Frey, Evolutionary game theory: theoretical concepts and applications to microbial communities, Physica A Stat. Mech. Appl. 389 (20) (2010) 4265–4298.
[49] A. d'Onofrio, P. Manfredi, E. Salinelli, Vaccinating behaviour, information, and the dynamics of SIR vaccine preventable diseases, Theor. Popul. Biol. 71 (3) (2007) 301–317.
[50] C. Bauch, A. d'Onofrio, P. Manfredi, Behavioral epidemiology of infectious diseases: an overview, in: Modeling the Interplay between Human Behavior and the Spread of Infectious Diseases, Springer, 2012, pp. 1–19.
[51] A. d'Onofrio, P. Manfredi, Information–related changes in contact patterns may trigger oscillations in the endemic prevalence of infectious diseases, J. Theor. Biol. 256 (3) (2009) 473–478.
[52] W.E. Boyce, R.C. DiPrima, D.B. Meade, Elementary Differential Equations and Boundary Value Problems, John Wiley & Sons, 2021.
[53] M. Assaf, B. Meerson, WKB theory of large deviations in stochastic populations, J. Phys. A Math. Theor. 50 (26) (2017) 263001.
[54] O. Ovaskainen, B. Meerson, Stochastic models of population extinction, Trends Ecol. Evol. 25 (11) (2010) 643–652.
[55] M. Assaf, B. Meerson, Spectral formulation and WKB approximation for rare-event statistics in reaction systems, Phys. Rev. E 74 (4) (2006) 041115.
[56] C.R. Doering, K.V. Sargsyan, L.M. Sander, Extinction times for birth-death processes: exact results, continuum asymptotics, and the failure of the Fokker–Planck approximation, Multiscale Model. Simul. 3 (2) (2005) 283–299.
[57] D.T. Gillespie, The chemical Langevin equation, J. Chem. Phys. 113 (1) (2000) 297–306.
[58] N.G. Van Kampen, Stochastic Processes in Physics and Chemistry, Elsevier, 1992.
[59] P. Poletti, M. Ajelli, S. Merler, The effect of risk perception on the 2009 H1N1 pandemic influenza dynamics, PLoS ONE 6 (2) (2011) e16460.
[60] P. Poletti, M. Ajelli, S. Merler, Risk perception and effectiveness of uncoordinated behavioral responses in an emerging epidemic, Math. Biosci. 238 (2) (2012) 80–89.
[61] A. d'Onofrio, P. Manfredi, E. Salinelli, Vaccinating behaviour and the dynamics of vaccine preventable infections, in: Modeling the Interplay between Human Behavior and the Spread of Infectious Diseases, Springer, 2012, pp. 267–287.
[62] M. Farkas, Periodic Motions, Springer, 1994.
[63] N. MacDonald, Time Lags in Biological Models, Springer, 1978.
[64] Y. Kuang, Delay Differential Equations, Academic Press, 1993.
[65] H. Wernecke, B. Sándor, C. Gros, Chaos in time delay systems, an educational review, Phys. Rep. 824 (2019) 1–40.
[66] B. Buonomo, A. Giacobbe, G. Mulone, Analysis of an epidemic model with peer-pressure and information-dependent transmission with high-order distributed delay, Ric. Mat. 68 (2) (2019) 453–468.
[67] D.V. Efimov, A.L. Fradkov, Oscillation conditions of nonlinear systems with static feedback, Autom. Remote Contr. 66 (2) (2005) 249–264.
[68] D.V. Efimov, A.L. Fradkov, Yakubovich's oscillatority of circadian oscillations models, Math. Biosci. 216 (2) (2008) 187–191.
[69] D.V. Efimov, A.L. Fradkov, Oscillatority of nonlinear systems with static feedback, SIAM J. Contr. Optim. 48 (2) (2009) 618–640.
[70] C.A. Braumann, Itô versus Stratonovich calculus in random population growth, Math. Biosci. 206 (1) (2007) 81–107.
[71] C.A. Braumann, Growth and extinction of populations in randomly varying environments, Comput. Math. Appl. 56 (3) (2008) 631–644.
[72] H.J. Kushner, Stochastic stability, in: Stability of Stochastic Dynamical Systems, Springer, 1972, pp. 97–124.
[73] R. Khasminskii, Stochastic Stability of Differential Equations, 66, Springer Science & Business Media, 2011.
[74] W. Horsthemke, R. Lefever, Noise-Induced Transitions in Physics, Chemistry, and Biology, Springer, 1984.
[75] G.I. Hagstrom, S.A. Levin, Phase transitions and the theory of early warning indicators for critical transitions, in: How Worlds Collapse, Routledge, 2023, pp. 358–374.
[76] M. Shiino, Dynamical behavior of stochastic systems of infinitely many coupled nonlinear oscillators exhibiting phase transitions of mean-field type: H theorem on asymptotic approach to equilibrium and critical slowing down of order-parameter fluctuations, Phys. Rev. A 36 (5) (1987) 2393.
[77] U.M. Ascher, Numerical Methods for Evolutionary Differential Equations, Society for Industrial and Applied Mathematics (SIAM), Philadelphia, PA, Philadelphia, PA, 2008.
[78] A. d'Onofrio, G. Caravagna, S. de Franciscis, Bounded noise induced first-order phase transitions in a baseline non-spatial model of gene transcription, Physica A Stat. Mech. Appl. 492 (2018) 2056–2068.
[79] D. Domingo, A. d'Onofrio, F. Flandoli, Boundedness vs unboundedness of a noise linked to Tsallis q-statistics: the role of the overdamped approximation, J. Math. Phys. 58 (3) (2017) 033301.
[80] R. Arthur, H.T.P. Williams, Scaling laws in geo-located Twitter data, PLoS ONE 14 (7) (2019) e0218454.
[81] C.T. Bauch, D.J.D. Earn, Vaccination and the theory of games, Proc. Natl. Acad. Sci. 101 (36) (2004) 13391–13394.
[82] P. Klepac, S. Funk, T.D. Hollingsworth, C.J.E. Metcalf, K. Hampson, Six challenges in the eradication of infectious diseases, Epidemics 10 (2015) 97–101.
[83] P.A. Gastañaduy, S. Funk, B.A. Lopman, P.A. Rota, M. Gambhir, B. Grenfell, P. Paul, Factors associated with measles transmission in the United States during the postelimination era, JAMA Pediatr. 174 (1) (2020) 56–62.
[84] M.T. Khan, S. Zaheer, K. Shafique, Maternal education, empowerment, economic status and child polio vaccination uptake in Pakistan: a population based cross sectional study, BMJ Open 7 (3) (2017) e013853.
[85] N. Stollenwerk, V. Jansen, Population Biology and Criticality: From Critical Birth-Death Processes to Self-Organized Criticality in Mutation Pathogen Systems, World Scientific, 2010.
[86] G. Brightwell, T. House, M. Luczak, Extinction times in the subcritical stochastic SIS logistic epidemic, J. Math. Biol. 77 (2) (2018) 455–493.
[87] A.B. Gumel, Causes of backward bifurcations in some epidemiological models, J. Math. Anal. Appl. 395 (1) (2012) 355–365.
[88] G. Tunnicliffe Wilson, Time Series Analysis: Forecasting and Control, Wiley, 2015.
[89] J.C. Butcher, Numerical Methods for Ordinary Differential Equations, Wiley, 2016.
[90] P. Kloeden, E. Platen, Numerical Solution of Stochastic Differential Equations: 23, Springer, 2010.
[91] A. d'Onofrio, "Noisy Oncology": Some Caveats in Using Gaussian Noise in Mathematical Models of Chemotherapy, Aspects of Mathematical Modelling: Applications in Science, Medicine, Economics and Management (2008) 229–234.
[92] R.V. Bobryk, Stability analysis of a SIR epidemic model with random parametric perturbations, Chaos Solitons Fractals 143 (2021) 110552.